

DTIC FILE COPY

2

AD-A230 090

VERSATILE HIGH PERFORMANCE
HOLOGRAPHIC OPTICAL COATINGS

December 15, 1990

SBIR Phase I Final Report
Contract N00014-90-C-0145
Solicitation Number SBIR SDIO90-001

Prepared for:

Strategic Defense Initiative Organization
ATTN: T/IS
The Pentagon
Washington, D.C. 20301-7100

Prepared by:

Dr. Jeffrey B. Shellan
JBS Technologies, Inc.
631 Kendale Lane
Thousand Oaks, CA 91360

DTIC
ELECTE
DEC 19 1990
S B D
Co

DISTRIBUTION STATEMENT A
Approved for public release;
Distribution Unlimited

REPORT DOCUMENTATION PAGE

1a. REPORT SECURITY CLASSIFICATION unclassified			1b. RESTRICTIVE MARKINGS		
2a. SECURITY CLASSIFICATION AUTHORITY			3. DISTRIBUTION/AVAILABILITY OF REPORT unlimited distribution		
2b. DECLASSIFICATION/DOWNGRADING SCHEDULE					
4. PERFORMING ORGANIZATION REPORT NUMBER(S)			5. MONITORING ORGANIZATION REPORT NUMBER(S)		
6a. NAME OF PERFORMING ORGANIZATION JBS Technologies, Inc.		6b. OFFICE SYMBOL (If applicable)	7a. NAME OF MONITORING ORGANIZATION Office of Naval Research		
6c. ADDRESS (City, State, and ZIP Code) 631 Kendale Lane Thousand Oaks, CA 91360			7b. ADDRESS (City, State, and ZIP Code) 800 North Quincy St. Arlington, VA 27217-5000		
8a. NAME OF FUNDING/SPONSORING ORGANIZATION SDIO		8b. OFFICE SYMBOL (If applicable) SDIO84	9. PROCUREMENT INSTRUMENT IDENTIFICATION NUMBER Contract No. N00014-90-C-0145 Solicitation No. SBIR SDIO 90-001		
8c. ADDRESS (City, State, and ZIP Code) The Pentagon, ATTN: T/IS Washington, D.C. 20301-7100			10. SOURCE OF FUNDING NUMBERS		
			PROGRAM ELEMENT NO.	PROJECT NO.	TASK NO.
			WORK UNIT ACCESSION NO.		
11. TITLE (Include Security Classification) Versatile High Performance Holographic Optical Coatings					
12. PERSONAL AUTHOR(S) Jeffrey B. Shellan					
13a. TYPE OF REPORT Final		13b. TIME COVERED FROM 90-6-7 TO 90-11-30		14. DATE OF REPORT (Year, Month, Day) 90-12-15	15. PAGE COUNT 118
16. SUPPLEMENTARY NOTATION					
17. COSATI CODES			18. SUBJECT TERMS (Continue on reverse if necessary and identify by block number)		
FIELD	GROUP	SUB-GROUP	Optical Coatings Holography		
19. ABSTRACT (Continue on reverse if necessary and identify by block number) The purpose of the work was to investigate the potential for fabricating holographic coatings (HCs) with nearly arbitrary reflectivity profiles. The desired reflectivity spectrum of the HC could, for example, be the optimum matched filter for detecting a specified target against a bright high clutter background. Once the desired spectral profile of the filter was calculated using well known matched filter theory, holographic techniques would be used to produce the filter. The analysis presented in this report has shown that such a procedure will work and allows the filter to be fabricated much more easily than would be the case for conventional multi-layer dielectric coatings, deposited one layer at a time. Detailed analysis is presented for the case of HCs designed for the detection of missile plumes against an Earth background in the UV and visible spectral regions.					
20. DISTRIBUTION/AVAILABILITY OF ABSTRACT <input checked="" type="checkbox"/> UNCLASSIFIED/UNLIMITED <input type="checkbox"/> SAME AS RPT. <input type="checkbox"/> DTIC USERS			21. ABSTRACT SECURITY CLASSIFICATION unclassified		
22a. NAME OF RESPONSIBLE INDIVIDUAL			22b. TELEPHONE (Include Area Code)		22c. OFFICE SYMBOL

TABLE OF CONTENTS

	<u>Page</u>
1. INTRODUCTION AND EXECUTIVE SUMMARY	1-1
2. BACKGROUND	2-1
2.1. MILITARY APPLICATIONS FOR MATCHED HOLOGRAPHIC FILTERS	2-1
2.1.1 MISSILE LAUNCH DETECTION IN THE IR	2-1
2.1.2 LASER RADAR	2-2
2.1.3 FRAUNHOFER LINE SURVEILLANCE - SINGLE FOCAL PLANE	2-3
2.1.4 FRAUNHOFER LINE SURVEILLANCE - DUAL FOCAL PLANE	2-5
2.1.5 WIDE-BAND MATCHED FILTER FOR BOOSTER DETECTION	2-7
2.2. COMMERCIAL APPLICATIONS FOR MATCHED HOLOGRAPHIC FILTERS	2-8
APPENDIX 2A. MATCHED FILTER SIGNAL PROCESSING	2A-1
2A.1 THEORY	2A-1
2A.2 CONCEPT DEMONSTRATION AND NUMERICAL ANALYSIS	2A-3
3. EXAMINATION OF APPROACHES FOR FABRICATING HOLOGRAPHIC MATCHED FILTERS	3-1
3.1. NARROW-BAND FILTERS	3-1
3.2. CONCEPT 1: CONTINUOUS EXPOSURE WITH PHASE CONTROL	3-2

<input checked="" type="checkbox"/>
<input type="checkbox"/>
<input type="checkbox"/>

Availability Codes	
Dist	Avail and/or Special
A-1	



3.2.1	DESCRIPTION OF CONCEPT 1 HOLOGRAM FABRICATION	3-2
3.2.2	CONCEPT 1 ANALYSIS	3-3
3.2.2.1	RELATIONSHIP BETWEEN REFLECTANCE PROFILE, $r(k)$, AND INDEX PROFILE, $n(z)$	3-3
3.2.2.2	CALCULATION OF HOLOGRAM EXPOSURE LEVELS	3-9
3.2.2.3	"INDEX STACKING"	3-13
3.3	CONCEPT 2: DISCRETE EXPOSURES	3-17
3.3.1	DESCRIPTION OF CONCEPT 2 HOLOGRAM FABRICATION	3-17
3.3.2	CONCEPT 2 ANALYSIS	3-19
	APPENDIX 3A-1	3A-1
3A.1	ANALYSIS	3A-1
3A.2	SAMPLE CALCULATION	3A-5
4.	PROPERTIES OF HOLOGRAPHIC RECORDING MATERIALS	4-1
4.1	BACKGROUND	4-1
4.2	THE DCG RECORDING PROCESS	4-1
4.3	DCG PROCESSING PROCEDURE TO CONTROL GRATING CHIRP	4-2
4.4	SEQUENTIAL RECORDINGS IN DCG	4-4
5.	COMPUTER MODELING OF OPTICAL COATING PERFORMANCES	5-1
5.1	UV PLUME SPECTRAL PROFILE	5-1
5.2	VISIBLE PLUME SPECTRAL PROFILE	5-3
5.3	HIGH REFLECTIVITY COATING FOR THE VISIBLE	5-3
5.4	PUBLICATION OF CONTRACT CONCLUSIONS	5-4

1. INTRODUCTION AND EXECUTIVE SUMMARY

This document is the final report (Item No. 0001AC) for SDIO contract number N00014-90-C-0145, "Versatile High Performance Holographic Optical Coatings." The contract has been monitored by ONR. The purpose of the work was to investigate the potential for fabricating holographic coatings (HCs) with nearly arbitrary reflectivity profiles. The desired reflectivity spectrum of the HC could, for example, be the optimum matched filter for detecting a specified target against a bright high clutter background. Once the desired spectral profile of the filter was calculated using well known matched filter theory, holographic techniques would be used to produce the filter. The analysis presented in this report has shown that such a procedure will work and allows the filters to be fabricated much more easily than would be the case for conventional multi-layer dielectric coatings, deposited one layer at a time.

Section 2. contains the background material which examines how filters can be used in target detection. Simple examples include the very narrow-band filters employed in laser radar and somewhat wider band IR filters used to detect missile plumes against an Earth background. In laser radar, the filters block all radiation wavelengths from reaching the detector except the narrow-band return laser wavelengths. Missile plume detection in the IR, against a high clutter Earth background, is best accomplished at the strong atmospheric water absorption line centered at 2.8 μm or the strong CO_2 absorption line centered at 4.3 μm . The Earth background is several orders of magnitude dimmer at these wavelengths (filter widths $\sim 0.2 \mu\text{m}$), allowing missile detection once the target breaks cloud cover. The filters for these applications can easily be made with conventional multi-layer coatings, but HCs offer an advantage even for these simple cases. These advantages include:

- Simplified fabrication, especially for higher performance filters where a fine spectral structure is desired within the narrow-band.
- Higher damage thresholds, both from nuclear events and from hostile laser irradiation.

In most of the HC applications investigated in this contract, the HC is used in a reflector mode. The target and background radiation passing through the camera beam train is reflected from the HC and onto the detector. The spectral filtering is thus performed through reflection and not transmission of the HC. The Fresnel reflection of the HC can easily be eliminated by recording the HC at an angle so that the interference planes of the coating are tilted slightly with respect to the surface of the HC.

The real advantage of the HC occurs for more complex applications than narrow-band filters. It is very difficult, for example, to detect missile plumes in the visible against the Earth background, which is especially intense in the visible. In a matched filter, the filter will allow wavelengths where the target is especially strong, and the background less intense, to be transmitted to the focal plane. It will also attenuate those wavelengths where the target is dimmer and the background is brighter from reaching the focal plane. Several examples are outlined in section 2 of this report which indicate that a matched filter could be used to detect missile plumes in the visible, contrary to the generally held belief of many "IR detector people." There are significant advantages to detecting missiles in the visible or near IR. These include:

- Cryogenic cooling is not required for silicon detectors used in the visible, thus greatly reducing the cost, complexity, and weight of such a system, compared to IR focal plane arrays.
- The silicon detectors represent a much more mature technology than HgCdTe or InSb detectors. They are also much less expensive, partly because of economics of scale. Silicon CCDs are mass produced for a commercial market.

Section 2 concludes with examples of how holographically produced filters could be used commercially. The use of these filters could help identify specific minerals and vegetation from a surveillance satellite.

In section 3, two basic concepts are examined for fabricating the general purpose HCs.

The analysis for both concepts is performed using the coupled mode theory. The final equations which determine the coating's reflectivity spectrum in terms of exposure wavelength, angle, and exposure time, must be solved numerically. Before this is done, we review a number of candidate hologram recording materials in section 4 of this report. The most attractive material, because of its high diffraction efficiency (large index of refraction modulation), high resolution ($> 10,000$ lines/mm), low scattering, and moderate exposure levels is dichromated gelatin (DCG). Section 4 reviews the properties of DCG and in particular how an unusual property of DCG can be exploited to simplify the filter fabrication for the "Concept 2" approach, described in section 3.

Section 5 contains the results of our numerical analysis. We considered "Concept 2" HCs designed for two military applications:

- Detection of missile plumes in the UV (3000 to 4000Å).
- Detection of missile plumes in the visible against an Earth background.

The section 5 analysis indicates that HCs can be made easily that accurately represent the ideal spectral profiles needed for the UV and visible plume detection. Some of the key results of this program have been submitted for publication and presentation at the 1991 SPIE International Symposium on Optical Applied Science and Engineering (21-26 July 1991, San Diego, CA; Conference No. 15). A draft copy of the paper is given in Appendix 5B.

2. BACKGROUND

Before discussing the novel approaches for fabricating optical filters which have been examined during Phase I of this program, we will review some of the potential uses of these filters in the fields of surveillance, target detection, and tracking. The primary emphasis during Phases 1 and 2 of this program will be in the development of the holographic filters for military applications, especially for SDI applications. These applications will be discussed in section 2.1. During Phase 3 of this work, as is often the case in SBIR programs, a greater emphasis will be placed on commercial uses of the holographic filters. These uses are examined in section 2.2.

2.1. MILITARY APPLICATIONS FOR MATCHED HOLOGRAPHIC FILTERS

2.1.1. MISSILE LAUNCH DETECTION IN THE IR

One of the most well known military uses of optical filters is in missile launch detection in the IR. The bright plume of a missile in the IR can be used to detect a missile from space, even with a bright Earth background, when viewed with a moderately narrow band optical filter ($\Delta\lambda \sim 0.2 \mu\text{m}$) centered at one of the absorption lines of the atmosphere. For example, the Earth background intensity drops several orders of magnitude around $2.8 \mu\text{m}$ and $4.3 \mu\text{m}$, due to strong water and carbon dioxide absorption lines, respectively. An optical filter centered at one of these lines will therefore block most of the Earth background radiance, but transmit the radiation from a plume, once the missile breaks cloud level and is above most of the attenuating atmosphere.

Of course, these optical filters can and have been made with conventional multi-layer deposition techniques (e.g. physical vapor deposition), but holographic filters offer a number of advantages. These include:

- Potentially narrower transmission lines and simplified fabrication, especially for advanced filters whose detailed spectral properties could be

matched to the atmospheric transmission in order to achieve even higher signal-to-clutter ratios (SCR).

- Higher damage thresholds, both from nuclear events and from hostile laser irradiation.

The principal investigator for this SBIR Phase I program, Dr. Jeffrey B. Shellan, experimentally demonstrated the high laser damage thresholds of holographic coatings under a subcontract to SAIC (No. DAA1-101-89-R-0065), which was funded by SDIO in 1989.

2.1.2. LASER RADAR

Another military (as well as non-military) application of optical filters is in laser radar systems. The laser radar can be used for target ranging, estimating target velocities (from the Doppler shifted return), and for background clutter suppression. For example, once a missile's bright plume is detected, a future space interceptor, such as Brilliant Pebbles may use laser radar to intercept the missile. The ladar could initially be used to obtain ranging information needed for calculating the optimum intercept trajectory. As the two vehicles converge, a "hard body handoff" is required--the interceptor must lock onto the missile body itself, rather than the much brighter plume. One approach for ensuring that this handoff is made is to use laser radar for actually imaging the hard body. A relatively large region near the tip of the plume is illuminated by the laser and the scattered laser light is detected by a CCD covered with a very narrow band filter. The filter, which is centered on the laser line, blocks nearly all the radiation from the plume and Earth background and detects the scattered laser light. For a liquid fueled missile, very little laser radiation is scattered from the plume itself, so centroid tracking can be used for hard body intercept. For solid fueled missiles, however, the fuel particles in the plume may actually scatter as much laser radiation as the missile. In this case, the target must be imaged using the focal plane array and an algorithm used which can identify the hard body silhouette.

Of course, the optical filter needed for the above mission could be fabricated by

conventional means, but holographic filters offer some advantages. In addition to those listed at the end of section 2.1.1, narrow line HCs can be made with larger fields-of-view (FOV) than standard coatings. This important point will be discussed in the next section.

2.1.3. FRAUNHOFER LINE SURVEILLANCE - SINGLE FOCAL PLANE

To first order, the solar spectrum can be approximated by a 5900°K black body. This spectrum does have a number of very narrow ($\sim 1 - 10\text{\AA}$) spectral holes, however, caused by solar atmospheric absorption. These regions of attenuated solar intensity are referred to as the Fraunhofer lines and the author of this report has investigated exploiting this effect in target detection. This work was done as part of a two year JBST contract from Lawrence Livermore National Laboratory.

Some of the most well known Fraunhofer lines are the H- α line (6562.8 \AA), the Mg II lines (2795.4 \AA and 2802.3 \AA), and the Ca II lines (8498.1 \AA , 8542.1 \AA , and 8662.2 \AA). At the center of the above six lines, the solar intensity is attenuated by 84%, 90%, 90%, 70%, 81%, and 79%, respectively. "Single focal plane Fraunhofer line surveillance" is realized by covering a focal plane with a narrow band filter centered at one of the Fraunhofer lines. Any background clutter produced by reflected sunlight will thus be attenuated by 70 to 90%. The self radiating targets, such as missile plumes, however, are not effected, since their radiation does not originate from the sun. This filter will thus increase the SCR by a factor of 5 to 10.⁽¹⁾ Larger apertures are required for this surveillance scheme to keep the SNR at an acceptable level, since this approach improves the SCR at the expense of the SNR.

It is doubtful that the target detection capability (SCR and SNR) of a "Fraunhofer detector" could ever equal that of the conventional IR approach described in section 2.1.1. There

⁽¹⁾SCR increases of two to three orders of magnitude can be realized using "dual focal plane Fraunhofer line surveillance," to be described in section 2.1.4.

is, however, one very important advantage of the Fraunhofer concept over the IR approach - the detection can be done with visible wavelength detectors. The potential advantages of using visible wavelength Si detectors is so great that LLNL has spent a considerable amount of time investigating a number of these novel schemes for their Brilliant Pebbles program. The important advantages of visible wavelength detectors over IR detectors include:

- Lower cost (economics of scale due to mass production of visible wavelength CCDs for commercial use)
- Lighter weight
- Well developed technology for large focal plane arrays with high quantum efficiency
- Cryogenic cooling is not required

Unfortunately, the Earth background is much brighter in the visible and typical targets are much dimmer in the visible, than in the IR. Thus novel techniques such as "Fraunhofer detection" will be needed if this economical target detection approach is to be realized.

A key difficulty which JBS Technology, Inc. encountered in designing the "Fraunhofer detector," as well as some other classified approaches to visible wavelength target detection, was the incompatibility of narrow line filters and wide fields-of-view. For laser radar filters, narrow receiver FOVs are often acceptable since the outgoing laser beam must be quite narrow in its angular extent to ensure an adequate return signal. For passive warning and detection systems, however, wide FOVs are often needed.

Figure 2.1 illustrates the spectral transmittance of a narrow line interference filter, designed for transmission at 0.500 μm when illuminated at normal incidence. As the filter illumination angle is increased, the peak transmittance shifts to shorter wavelengths and broadens.

This characteristic of interference filters would severely restrict a system's FOV, which used a narrow band filter. Figure 2.2 is a plot of a filter's FOV as a function of its percentage half width. The half width of the H- α Fraunhofer line is about 2Å or about 0.03% of the wavelength (2/6562). Figure 2.2 indicates that the full cone FOV of this system would only be about 4° for a filter with an effective index of 3.

One method for increasing the surveillance camera's FOV would be to put the narrow band filter on a curved surface as illustrated in figure 2.3. This approach was investigated by the author of this report several years ago, but we were unable to find a single vendor able to deposit a multi-layer ("conventional") coating, to the required layer thickness control, over a large curved substrate. This coating could easily be made, however, using holographic methods. A photosensitive material, such as dichromated gelatin (DCG), would be deposited on the curved glass substrate. A converging and diverging beam could then be interfered in the DCG to produce the desired interference filter.

2.1.4 FRAUNHOFER LINE SURVEILLANCE - DUAL FOCAL PLANE

In section 2.1.3 we saw that the background clutter could be reduced by 70% to 90% by the use of narrow band filters centered at Fraunhofer lines. It has been shown by JBS Technologies, Inc. that the use of a pair of focal planes covered by two different narrow band filters, one centered at a Fraunhofer line and the other filter shifted several angstroms off of the Fraunhofer line, can increase the SCR by at least three orders of magnitude! A similar improvement in SCR could be realized by using atmospheric absorption lines in the near IR, such as the water absorption line at 0.92 μm (visible wavelength Si CCDs can be used up to $\sim 1 \mu\text{m}$).

Figure 2.4 is a schematic diagram of the hardware needed for this concept. The signals from the two co-registered focal planes, which measure very closely spaced spectral bands, can be combined in an optimum manner which nearly cancels the background clutter completely. Some details involved in this signal processing are discussed in Appendix 2A. Appendix 2A also

presents an example of the power of this scheme using real Earth scene data, as previously prepared by JBST under a LLNL contract.

It is commonly believed that boosters cannot be detected at visible wavelengths from space with a bright Earth background. Although, for reasonably sized camera apertures, the booster plume radiant intensity is high enough to generate an acceptable SNR,⁽¹⁾ the background clutter is too large to allow detection by conventional means--the SCR is too low.

Figure 2.5 is a plot of the detection range as a function of camera lens diameter for a third stage booster,⁽²⁾ as seen at 0.656 μm (the Fraunhofer H- α line). We assume that both a SNR and SCR of 5 are needed for detection. The plot indicates that if no filters are used, the detection range is only 80 km, so the booster could not be detected at cloud break, as desired, from a surveillance satellite at 400 km. Note that the detection range of 80 km is independent of the camera lens diameter, since it is SCR limited and not SNR limited. Larger lens diameters allow more target photons to be collected, but more background photons are also collected so the detection range cannot be increased. The use of a narrow band filter centered at the H- α Fraunhofer line and a single focal plane can increase the detection range to about 120 km, since the background intensity can be preferentially reduced with this filter. This detection range is still too limited to be of interest.

If a dual focal plane with complementary narrow band holographic filters is used, however, the detection range can be extended to several hundred kilometers. A 10 cm aperture provides a large enough signal to allow detection at 550 km. Since nearly all the background clutter can be suppressed with this scheme, the camera's performance is limited by SNR and not

⁽¹⁾That is, readout noise, detector noise, shot noise, etc. are all low enough relative to the target signal.

⁽²⁾The booster type will not be given in order to keep this report unclassified.

the SCR. This is an important conclusion since visible wavelength detection of boosters offers some advantages over IR detection, as outlined in section 2.1.3.

2.1.5. WIDE-BAND MATCHED FILTER FOR BOOSTER DETECTION

Most of the SDI related filter designs discussed thus far have been narrow band filters. For the detection of dim targets against a fairly uniform background, it may be desirable to use a wider band filter so that more target photons can be transmitted to the focal plane. A "matched filter" has a spectral profile which blocks transmission of radiation to the focal plane at wavelengths where the background is bright and the target is dim. It has a high optical throughput at wavelengths where the target is brighter and the background is dim. If the spectral profile of the background and target are known a priori, then a filter with the ideal spectral profile can be designed. As a final example of a military application for holographic filters, we will consider the design of such a broad band filter for the detection of a solid fueled missile against an Earth background.

A solid fueled missile plume can be modeled, to first order, as a 2350°K black body. The Earth background, in the visible, will be modeled as a 5900°K black body (reflected solar spectrum) which has been modified by the spectral transmission of the Earth's atmosphere.

Figure 2.6 is a normalized plot of the black body curves for a 5900°K radiator, whose spectral peak is at 0.5 μm , and a 2350°K radiator, with a peak at $\sim 1.2 \mu\text{m}$. Figure 2.7 is a plot of the Earth background radiance, found by taking the product of the spectral profile of the 5900°K black body and the atmospheric transmission (double pass), as calculated using the Lowtran 7 atmospheric model. Two different curves are plotted in figure 2.7 - one for the Lowtran Mid-Latitude Summer atmospheric model and one for the Sub-Arctic Winter atmospheric model.

If the Earth background profile, as shown in figure 2.7, is combined with the 2350°K plume profile, as plotted in figure 2.6, an optimum filter spectral profile can be calculated. This

matched filter is the ideal filter for detecting the target. The reflectivity profile of the desired holographic filter is shown in figure 2.8. We have designed the filter to operate in a reflectivity mode, so the detector receives radiation reflected by the hologram (rather than transmitted). Two different reflectivity profiles are indicated in figure 2.8, corresponding to the two different atmospheric models. The figure shows that it may be desirable to use a filter wheel containing several holographic filters. The best filter, depending on atmospheric conditions, could then be rotated in place in front of the detector.

A more attractive application of a holographic matched filter for plume detection can be realized when the target has some detailed spectral structure. Examples of this, in the UV regime, are illustrated in figure 2.9. A holographic matched filter could be fabricated which would pass a large portion of the spectrum where the missile plume is intense and block the wavelengths between the intensity spikes shown in figure 2.9.

2.2 COMMERCIAL APPLICATIONS FOR MATCHED HOLOGRAPHIC FILTERS

Most of the Phase II efforts will be directed toward developing HCs which have a direct military application. This technology can also be used in commercial applications, such as improved identification of specific vegetation or minerals from satellite cameras. In fact airborne imaging spectrometers have already been used to identify various types of vegetation (and even the health of the vegetation) and numerous minerals--all from the "spectral fingerprint" of the specific material being searched for. This technology could eventually be used for worldwide surveys to predict crop yields, for monitoring illegally grown crops (coca, marijuana, the opium poppy), and to conduct rapid geological surveys for mining and soil type delineation. It could be used to detect vegetation stress, to monitor tropical forest changes, to perform forest structure analysis and forest biomass estimates, and even to measure plankton type and concentration (to predict the location of fish). This could all be done from orbiting satellites.

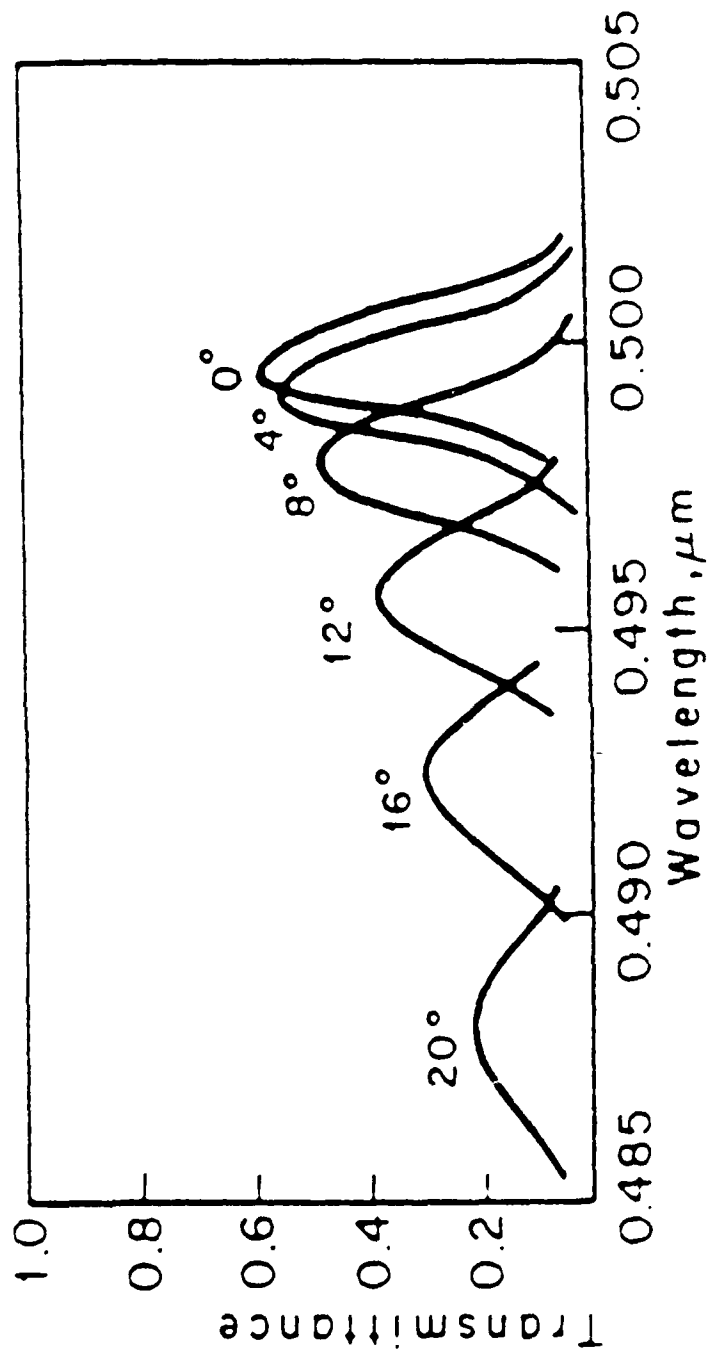
The AIS (airborne imaging spectrometers) hardware being developed by JPL for these

measurements uses a dispersing grating to direct various wavelength bands to the N rows of a 2-D focal plane array. Each row of the CCD thus images the same 1-D strip of the scene being viewed, to obtain a spectrally resolved 1-D view of the target area. The 2-D spatial image is generated by "push broom imaging" of the Earth scene passing below the camera. Since most materials have a characteristic spectral fingerprint, this technology represents a major advance in remote sensing. The concept is illustrated in figure 2.10. Figure 2.11 and 2.12 illustrate this spectral fingerprint for several different plants and minerals, as measured with a spectrometer.

In the imaging spectrometer (IS) concept, a separate image is generated at numerous wavelengths (over 200 separate wavelengths in the advanced JPL devices) and this wealth of data is then processed to identify material in the scene. Commercial applications of holographic matched filter technology, which we hope to develop in Phase III of this program, will complement the IS systems. Rather than generating hundreds of images of the same scene, as viewed at different wavelengths, only one, or at most a handful, of images are taken. Rather than using very narrow band filters or, equivalently, a dispersive grating, filters with complex spectral properties could be used in the holographic matched filter concept. A holographic filter would be designed to highlight a specific material in the scene. The approach is not as powerful as IS, but is much simpler, requires far less computer power, and may be more useful for rapid surveys of large areas where it is desirable to use the entire 2-D focal plane for imaging, and not just one row.

A filter wheel placed in front of the CCD could contain special holographic matched filters designed to highlight areas of the scene with a desired spectral characteristic. For example, the DEA may wish to mount a coca, marijuana, and opium holographic filter on their camera, while the Agriculture Department might want space reserved for a corn or soybean filter! These holographic filters have the property that they allow radiation to reach the focal plane at wavelengths for which the material of interest radiates strongest. The filters block the transmission at wavelengths for which the material does not radiate strongly. As was the case for the military targets discussed in section 2.1, much higher SCR enhancement will be realized if a dual focal plane configuration is used with complementary holographic matched filters.

We believe that many of the filters described in the last two sections, especially ones with complex spectral properties, can best be fabricated holographically. Now that the motivation for the development of these complex filters has been presented, we will describe some approaches for fabricating them and analyze their performance.



(a)

Figure 2.1 Angular properties of all-dielectric interference filters. Measured variation with angle of incidence of the spectral transmittance of a typical commercial interference filter.

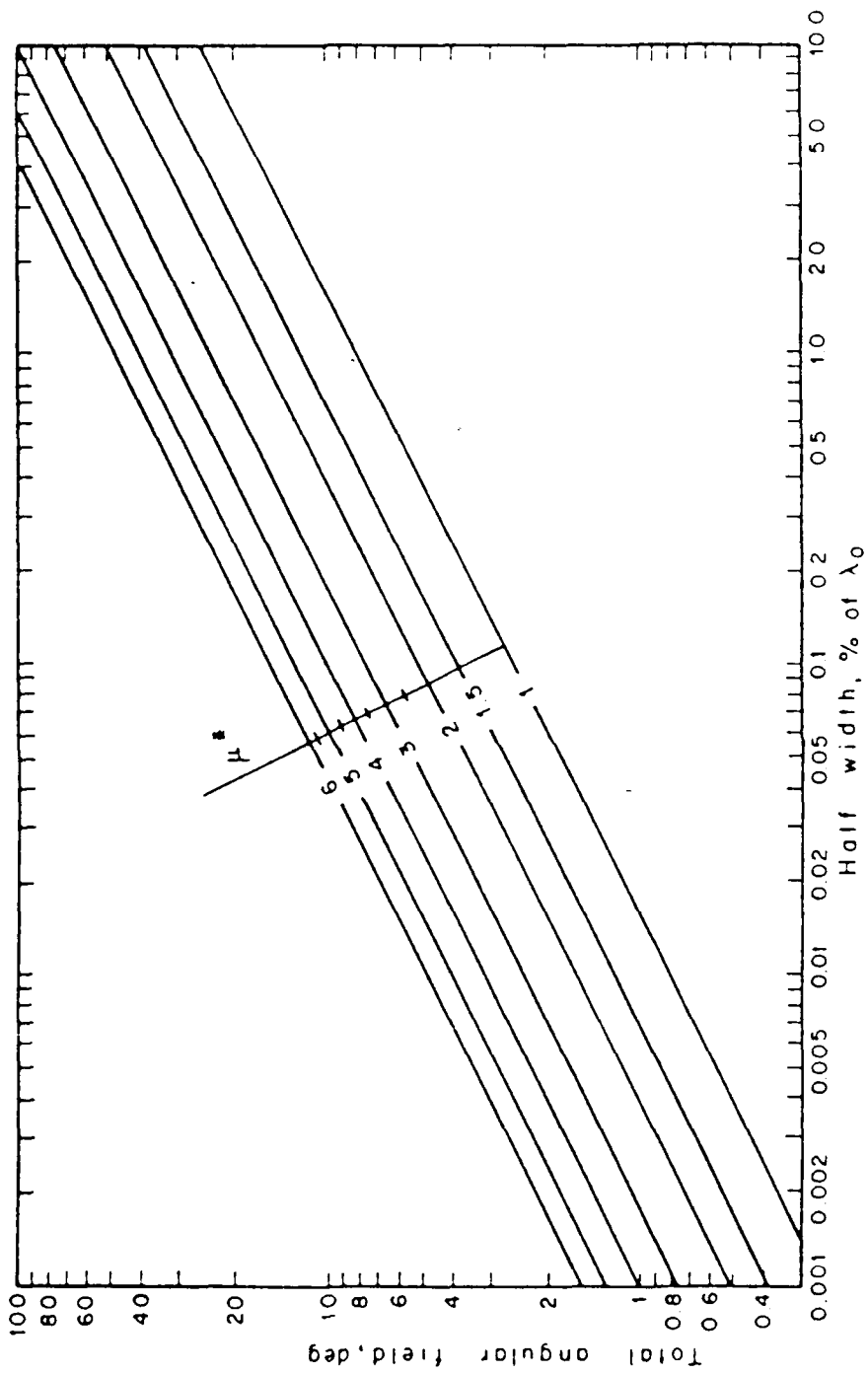


Figure 2.2 Angular field of FP filters as a function of the half width for different effective indexes μ .

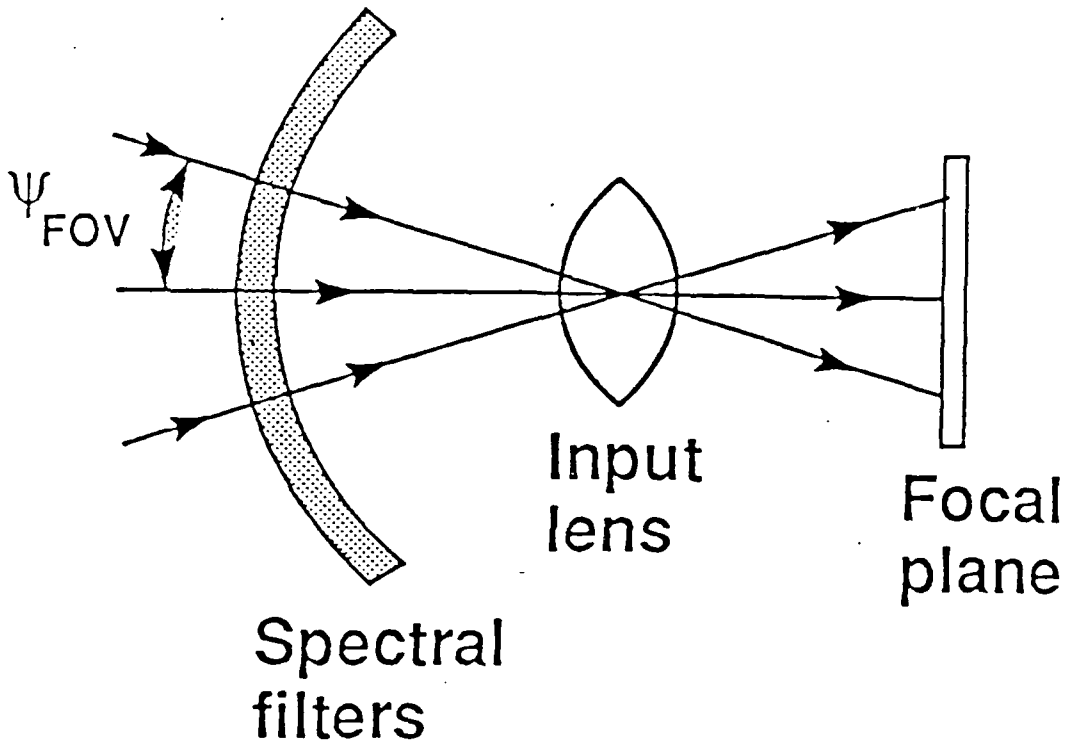


Figure 2.3 Fabricating a narrow band filter over a curved surface can be used to increase FOV of a surveillance camera.

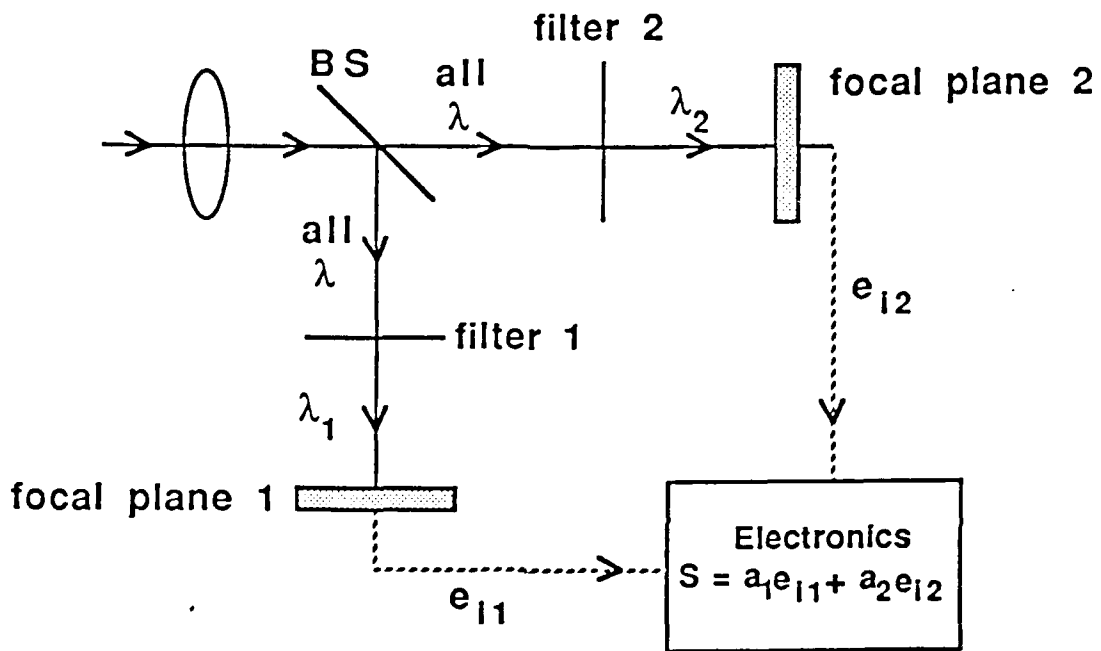


Figure 2.4 Schematic diagram of two focal plane spectral signal processing concept

THE COMBINATION OF AN H-ALPHA FRAUNHOFER FILTER AND SIGNAL PROCESSING
 ALLOWS THE DETECTION OF A THIRD STAGE BOOSTER AT VISIBLE WAVELENGTHS
 WHICH WOULD OTHERWISE REMAIN HIDDEN BY EARTH BACKGROUND CLUTTER

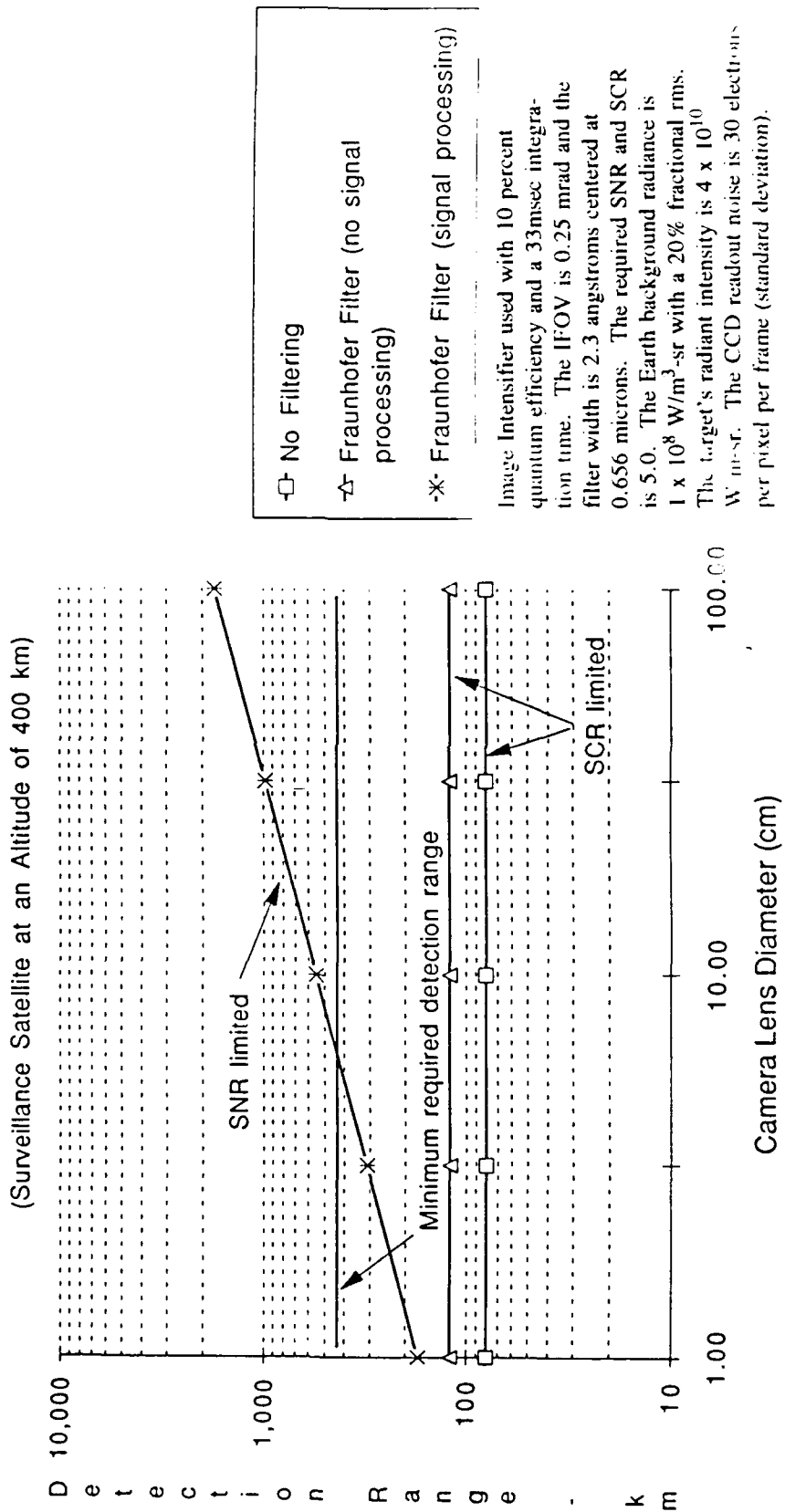


Figure 2.5

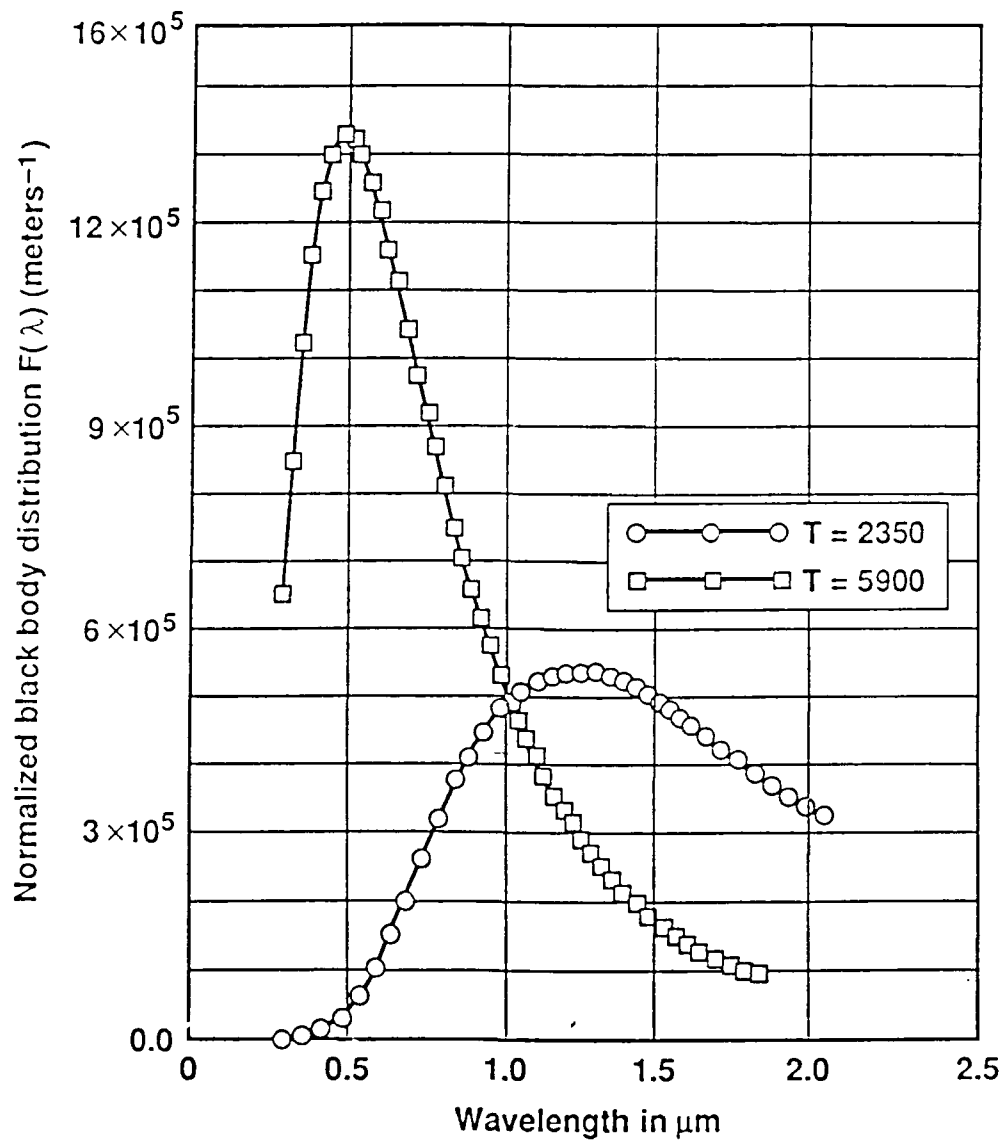


Figure 2.6 Plot of the Normalized Black Body Curves for 2350°K and 5900°K Radiators

EARTH BACKGROUND RADIANCE (WATTS/(M²-MICRON-SR)) AS A
 FUNCTION OF WAVELENGTH AND LOWTRAN 7 ATMOSPHERIC MODEL

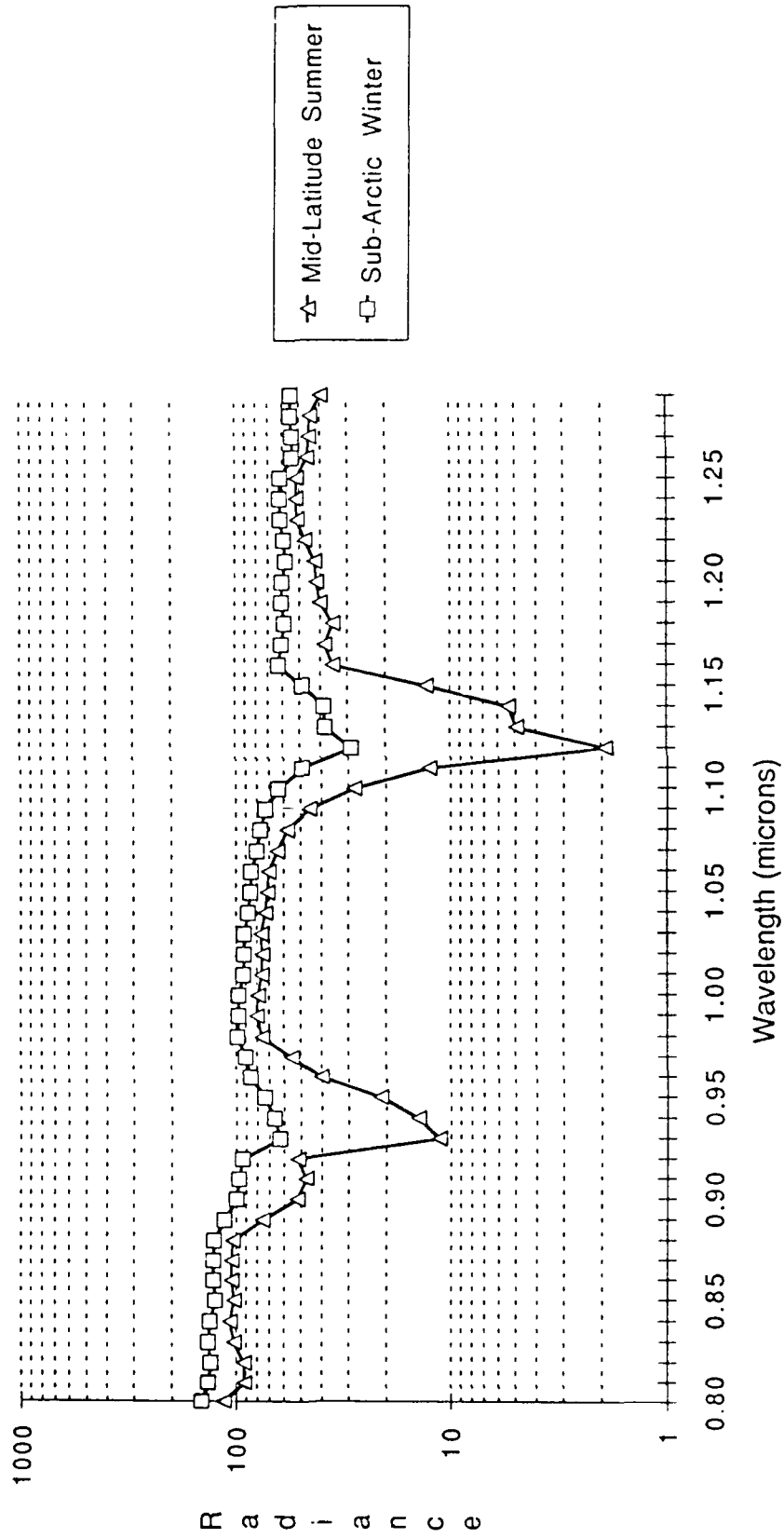


Figure 2.7

OPTIMUM MATCHED FILTER REFLECTIVITY AS A FUNCTION OF WAVELENGTH FOR THE DETECTION OF A SOLID FUELED BOOSTER AGAINST AN EARTH BACKGROUND USING A SILICON DETECTOR

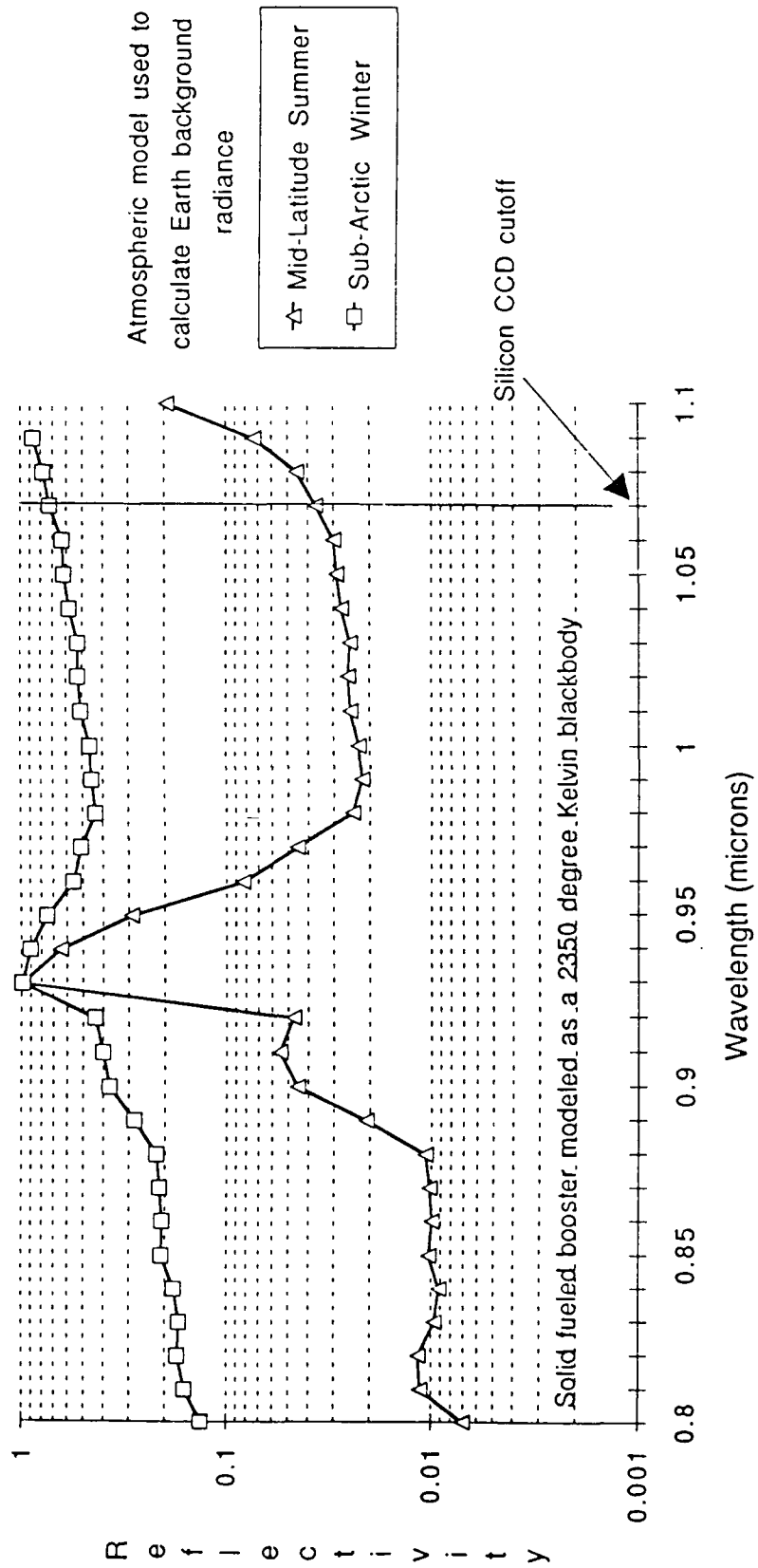
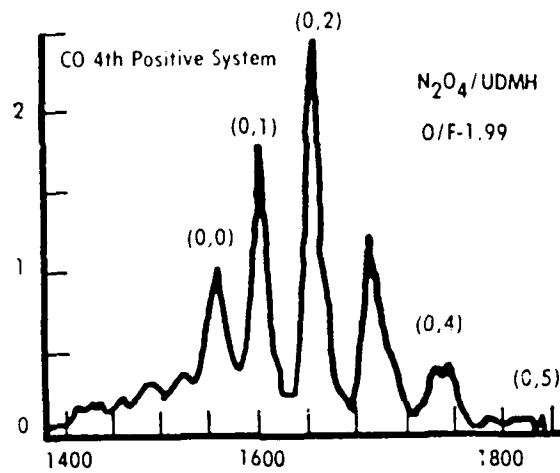
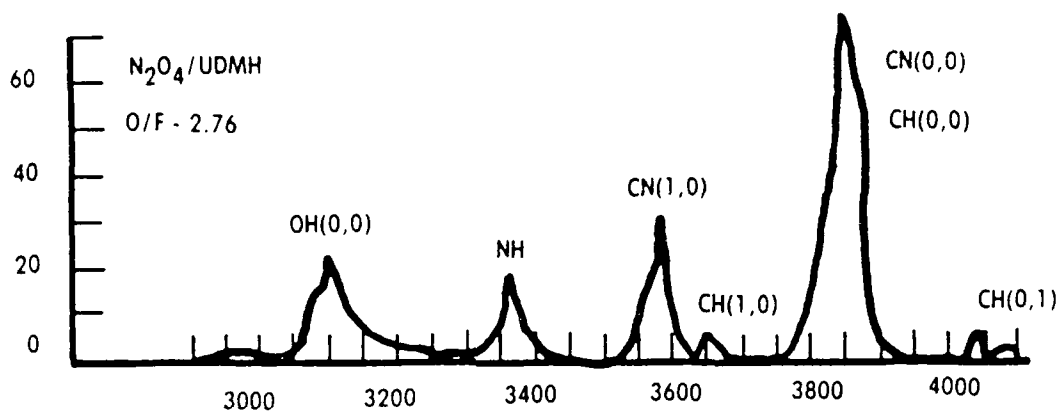


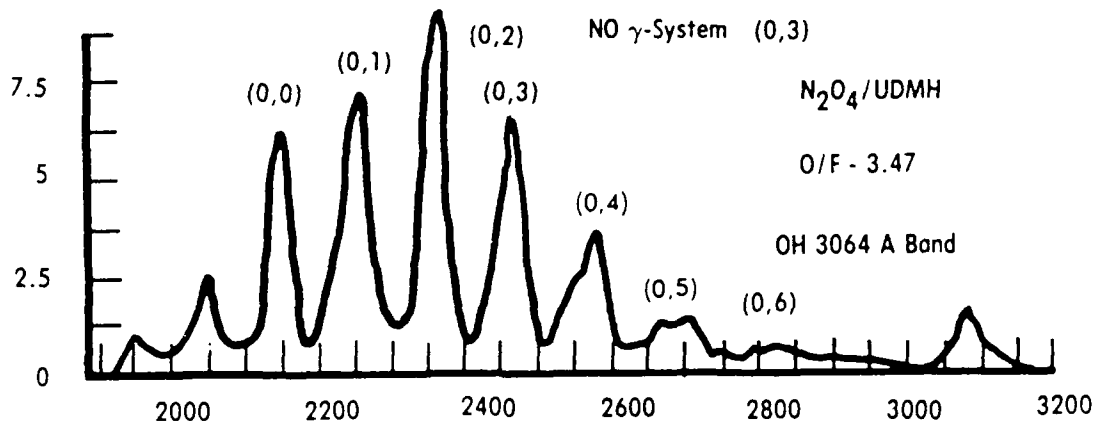
Figure 2.8



Wavelength range - 1400 to 1900 Å°



Wavelength Å°



Wavelengths range - 1900 to 3300 Å°

Figure 2.9 Examples of UV Spectra From Storable Propellant Rocket Plumes.

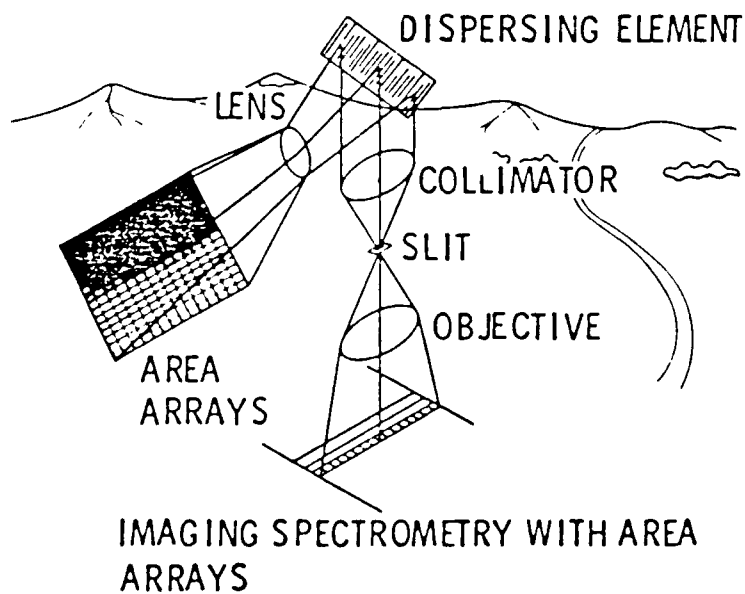
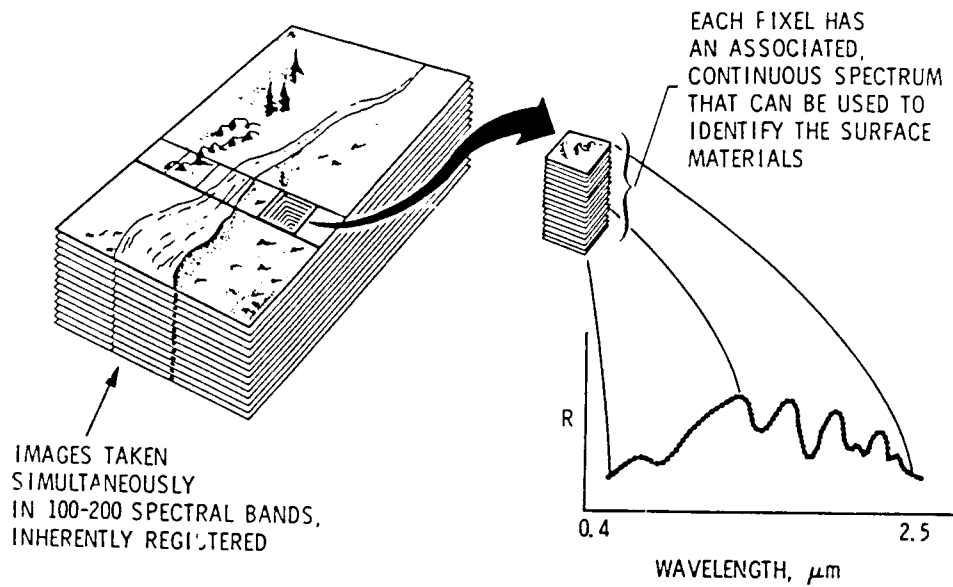
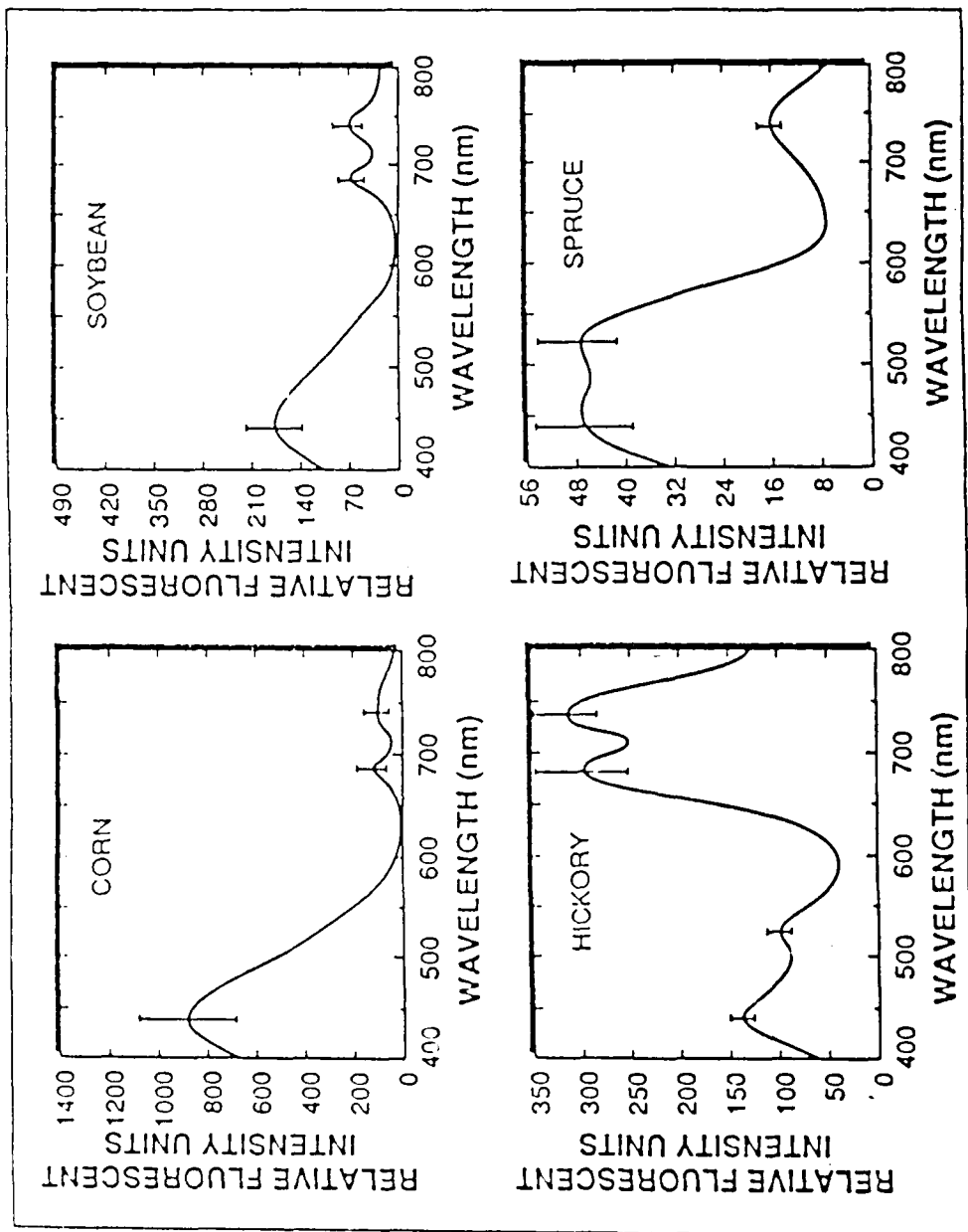
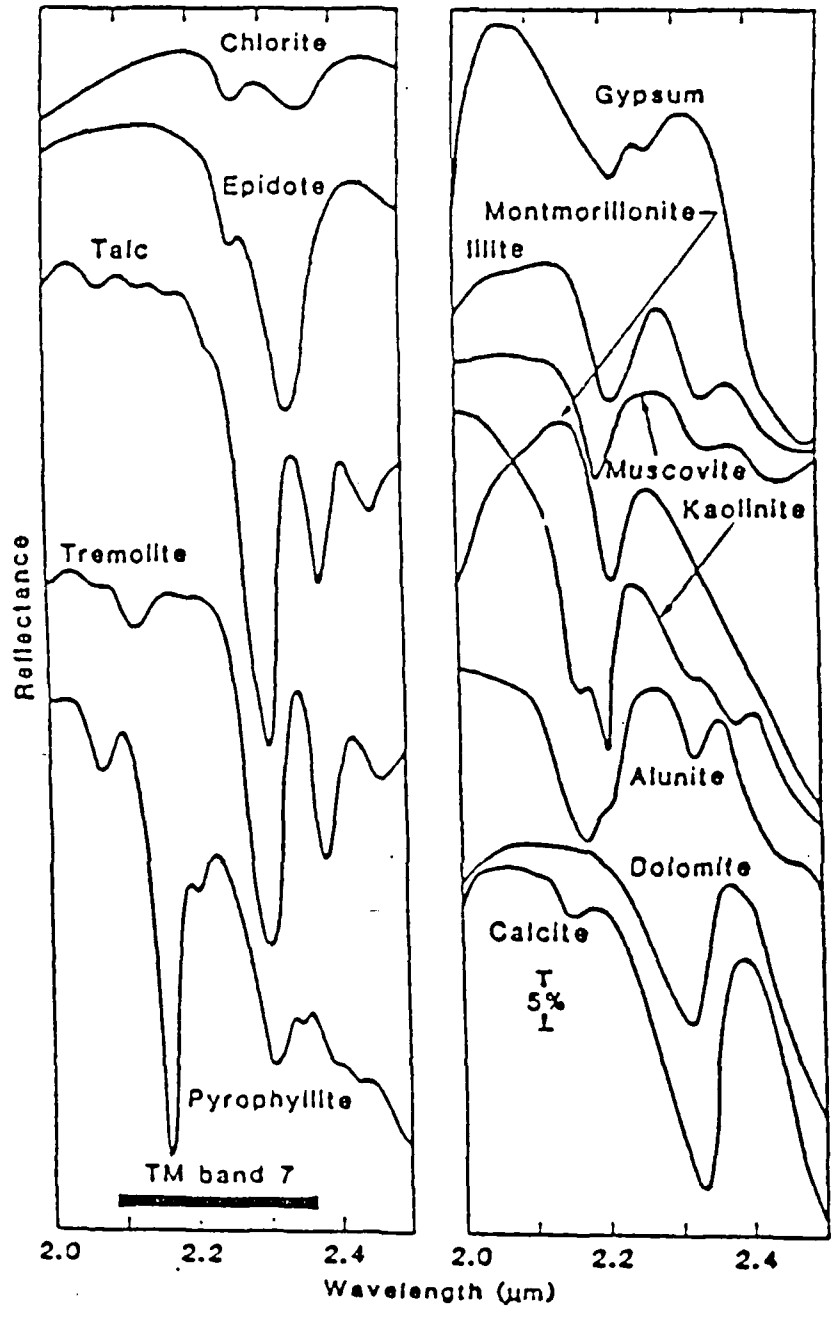


Figure 2.10. JPL's AIS Concept.



(1) J. W. Chappelle, et al., "Lasers may help in remote assessment of vegetation," Laser Focus World, 123 (June 1989).

Figure 2.11 Fluorescence Spectra of Plants of Four Major Plant Types Provide Information Regarding Type of Plant Stress and Identification of Specific Plant Types.⁽¹⁾ (Active IS)



⁽¹⁾Alexa: F.H. Goetz, et al, "Imaging Spectrometry for Earth Remote Sensing," *Science* 228, 1147 (1985)

Figure 2.12 Examples of Short IR Spectra of Twelve Minerals⁽¹⁾ (Passive IS)

APPENDIX 2A. MATCHED FILTER SIGNAL PROCESSING

2A.1 THEORY

This Appendix will summarize some of the mathematical details which support our contentions in section 2.1.4 that SCR enhancements of several orders of magnitude are achievable if complementary optical filters cover co-registered focal plane arrays. This spectral sampling and signal processing scheme does require that the spectral bands be judiciously chosen. Examples include the Fraunhofer lines (section 2.1.4) or Earth atmospheric absorption lines.

We will define the signal received in pixel number i , focal plane number j , as e_{ij} . The signal e_{ij} depends not only on the scene being observed, but also on the optical transmission property of the filter covering focal plane j . The energy measured, e_{ij} , consists of a possible target signal t_{ij} and a background signal b_{ij} :

$$e_{ij} = b_{ij} + t_{ij} \quad 1.$$

We wish to form a linear sum of the signals from pixel number i from each focal plane and will define this processed signal as s_i :

$$s_i = s_i^{(t)} + s_i^{(b)} \quad 2.$$

where:

$$s_i^{(t)} = \sum_{j=1}^2 a_j t_{ij} \quad 3.$$

$$s_i^{(b)} = \sum_{j=1}^2 a_j b_{ij} \quad 4.$$

The sums in equations 3 and 4 are over the two focal planes in our system. The coefficients a_j to be used in the signal processor are chosen so that the variance of the background signal over the field of pixels is as small as possible, while at the same time, the processed target signal $s_i^{(t)}$ is as large as possible. This is a classical matched filter problem, and the details involved in solving the problem will not be presented here. They were presented by Dr. Shellan in reference 1. The result is given by:

$$\underline{a} = \frac{\underline{\underline{B}}^{-1} \underline{t}}{\underline{t}^T \underline{\underline{B}}^{-1} \underline{t}} \quad 5.$$

In equation 5, the filter coefficients a_j are expressed by the column vector \underline{a} whose components are the desired coefficients a_j . The column vector \underline{t} represents the total target signal measured in each of the two focal planes. The superscripts "T" and "-1" denote transpose and matrix inverse, respectively. The matrix $\underline{\underline{B}}$ is found from background spectral correlation properties, and the j, k component of this matrix, B_{jk} , is related to the b_{mn} coefficients by:

$$B_{jk} = \frac{1}{p} \sum_{i=1}^p b_{ij} b_{ik} - \left(\frac{1}{p} \sum_{i=1}^p b_{ij} \right) \left(\frac{1}{p} \sum_{i=1}^p b_{ik} \right) \quad 6.$$

The integer p in the summation in equation 6 represents the number of pixels in our field

of interest. The output target signal from our signal processor $\left(\sum_i s_i^{(t)} \right)$, divided by the rms background signal, is defined as the signal-to-clutter ratio of the signal processor. It can be shown⁽¹⁾ to be given by:

$$\text{SCR} = (\underline{t}^T \underline{\underline{B}}^{-1} \underline{t})^{1/2} \quad 7.$$

Now that we have outlined some of the mathematics involved in this problem, we will explain in more physical terms how these results will be used to design a system best able to detect targets. The parameters that determine the signal-to-clutter ratio (SCR in equation 7) are the total target energy measured by each focal plane and the Earth background spectral statistics as given by the matrix elements B_{jk} .

The matrix elements B_{jk} simply represent various spectral/spatial correlation properties of the background scene. Analysis indicates that for the novel sampling/signal processing scheme proposed, the output SCR is proportional to $\alpha t / \Delta \lambda$, where the variables α , t , and $\Delta \lambda$ represent the atmospheric absorption, target signal, and separation of the two sampled wavelengths, respectively. Thus, we expect that the SCR can be driven to very high levels by exploiting narrow atmospheric absorption lines which in turn allow the use of closely spaced sampling, $\Delta \lambda$. Fraunhofer lines may allow even smaller $\Delta \lambda$ values to be used.

2A.2 CONCEPT DEMONSTRATION AND NUMERICAL ANALYSIS

Figures 2A.1a and 2A.1b show a pair of coregistered and radiance-calibrated images

⁽¹⁾The variable α actually represents the differences in the atmospheric absorption between the target and more distant background. If the sampling is done with a Fraunhofer line, then α represents the strength of the Fraunhofer line dip.

collected over the Australian desert by the TIMS sensor in two adjacent LWIR wavebands separated by $\Delta\lambda = 400$ nm (center-to-center). The measured spectral covariance matrix for these scenes (denoted as $\underline{\underline{B}}$ in section 2.A.1) is

$$\underline{\underline{B}} = \begin{bmatrix} B_{11} & B_{12} \\ B_{12} & B_{22} \end{bmatrix} = \begin{bmatrix} 47.16 & 49.50 \\ 49.50 & 52.38 \end{bmatrix} \quad 8.$$

This reveals that the clutter has nearly the same average power in each band and an extremely high correlation coefficient of $\rho_{12} = B_{12}/\sqrt{B_{11}B_{22}} = 0.996$ between bands. If a target response were present with roughly equal magnitude t in bands 1 and 2, very little could be gained by combining the bands on a pixel-by-pixel basis. For example, with $t = 7$, the SCR in either band is on the order of unity, the signal vector is $\underline{t}^T = [7 \ 7]$, and from equation 7, the largest SCR available from combining both bands is

$$\text{SCR} = (\underline{t}^T \underline{\underline{B}}^{-1} \underline{t})^{1/2} \approx 0.96 \quad 9.$$

which is far too low for reliable detection

However, if the clutter response in one of the two bands (say, Band 1 in figure 2A.1a) is synthetically attenuated to simulate the effect of selective background absorption, the situation changes significantly. Figures 2A.2a and 2A.2b show grey-scale plots for the central 64×64 portion of the two images in figure 2A.1. If the apparent pixel radiances in the Band 1 subimage of figure 2A.2a are scaled by the factor $\alpha = 0.5$ but those in Band 2 are left unchanged, then the measured spectral correlation matrix becomes

$$\underline{\underline{B}} = \begin{bmatrix} B_{11} & B_{12} \\ B_{12} & B_{22} \end{bmatrix} = \begin{bmatrix} 11.79 & 24.75 \\ 24.75 & 52.38 \end{bmatrix} \quad 10.$$

Repeating the SCR calculation using equation 10 with the same signal $\underline{t}^T = [7 \ 7]$, we now find that

$$\text{SNR} = (\underline{t}^T \underline{\underline{B}}^{-1} \underline{t})^{1/2} = 12$$

11.

To demonstrate that such a signal is now readily detectable, the unresolved additive target response shown in figure 2A.2c is synthetically injected into both the attenuated Band 1 subimage and the Band 2 subimage with a magnitude of 7 units. Figure 2A.2d shows the results of taking the optimum linear combination of the two resulting scenes, as defined by equation 5 (the output image is plotted on the same grey-scale as figures 2A.2a and 2A.2b to facilitate a direct comparison).

In analysis conducted by the principal investigator, expressions for the SCR gain of the proposed concept were developed as a function of α , $\Delta\lambda$, and a set of physical parameters which are related to the measured spectral correlation of the background in the two bands.⁽¹⁾ For example, using the data in the two TIMS images in figure 2A.1 to estimate the model parameters, the achievable SCR gain against this terrain background can be locally parameterized by α and $\Delta\lambda$ as shown in figure 2A.3. This family of curves clearly demonstrates the benefits of selective absorption and small wavelength differentials for a specific case. Note the relatively high SCR achievable even with absorption coefficients as small as 5% for small $\Delta\lambda$ values.

⁽¹⁾Jeffrey B. Shellan, "Clutter Suppression Through Differences in Target and Background Spectral Content," J.B.S. Technologies, Inc., report to Lawrence Livermore National Laboratory, Contract B056075 (October 12, 1988).

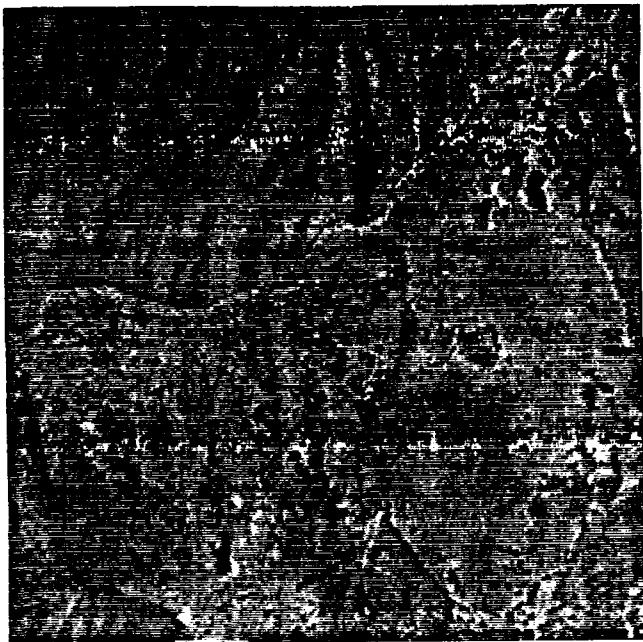


Figure 2A.1a TMS Band 1 LWIR Image of the Australian Desert (10 m ground resolution)

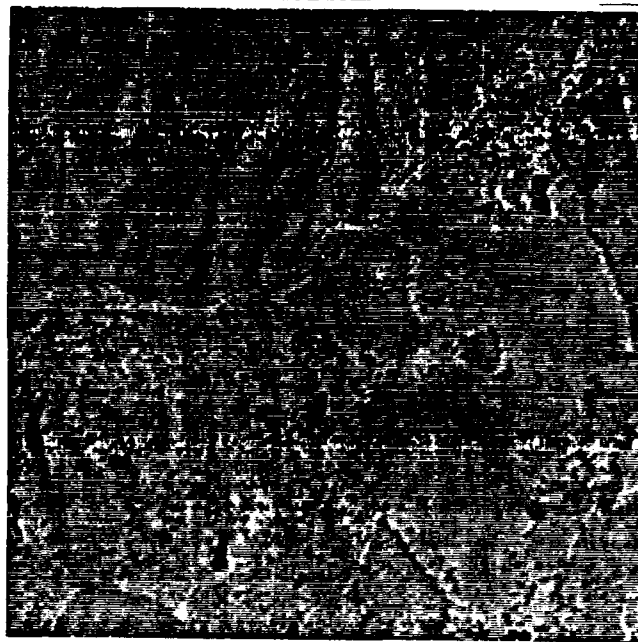


Figure 2A.1b TMS Band 2 LWIR Image of the Australian Desert (10 m ground resolution)

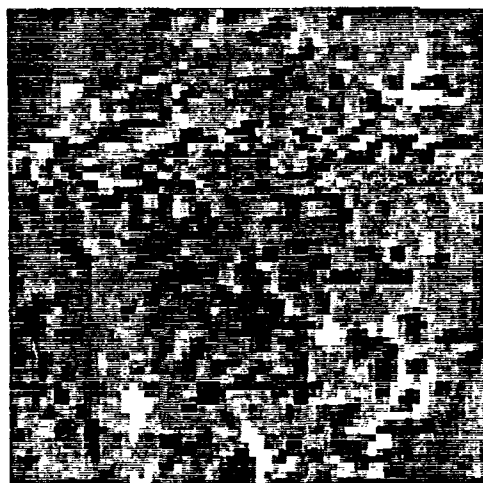


Figure 2A.2a TMS Band 1 subimage



Figure 2A.2b TMS Band 2 subimage

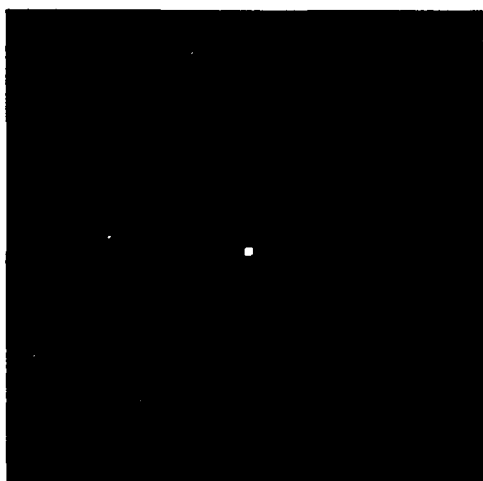


Figure 2A.2c Point target response injected into the Band 1 and Band 2 subimages

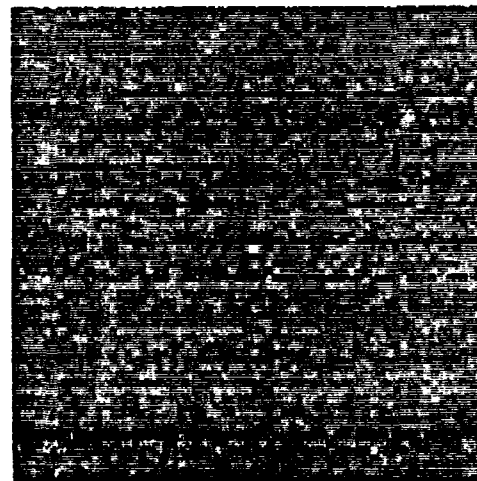


Figure 2A.2d Results of optimum linear processing of Bands 1 and 2 with injected target. (Band 1 background clutter attenuated by $\alpha = 0.5$ to simulate selective absorption.)

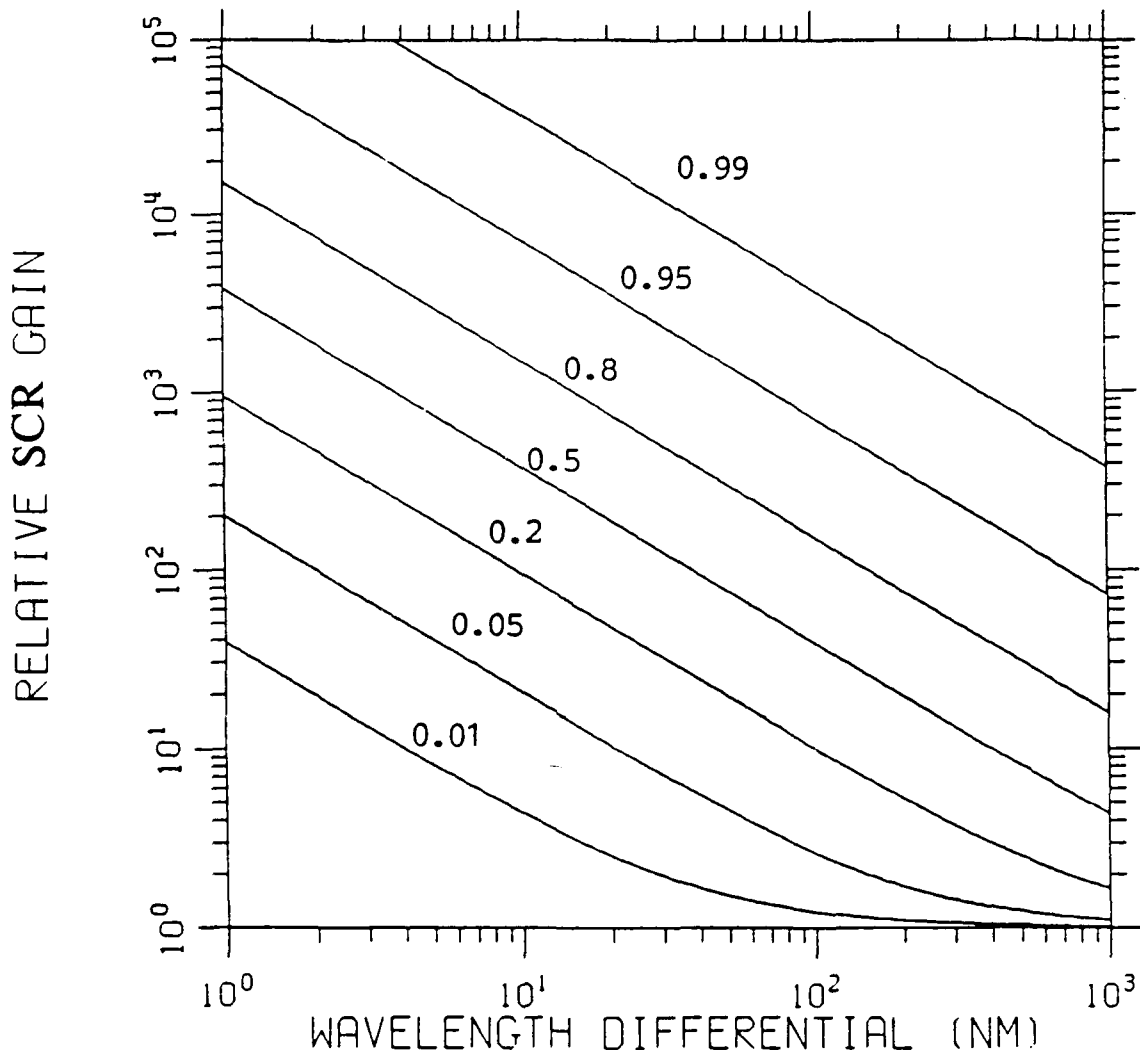


Figure 2A.3 SCR gain vs. wavelength differential ($\Delta\lambda$) for various absorption coefficients α . Gain is measured relative to SCR obtained by linear processing of two bands outside absorption region.

3. EXAMINATION OF APPROACHES FOR FABRICATING HOLOGRAPHIC MATCHED FILTERS

3.1 NARROW-BAND FILTERS

The simplest HC to fabricate is the narrow-band filter which reflects radiation over a narrow spectral band and transmits nearly all the radiation outside of this band. This kind of filter has been fabricated for years and is reviewed here simply as a means to introduce the complex filters to be developed in this program.

The HC is fabricated by interfering two counter propagating plane waves in a photo-sensitive material such as dichromated gelatin (DCG). This is usually accomplished by placing a reflector plate behind the hologram being recorded so that the incident wave is reflected, thus producing the desired standing wave pattern. This geometry is illustrated in figure 3.1. The intensity modulation will, in turn, produce an index of refraction modulation in the developed hologram. The period of the index modulation, Λ_g , is equal to $\lambda_r/(2n_o)$, for a hologram recorded with normally incident light (λ = wavelength of recording radiation in vacuum, n_o = average index of refraction of photosensitive layer). This index of refraction period is the period which will produce the greatest reflectivity when the hologram is subsequently re-illuminated with radiation at wavelength λ_r (normal incidence).

For hologram recording at oblique incident angles, as shown in figure 3.2, the fringe spacing, Λ_g , will be greater than for normal incident recordings. For a reflection hologram recorded at an incident angle ϕ_r , the period of the index modulation will be:

$$\Lambda_g = \frac{\lambda_r}{2(n_o^2 - \sin^2 \phi_r)^{1/2}} \quad 3.1$$

The above grating will only reflect strongly at wavelength λ_r , under subsequent re-

illumination, if the "playback" incident angle is also ϕ_r . For normal incidence operation, the grating period given in equation 3.1 will reflect most strongly when illuminated by radiation of wavelength λ_p given by:

$$\lambda_p = \frac{n_o \lambda_r}{(n_o^2 - \sin^2 \phi_r)^{1/2}} \quad 3.2$$

It is thus straightforward to record a hologram at wavelength λ_r which can strongly reflect at a longer wavelength, λ_p , when the hologram is later illuminated at normal incidence. If the DCG is sequentially exposed at a number of incident angles, $\phi_1, \phi_2, \dots \phi_n$, by radiation at a single wavelength, λ_r , then, after development, the resulting hologram will strongly reflect at a number of discrete wavelengths, $\lambda_1, \lambda_2, \dots \lambda_n$, determined from equation 3.2. This effect has been demonstrated by many groups and, in fact, is the basis for some filters designed to protect space surveillance sensors from blinding hostile laser radiation. It has also been used to fabricate laser goggles which can provide the user with eye protection from several common laboratory lasers. We will now show how this concept can be used to fabricate holographic filters with arbitrary complex reflectivity profiles, such as those needed for the "matched filters" described in section 2.

3.2 CONCEPT 1: CONTINUOUS EXPOSURE WITH PHASE CONTROL

3.2.1 DESCRIPTION OF CONCEPT 1 HOLOGRAM FABRICATION

In section 3.1 it was pointed out that if the holographic recording medium is sequentially exposed to recording beams at a number of different incident angles, the index of refraction modulation of the developed hologram will consist of a superposition of gratings, each with a different period. This structure will then reflect strongly at a number of different wavelengths. For normal incidence, the hologram will reflect strongly at wavelengths equal to $2n_o \Lambda_g^{(p)}$, where

$\Lambda_g^{(p)}$ is the period of the p^{th} grating within the recording medium.

The basic concept to be investigated in this program is whether a hologram with an arbitrary reflectivity profile can be fabricated by sequentially recording gratings with the desired period. To fabricate a hologram with a continuous reflectivity spectral profile, $R(\lambda)$, the hologram could be recorded by exposing the DCG (or other photosensitive material) to a continuum of incident angles, before the DCG is actually developed. The strength of the reflectivity desired at a specific wavelength would be controlled by modulating the intensity of the laser used to record the hologram, as the angle of incidence of the recording beam was changed. The geometry for such a system is illustrated in figure 3.3. The above approach for fabricating a hologram with any desired reflectivity profile will be referred to as "Concept 1."

In the following section we will analyze the expected performance of the novel holographic filter fabricated by the procedure described above. Obviously the key issue to investigate is how the continuum of "off resonance" Fourier grating components effects the reflectivity of the beam. Although it has been experimentally demonstrated that recording a "reasonable" number of different grating periods in one hologram can produce a structure that will then reflect at each of the corresponding radiation wavelengths, this has not been demonstrated in the limit of an infinite number of different grating periods--that is, for the case of a continuum of grating periods.

3.2.2. CONCEPT 1 ANALYSIS

3.2.2.1 RELATIONSHIP BETWEEN REFLECTANCE PROFILE, $r(k)$, AND INDEX PROFILE, $n(z)$

This problem will be analyzed using the coupled mode theory, as described in the references of Yariv,⁽¹⁾ Yeh,⁽²⁾ Shellan,⁽³⁾ and Kogelnik.⁽⁴⁾ We will briefly summarize this theory. The propagation of radiation is described by the wave equation, which for an electric field with time dependence $\exp(-i\omega t)$ reduces to:

$$\frac{d^2 E}{dz^2} + k^2 n^2 E = 0 \quad 3.1$$

where:

- E(z) ▪ electric field in the holographic coating
- z ▪ coordinate of a point within the coating, as measured normal to the coating/air interface (z = 0 is the coordinate at the coating surface)
- k ▪ radiation wave number in vacuum = ω/c , where ω is the radian frequency of the radiation and c is the speed of light
- n = n(z) = index of refraction of the HC

If the hologram were recorded with light at a single angle of incidence, then the index of refraction could be represented by a sinusoidal modulation of the form:

$$n^2(z) = n_o^2 + 2 n_o n_1 \cos \left(\frac{2\pi}{\Lambda_g} z + \gamma \right) \quad 3.2$$

(for $n_1 \ll n_o$)

where:

- n_o = average index
- n_1 = amplitude of index modulation
- Λ_g = grating period
- γ = phase factor for grating

In our case, however, the hologram will be created by sequentially exposing the DCG to radiation from a continuum of angles, as illustrated by the hardware in figure 3.3. In this case the index of refraction of the DCG after development must be represented by a continuum of grating periods:

$$\begin{aligned}
 n^2(z) = n_0^2 + 2n_0 \int_{K_g^{(min)}}^{K_g^{(max)}} \hat{n}_+(K_g) \exp(i K_g z) dK_g \\
 + 2n_0 \int_{K_g^{(min)}}^{K_g^{(max)}} \hat{n}_-(K_g) \exp(-i K_g z) dK_g
 \end{aligned}
 \tag{3.4}$$

where:

$$K_g = \frac{2\pi}{\Lambda_g} = \text{grating vector}$$

$K_g^{(min)}$ and $K_g^{(max)}$ are the minimum and maximum values of the grating vector which make up the complex hologram profile.

\hat{n}_+ and \hat{n}_- are the Fourier coefficients which describe the hologram profile.

The third expression needed to derive the coupled mode equations is the equation for the form of the electric field. The field $E(z)$ will be written as:

$$E(z) = F(z) \exp(i n_0 k z) + B(z) \exp(-i n_0 k z) \tag{3.5}$$

In equation 3.5, $F(z)$ represents the amplitude of the incident wave as it travels within the hologram and $B(z)$ represents the amplitude of the reflected wave within the hologram. In coupled mode analysis, we use the fact that B and F are relatively slowly varying functions of z , so that:

$$\frac{d^2F}{dz^2} \ll k^2 n_0^2 F \quad 3.6$$

$$\frac{d^2B}{dz^2} \ll k^2 n_0^2 B \quad 3.7$$

If we combine equations 3.1, 3.4, and 3.5 and ignore the second derivatives of B and F , we find:

$$\begin{aligned} & 2 i n_0 k \frac{dF}{dz} \exp(i n_0 k z) - 2 i n_0 k \frac{dB}{dz} \exp(-i n_0 k z) \\ & + 2 n_0 k^2 [F \exp(i n_0 k z) + B \exp(-i n_0 k z)] \cdot \\ & \cdot \int_{K_g^{(min)}}^{K_g^{(max)}} \hat{n}_-(K_g) \exp(i K_g z) dK_g \\ & + 2 n_0 k^2 [F \exp(i n_0 k z) + B \exp(-i n_0 k z)] \cdot \end{aligned} \quad 3.15$$

$$\cdot \int_{K_g^{(min)}}^{K_g^{(max)}} \hat{n}_-(K_g) \exp(-i K_g z) dK_g = 0$$

Since F and B vary relatively slowly with z and the terms $\exp(i n_o k z)$ and $\exp(-i n_o k z)$ vary rapidly with z, equation 3.15 can be broken up into two different equations. This is the key step in the derivation of the coupled mode equations and is discussed in detail in any one of the four references given above. The result is:

$$\frac{dF}{dz} - i k B \int_{K_g^{(min)}}^{K_g^{(max)}} \hat{n}_+(K_g) \exp [i (K_g - 2n_o k) z] dK_g = 0 \quad 3.16$$

$$\frac{dB}{dz} + i k F \int_{K_g^{(min)}}^{K_g^{(max)}} \hat{n}_-(K_g) \exp [-i (K_g - 2n_o k) z] dK_g = 0 \quad 3.17$$

Equations 3.16 and 3.17 cannot be solved analytically for the general case, but we can find an approximate analytic solution in the low reflectivity limit. This case is referred to as the undepleted incident wave approximation, since we replace F(z) with its value at $z = 0$ in equation 3.17. Using $F(z) = F(0) = 1$, equation 3.17 can be rewritten as:

$$\frac{dB}{dz} \sim -i k \int_{K_g^{(min)}}^{K_g^{(max)}} \hat{n}_-(K_g) \exp [-i (K_g - 2n_o k) z] dK_g \quad 3.18$$

If we integrate each side of equation 3.18 over z, from $z = 0$ to $z = L$ (L = holographic coating thickness), and use the boundary conditions:

$$B(L) = 0$$

$$B(0) = r = \text{coating reflectance},$$

we can relate the coating's reflectance profile $r(k)$ to the Fourier component \hat{n}_- . The result is:

$$r(k) \sim i k L \int_{K_g^{(min)}}^{K_g^{(max)}} \hat{n}_-(K_g) \exp [i(2n_0 k - K_g) L/2] \cdot \text{sinc} [(2n_0 k - K_g) L/2] dK_g \quad 3.19$$

$$\left(\text{sinc } u = \frac{\sin u}{u} \right)$$

For large values of L (thick holographic coatings), the sinc term in the integrand of equation 3.19 acts like a delta function. Thus if:

$$(2n_0 k - K_g^{(min)}) L/2 \gg 1 \quad 3.20$$

$$\text{and } (2n_0 k - K_g^{(max)}) L/2 \ll 1, \quad 3.21$$

equation 3.19 can be approximated as:

$$r(k) \sim i 2 k \hat{n}_-(2n_0 k) \int_{-\infty}^{\infty} \text{sinc } u e^{iu} du \quad 3.22$$

$$\Rightarrow \hat{n}_-(2n_0 k) \sim \frac{-i}{\pi k} r(k) \quad 3.23$$

Equation 3.23 shows that the Fourier component $\hat{n}_-(K_g)$ is proportional to the coating's reflectance evaluated at the wavenumber $k = K_g/(2n_0)$. If we combine equations 3.4 and 3.23, and use the fact that $n^2(z)$ is real, we can find what the coating's index of refraction profile must

be in terms of its reflectance spectrum. The result is:

$$n^2(z) \approx n_o^2 + \frac{4n_o^2}{\pi} \left[i \int_{k_{\min}}^{k_{\max}} \frac{1}{k} r(k) \exp(-i2n_o kz) dk + c.c. \right] \quad 3.24$$

where:

$$k_{\min} = K_g^{(\min)}/(2n_o)$$

$$k_{\max} = K_g^{(\max)}/(2n_o)$$

"c.c." represents complex conjugate

For relatively small index modulations, equation 3.24 can be rewritten as:

$$n(z) \approx n_o + \frac{2n_o}{\pi} \left[i \int_{k_{\min}}^{k_{\max}} \frac{1}{k} r(k) \exp(-i2n_o kz) dk + c.c. \right] \quad 3.25$$

3.2.2.2 CALCULATION OF HOLOGRAM EXPOSURE LEVELS

In this initial analysis we will assume that the index of refraction modulation of the developed hologram is proportional to the exposure of the DCG during the recording process. That is, non-linear terms, which can be especially important if the DCG is over exposed, will not be considered here. If δn represents the change in the index from its unexposed value, then

$$\delta n = c_o H \quad 3.26$$

where:

- H = exposure of DCG (Joules/cm²)
c₀ = proportionality constant between H and δn

If I₀ is the intensity of the exposure beam used to create the hologram, then the standing wave pattern formed in the hologram during exposure will have an intensity ranging from 0 to 4I₀ (This assumes that the two counterpropagating beams forming the standing wave pattern each have intensity I₀). If H represents the DCG exposure that would result from only one of the two counterpropagating beams, then the total peak-to-valley index modulation produced by the standing electric field is 4c₀H.

For fabrication "Concept 1," illustrated in figure 3.3 and described in section 3.2.1, the DCG is exposed through a range of angles by rotating the mirror indicated in figure 3.3. The rotating mirror will turn at a constant rate during the exposure and the laser output will be modulated so that the exposure level is a function of the angle of incidence of the laser. This will control the amplitude of the various grating periods, which in turn determines the reflectivity spectral profile of the hologram after development. We will now calculate what the intensity of the exposing laser beam should be as a function of incident angle, in terms of c₀ and the desired hologram reflectivity profile.

If H(θ)dθ represents the differential hologram exposure due to a single beam as it swings through the angular range θ to θ + dθ, then the modulation of the square of the index of refraction, Δn², can be expressed as:

$$\Delta n^2 = 4 n_0 c_0 \int H(\theta) \cos [K_g(\theta) z + \gamma(\theta)] d\theta \quad 3.27$$

where:

- n₀ = average DCG index of refraction
γ(θ) = a phase term which represents the relative phasing of the Fourier components which form the index of refraction profile

The integration in equation 3.27 is over the range of recording angles. The term $K_g(\theta)$ is equal to $2\pi/\Lambda_g(\theta)$, where $\Lambda_g(\theta)$ is the period of the grating formed by a recording beam incident at angle θ . If the recording wavelength is λ_r (in vacuum) and a superstrate of index n_s covers the DCG during the exposure, then K_g is given by:

$$K_g(\theta) = \frac{4\pi}{\lambda_r} [n_o^2 - n_s^2 \sin^2 \theta]^{1/2} \quad 3.28$$

If we compare equations 3.24 and 3.27, we can find an expression for $H(\theta)$ in terms of $r(k)$. The result is:

$$\begin{aligned} & 4 n_o c_o \int H(\theta) \cos [K_g(\theta)z + \gamma(\theta)] d\theta \\ & = \frac{4 n_o^2}{\pi} \left[i \int \frac{1}{k} r(k) \exp(-i 2 n_o k z) dk + c. c. \right] \end{aligned} \quad 3.29$$

If we express $\cos(K_g z + \gamma)$ as $\frac{1}{2} \{ \exp[i(K_g z + \gamma)] + c. c. \}$ and equate integrands on each side of equation 3.29, we find:

$$H(\theta) = \frac{2 n_o i}{\pi c_o} \exp(i\gamma) \frac{1}{k} r(k) \frac{dk}{d\theta} \quad 3.30$$

The HC reflectivity, $R(k)$, is related to the reflectance, $r(k)$, by:

$$r(k) = \sqrt{R(k)} \exp[-i\beta(k)] \quad 3.31$$

where β = reflectance phase shift

Since $H(\theta)$ must be real and positive, we must have:

$$i \exp [i(\gamma - \beta)] = -1 \quad 3.32$$

and thus:

$$H(\theta) = \frac{-2 n_o}{\pi c_o k} \sqrt{R(k)} \frac{dk}{d\theta} \quad 3.33$$

The wave vector $k = k(\theta)$ in equation 3.33 is equal to $K_g(\theta)/(2n_o)$, where $K_g(\theta)$ is given by equation 3.28. We can use these relationships to calculate $dk/d\theta$. Also, if the "rotating mirror" in figure 3.3 turns at an angular velocity of Ω (radians/second), the exposure variable $H(\theta)$ is related to the incident intensity at angle θ , $I(\theta)$, by

$$I(\theta) = \Omega H(\theta) \quad 3.34$$

Combining equations 3.28, 3.33, 3.34 and $k = K_g/(2n_o)$ yields our desired result:

$$I(\theta) = \frac{2 n_o n_s^2 \Omega}{\pi c_o} \cdot \frac{\sin \theta \cos \theta}{(n_o^2 - n_s^2 \sin^2 \theta)} \cdot \left\{ R \left[\frac{2 \pi}{n_o \lambda_r} (n_o^2 - n_s^2 \sin^2 \theta)^{1/2} \right] \right\}^{1/2} \quad 3.35$$

Equation 3.35 indicates exactly what the recording laser intensity should be, at each exposure angle θ , in order to create a hologram with the desired reflectivity spectrum $R(k)$. The required intensity is proportional to Ω/c_o and increases as R increases, as expected.

3.2.2.3 "INDEX STACKING"

Equation 3.35 indicates that a coating with an arbitrary reflectivity spectrum can be created by properly modulating the recording beam as the hologram exposure angle is changed. Equation 3.25 gives the required index profile as a function of the desired reflectance. We will now apply equation 3.25 to a specific case to see if things are as simple as they appear!

We will consider, as an example, the case of a coating with a uniform reflectivity of 10% over the visible wavelength spectrum (0.4 to 0.7 μm) and zero reflectivity elsewhere. If we take $\beta = \frac{-\pi}{2}$ so that $r(k) = i\sqrt{R(k)} \approx +0.316 i$ (equation 3.31) and evaluate the index of refraction $n(z)$ at the hologram surface ($z = 0$), then equation 3.25 predicts:

$$\begin{aligned}n(0) &= n_o \left[1 - \frac{4}{\pi} |r(k)| \ln(k_{\max}/k_{\min}) \right] \\ \rightarrow n(0) &= n_o \left[1 + \frac{4}{\pi} \times 0.316 \ln(0.7/0.4) \right] \\ n(0) &= n_o [1 + 0.225]\end{aligned} \tag{3.36}$$

For DCG, the average background index, n_o , is about 1.5, so equation 3.36 indicates that the index at the surface of the hologram must be equal to 1.84, or 0.34 higher than the average DCG index. This level of index modulation, however, is impossible to achieve in DCG or any other holographic recording material! Experiments have shown that the highest peak-to-valley index modulation achievable in DCG is about 0.2. The linear relationship between DCG exposure and index modulation shown in equation 3.26 does not, of course, hold for arbitrarily large exposures. A more accurate model for the relationship between δn and H is a non-linear one:

$$\delta n = \delta n_{\max} \left[1 - \exp \left(\frac{-c_o H}{\delta n_{\max}} \right) \right] \quad 3.37$$

For small exposure levels, equation 3.37 reduces to the linear result given in equation 3.26, but as H increases the index change saturates at the value δn_{\max} .

Achieving a 10% reflectivity at a "single wavelength" requires only a small index modulation for a holographic coating with a reasonable thickness. For example, the peak-to-valley sinusoidal index modulation would only need to be about 5×10^{-3} to achieve a reflectivity of 10% at $\lambda = 0.5 \mu\text{m}$ for a $20 \mu\text{m}$ thick coating. It was the broad-band reflectivity requirement (0.4 to $0.7 \mu\text{m}$) which drove the index modulation (at the coordinate $z = 0$) up to 0.34 for the example given above. In order to produce the broad-band spectrum, the index of refraction profile must contain Fourier components corresponding to all wavelengths in the band. When these various Fourier components are added up, there will be regions in the coating where they tend to add up in phase, thus producing a large localized index modulation. These large localized index changes, however, cannot physically be produced in the recording material so the intensity recording profile given in equation 3.35 will not, in reality, always produce the desired profile. We will refer to this effect as "index stacking." Although the amplitude of the individual Fourier components making up the desired grating structure of the hologram may be small, there can often be regions in the coating where these components add in phase, thus resulting in δn values that are unachievable.

Figure 3.4 illustrates the concept of index stacking with a simple example--a grating consisting of two Fourier components shown in the top two curves in the figure. The longer period grating (profile A) will reflect longer wavelength radiation and the shorter period grating (profile B) reflects shorter wavelength radiation. When the two index profiles are added ("A + B (Non-Chirp Sum)") as shown in the third curve in the figure, the resulting structure will reflect both the long and short wavelength radiation. Notice, however, the peak-to-valley index modulation for the third curve is equal to ~ 0.35 , as compared to 0.20 for the top two curves (0.1 separation between dashed lines in the figure). When many different Fourier components

are added, index stacking can present a real problem.

One way to control, and even eliminate, index stacking is to judiciously select the phasing between the Fourier components being summed. The phasing should be selected to minimize the index stacking. In many cases of interest we are only concerned with the coating reflectivity profile, $R(k)$, and not in the phase, β , of the reflected radiation. Thus we can replace $r(k)$ in equation 3.25 with $\sqrt{R(k)} \exp[-i\beta(k)]$ and select the function $\beta(k)$ which minimizes index stacking! That is, we must find the function $\beta(k)$ which minimizes the term in brackets, [], in equation 3.25, at the worst possible value of z between 0 and L . Once we calculate the optimum $\beta(k)$, this ideal phase term can be used to find the desired phase relationship between the Fourier components, γ (see equation 3.32). This in turn can be used to determine the location of the back reflector plate, shown in figure 3.3, during the recording of the hologram. Thus as the rotating mirror in figure 3.3 is turned at a uniform rate, the laser intensity and back reflector plate location are adjusted in a previously calculated manner. The changing laser intensity determines the amplitude of the particular Fourier grating components being recorded, and the back plate position determines the relative phase of that Fourier component.

Although it is not obvious from examining equation 3.25 that an ideal $\beta(k)$ can be found which significantly reduces the effect of index stacking, some simple physical reasoning shows that this is the case. This physical reasoning also can be used to directly determine what the function $\beta(k)$ must be.

The bottommost curve in figure 3.4 ("A + B (Chirp Sum)") illustrates the approach that can be used to minimize index stacking. We must find the phasing, β , to use which generates a chirped grating with constant amplitude. The bottommost curve in the figure is a chirped grating which contains the frequency components of the top two curves, so it will reflect strongly at the two desired wavelengths. This curve also has a peak-to-valley index modulation of only 0.2, in contrast to the value of 0.35 in the third curve.

Our approach for fabricating "Concept 1" holographic filters can be summarized as follows:

1. Calculate the angle of incidence dependent laser intensity needed to generate the Fourier spectrum required for the desired $R(k)$ profile.
2. Calculate the Fourier component phasing term, γ , which will produce a uniform amplitude chirped grating, as shown at the bottom of figure 3.4, thus minimizing the index stacking problem.
3. Program the laser output modulator and the computer controlled translation stage holding the back reflector plate to respond according to the profiles calculated in steps 1 and 2.
4. Record the hologram by turning the "rotating mirror" in figure 3.3 through the required range of angles.

The laser intensity profile needed for step 1 is given in equation 3.35. The Fourier phasing term, γ , needed in step 2 is calculated in Appendix 3A

The Fourier component phase shift term $\gamma(\theta)$ is adjusted by precision movement of the back mirror during the recording process. This can be done by using a programmable computer controlled translation stage, such as Klinger Corporation's MT160 Holodrive linear translation stage.

We introduced the issue of index stacking at the beginning of this section with the example of a 10% reflectivity broad-band (0.4 to 0.7 μm) HC. We will conclude this topic by considering another, more stressing, coating design. The desired coating must have 30% reflectivity from 0.367 μm to 1.10 μm and 0% reflectivity outside of this band. Since we do not have any requirement on the phase of the reflectance, $\beta(k)$, this parameter can be chosen to

produce a hologram with a uniform amplitude index modulation, thus minimizing the index stacking problem.

Figure 3.5 is a plot of the index modulation needed to produce the wide band 30% reflectivity coating if we simply take $\beta(k) = 0$. That is, we do nothing to minimize the index stacking. The coating has a total thickness of 20 μm and figure 3.5 is a plot of the index modulation for the outermost 0.5 μm of the structure. The maximum peak-to-valley index modulation in the outer portion of the HC is nearly equal to 1.4 (1 + 0.4), far more than the 0.2 maximum which can be recorded in DCG. If on the other hand, we record the same Fourier spectrum as in figure 3.5, but choose $\beta(k)$ in an optimum manner (see Appendix 3A), the peak-to-valley index modulation can be reduced to 0.2. Figure 3.6 is a plot of the index modulation in this case, for the outermost 0.5 μm of the HC. The entire profile for this physically realizable coating is a uniform amplitude chirped grating, with the longest period portion of the grating (which reflects "strongly" (30%) at 1.10 μm) at the outermost part of the DCG layer. The period of the grating near the substrate is 0.122 μm and that portion of the structure reflects 30% of the light at 0.367 μm .

3.3 CONCEPT 2: DISCRETE EXPOSURES

3.3.1 DESCRIPTION OF CONCEPT 2 HOLOGRAM FABRICATION

Shortly after completing the analysis for the "Concept 1" hologram, we realized that a simpler approach was available for fabricating the HCs if DCG were used. When a hologram is recorded by a beam at a single incident angle, the period of the intensity fringe pattern, Λ_g , will be as given in equation 3.1 (air superstrate). In section 3.2 we assumed that the index of refraction modulation of the developed hologram will also have spacing Λ_g . This holds for an ideal recording medium, but in any real recording material nonlinearities will be present so that the index of refraction profile may not be a faithful reproduction of the material's exposure profile. Although DCG is one of the best holographic recording materials discovered to date, these nonlinearities are present and prevent a perfect reproduction of the exposure pattern.

It turns out that certain exposure and development procedures, to be described in section 4, can significantly reduce the ability of DCG to faithfully turn a recording intensity pattern into a corresponding index of refraction profile. In the "Concept 2" approach to matched filter fabrication, we will take advantage of these nonlinearities to fabricate holographic filters with an arbitrary reflectivity profile. This technique is expected to be simpler than the "Concept 1" approach described in section 3.2.

In particular, even after recording a hologram with a plane wave at a single angle of incidence, the exposure and development can be performed under conditions that produce a chirped grating--a grating with a period that changes somewhat through the thickness of the hologram. By carefully controlling the wet processing of the exposed DCG, the degree of swelling and dehydration of the developing HC can be altered. If the hologram is fabricated with a process, for example, which causes the innermost portion of the coating (near the substrate) to swell, the period of the index of refraction modulation will be greater near the back of the coating than the front surface. This structure will thus reflect radiation over a broader bandwidth than would be the case for a uniform period coating. Examples of previous applications of this property of DCG will be given in section 4.

Figure 3.7 illustrates the reflectivity spectrum of a uniform period grating and a chirped grating. The spectral response of the chirped grating is much wider than the uniform period grating. Also, for a fixed amplitude modulation, the peak reflectivity of the chirped structure will be less than the single period grating.

In the "Concept 2" approach to holographic filter fabrication, a holographic exposure is made at a number of discrete incident angles, rather than over a continuum of angles. If the gratings from each exposure are not chirped, the reflectivity of the HC will consist of a series of narrow peaks--a "comb filter." This spectral response is illustrated in figure 3.8a, along with the continuous profile of some coating which we wish to fabricate. The comb filter is a poor representation of the desired reflectivity profile. If we were to make exposures at many more discrete angles, the resulting hologram would more closely match the desired curve. In the limit

of one long exposure through a continuum of angles, the process would be equivalent to "Concept 1."

Figure 3.8b indicates what the spectral response of the HC would be if the five grating Fourier components which produced the comb filter in figure 3.8a were processed under conditions which resulted in chirped gratings. The sum of the reflectivities from each of the individual chirped gratings can closely approximate the desired reflectivity profile. If more angles are used for recording and the chirp is reduced for the separate Fourier component, then complex reflectivity profiles can be more accurately fabricated. If too many separate angles are recorded, however, the process starts to resemble "Concept 1" and the relative phasing of the various gratings will have to be controlled in order to avoid "index stacking." If the reflectivity spectrum can be approximated by only a few (perhaps less than 10) separately recorded chirped gratings, then index stacking will often not be a problem.

In the following sections we will analyze in detail the spectral response of a HC fabricated with the "Concept 2" technique. This analysis will also help determine the best angles and exposure levels for recording each chirped grating.

3.3.2 CONCEPT 2 ANALYSIS

In order to determine the performance of the "Concept 2" HC's we need to solve coupled equations 3.16 and 3.17, in the general case ($|B|$ not necessarily small). This can best be accomplished by defining a new variable ρ :

$$\rho(z) = \frac{B(z)}{F(z)} \left[\frac{Q(z)}{Q^*(z)} \right]^{1/2} \quad 3.38$$

where:

$$Q(z) = \int_{K_g^{(\min)}}^{K_g^{(\max)}} \hat{n}_r(K_g) \exp [i(K_g - 2n_0 k) z] dK_g \quad 3.39$$

and $Q^*(z) =$ complex conjugate of $Q(z)$

The reflectivity of the HC, R , is equal to $|\rho(0)|^2$.

If we take the derivative with respect to z of each side of equation 3.38 and use equations 3.16 and 3.17, we can find a differential equation for $\rho(z)$, which resembles the Riccati differential equation. The result is:

$$\rho' = -ik |Q| (\rho^2 + 1) + \frac{1}{2} \left[\frac{Q'}{Q} - \frac{Q^{*'}}{Q^*} \right] \rho \quad 3.40$$

where:

$$\rho' = \frac{d\rho}{dz}$$

$$Q' = \frac{dQ}{dz}$$

The boundary condition on $\rho(z)$ is $\rho(L) = 0$ ($L =$ coating thickness, $z = 0$ is at the surface of coating and $z = L$ is at the coating substrate interface). If the index of refraction profile results from the superposition of N different chirped gratings, then we can write $n^2(z)$ as:

$$n^2(z) = n_0^2 + 2n_0 \sum_{p=1}^N n_p \cos \left[\frac{2\pi}{\Lambda_p^{(0)}} (1 + \epsilon(z)) z + \alpha_p \right] \quad 3.41$$

In equation 3.41 n_p is one-half the peak-to-valley index modulation of the p^{th} chirped grating making up the HC. The period of the p^{th} grating would be $\Lambda_p^{(0)}$ if there were no chirp. The fractional differential contraction (i.e. the strain) of the DCG at coordinate z is defined as $\epsilon(z)$ ($\epsilon \ll 1$), so that the local period of the p^{th} grating is equal to approximately $\Lambda_p^{(0)} (1 - \epsilon(z))$. The term α_p in equation 3.41 represents the phase shift for the p^{th} chirped grating.

Comparing equations 3.4 and 3.41 yields:

$$\int_{K_g^{(\min)}}^{K_g^{(\max)}} \hat{n}_p(K_g) \exp(i K_g z) dK_g \quad 3.42$$

$$= \frac{1}{2} \sum_{p=1}^N n_p \exp \left[\frac{i 2 \pi}{\Lambda_p^{(0)}} (1 + \epsilon(z)) z + i \alpha_p \right]$$

From the definition of Q , we find:

$$Q(z) = \frac{1}{2} \sum_{p=1}^N n_p \exp \left\{ i \left[\frac{2 \pi}{\Lambda_p^{(0)}} (1 + \epsilon(z)) - 2 n_o k \right] z + i \alpha_p \right\} \quad 3.43$$

Numerical methods can now be used to solve for equation 3.40, using equation 3.43 for $Q(z)$ if the index profile can be expressed as a sum of chirped gratings of constant amplitude.

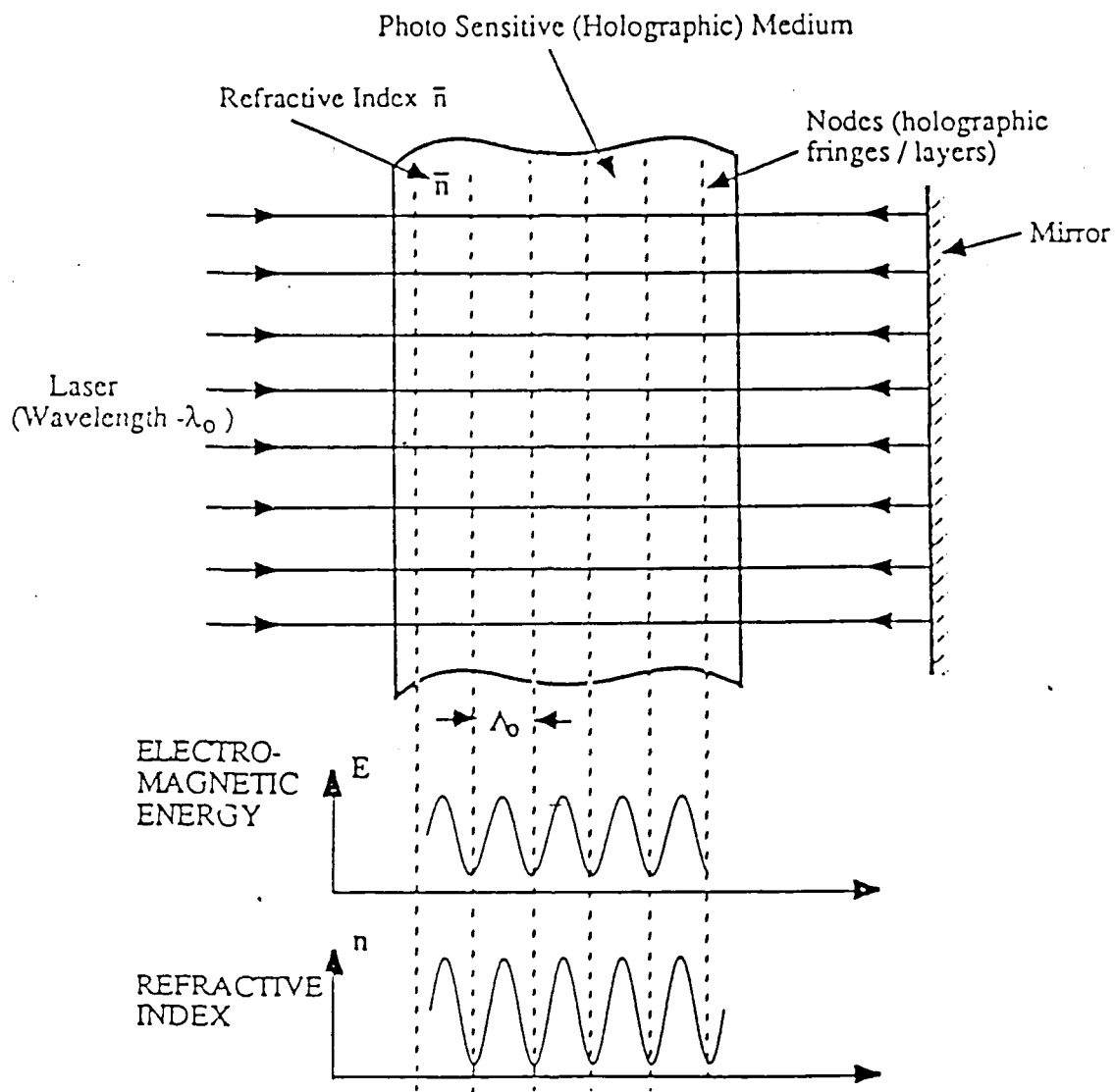


Figure 3.1 Standing Wave Holographic Recording Geometry (Normal Incidence)

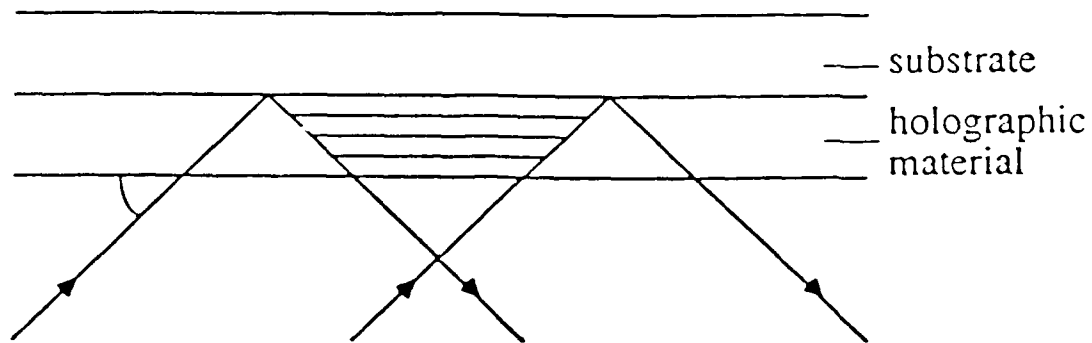


Figure 3.2 Geometry of a Lippmann holographic recording at oblique recording angles.

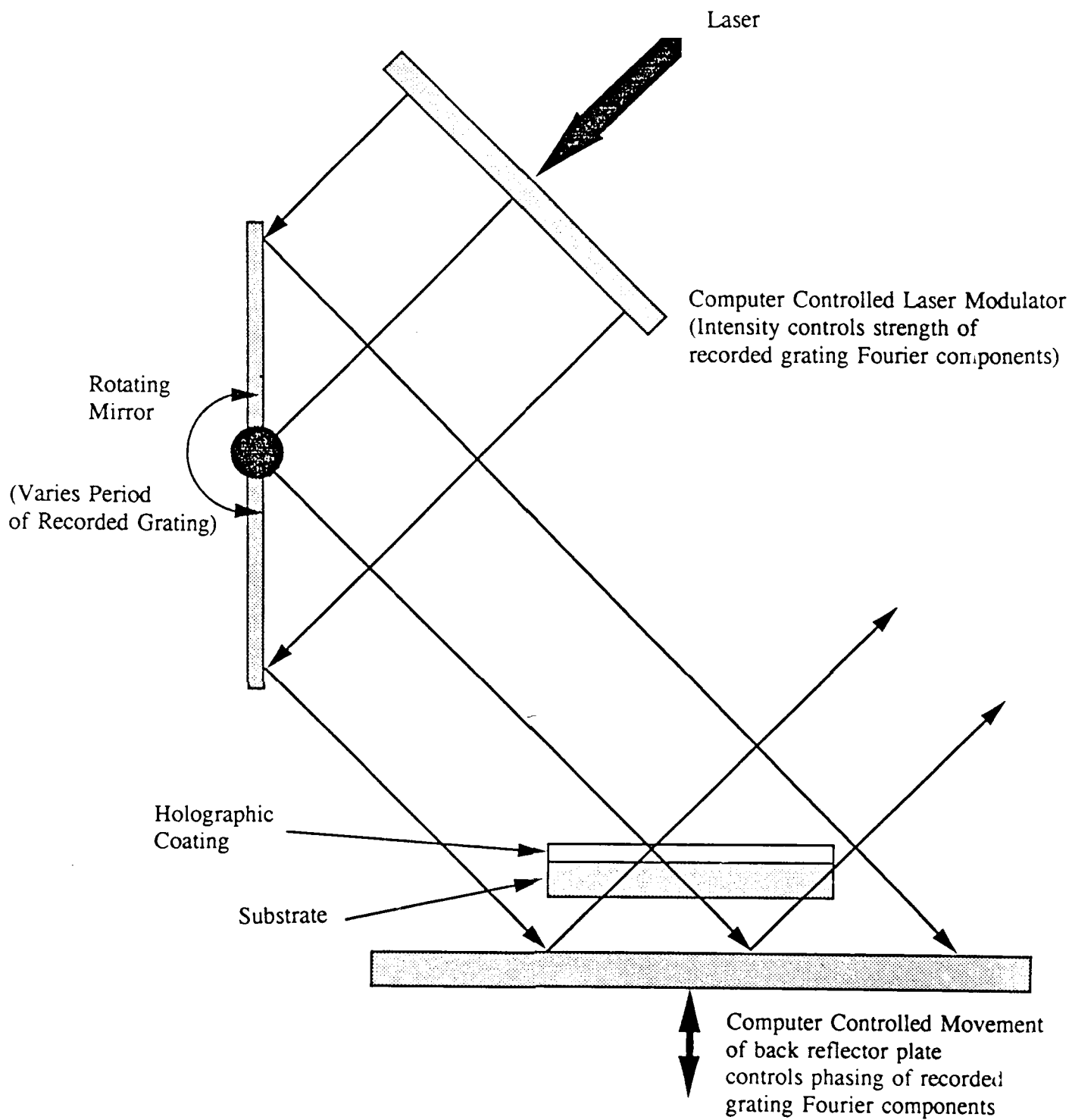
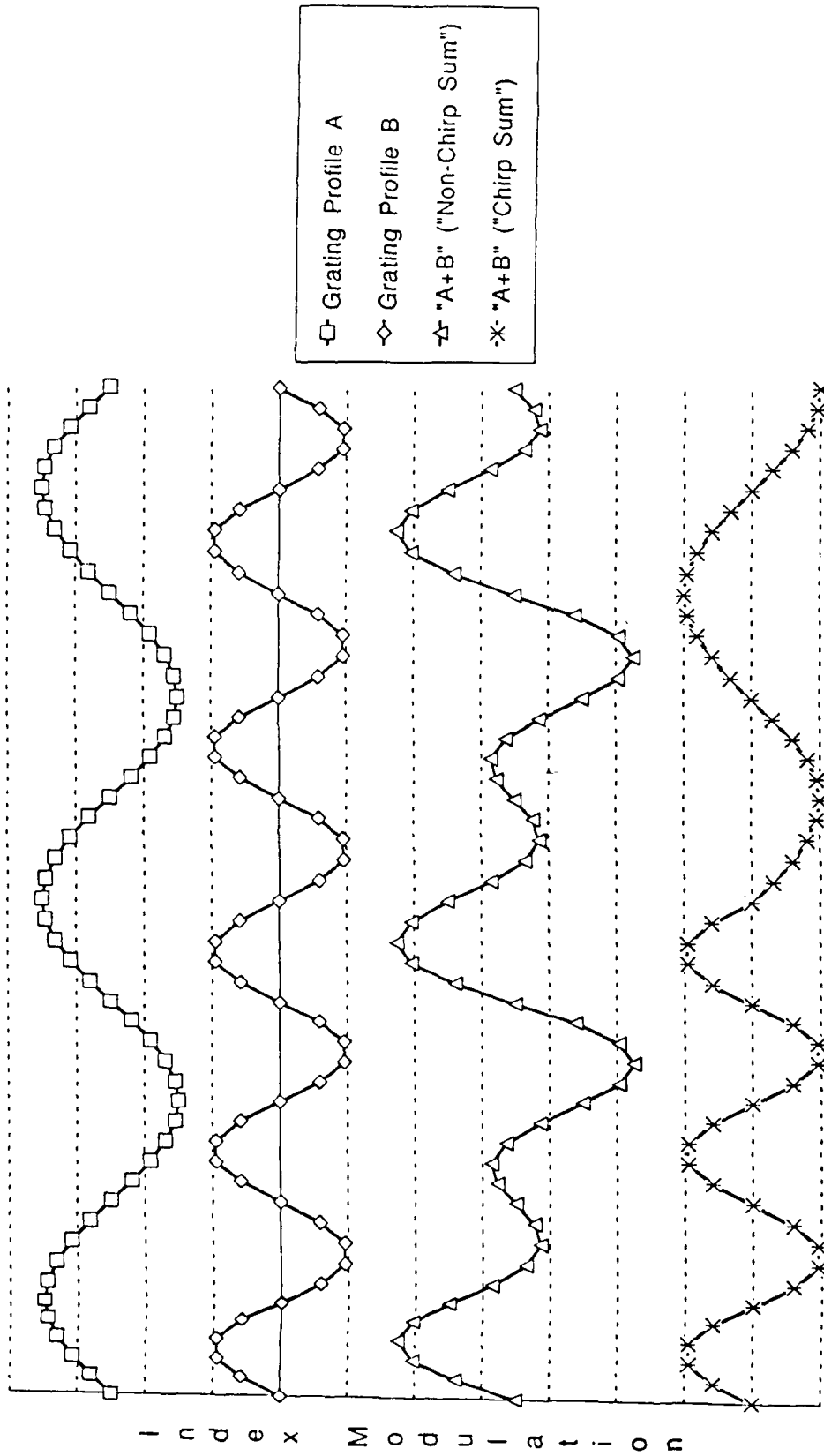


Figure 3.3 Schematic Diagram of Holographic Filter Fabrication



Distance from Surface of Holographic Coating, z (microns)

Figure 3.4 Index Stacking can be Controlled by Adjusting Phase Relationship Among Fourier Components of Recorded Beam.

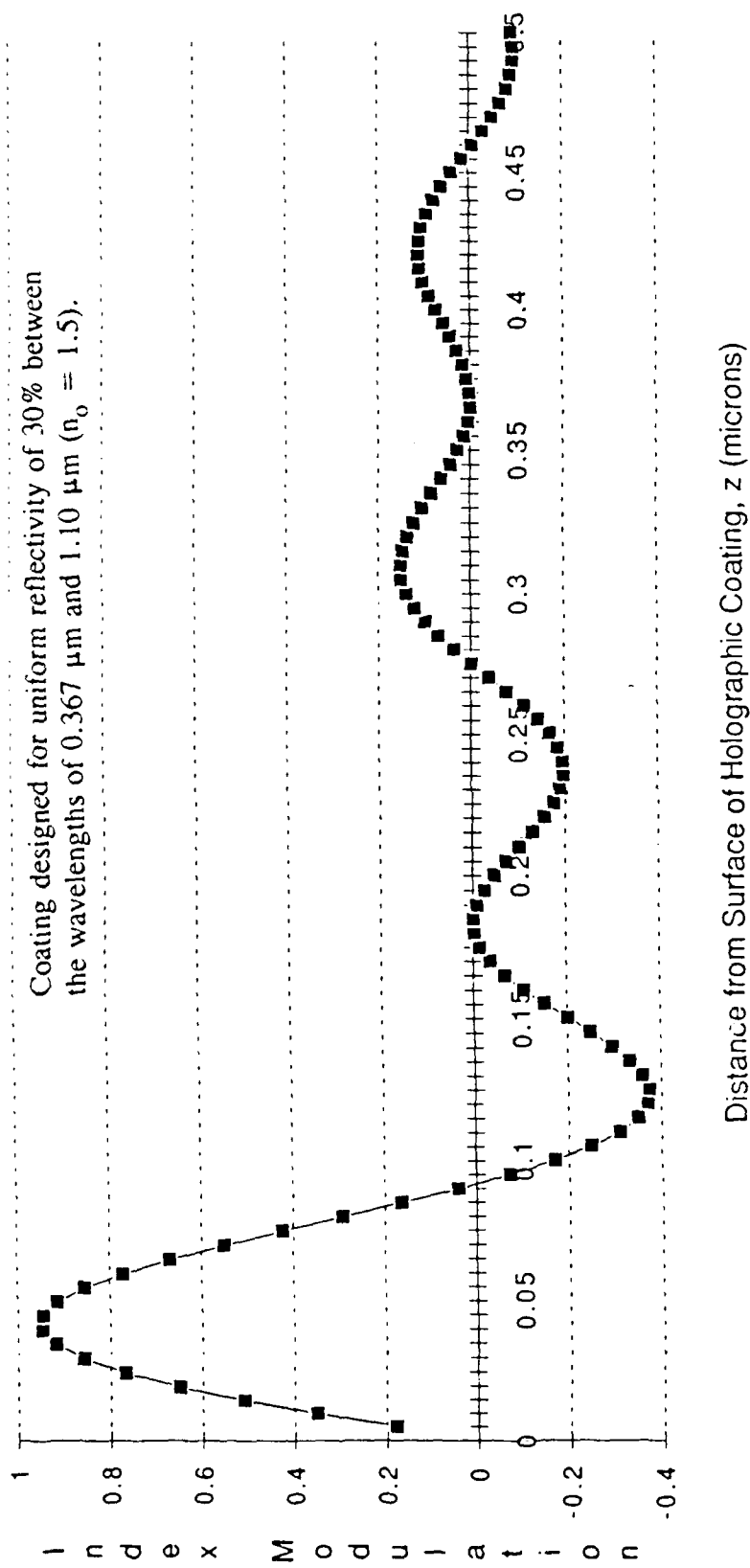


Figure 3.5 Index Modulation for the Outer Portion of a 20 Micron Thick Broadband Holographic Coating with a Constant Reflectance Phase Shift.

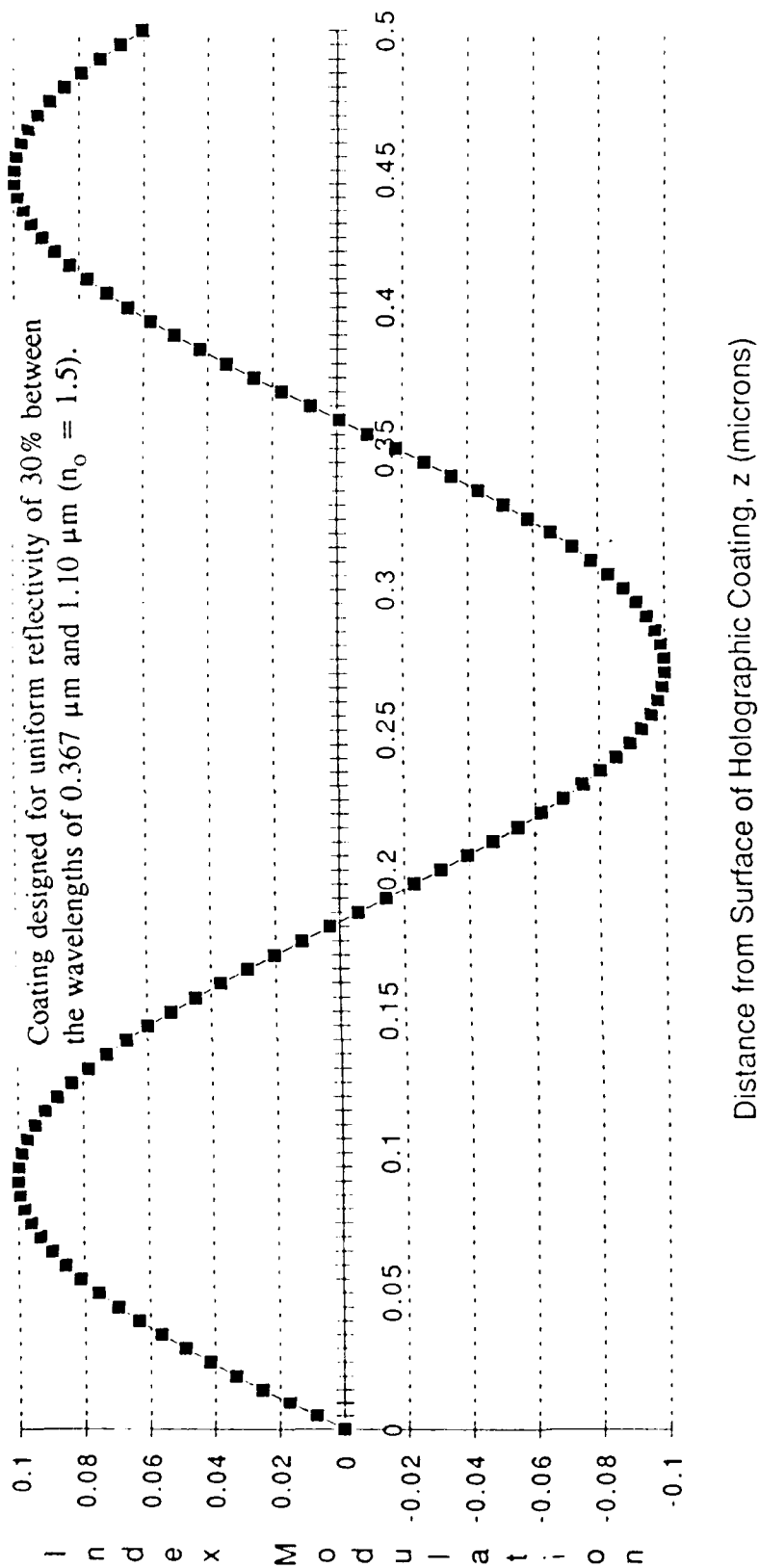


Figure 3.6 Index Modulation for the Outer Portion of a 20 Micron Thick Broadband Holographic Coating Designed to Minimize "Index Stacking."

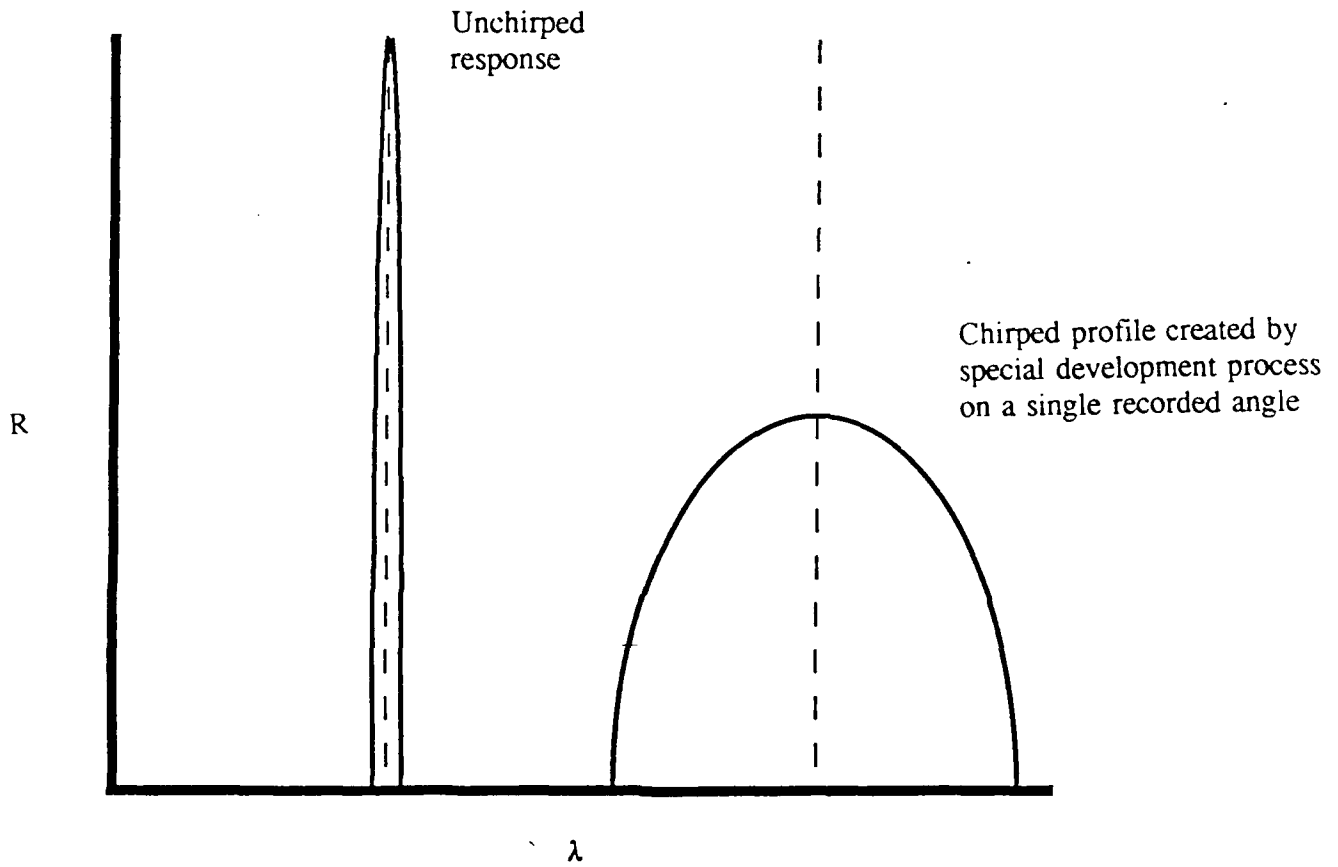


Figure 3.7 Reflectivity Spectrum of a Uniform and Chirped Grating.

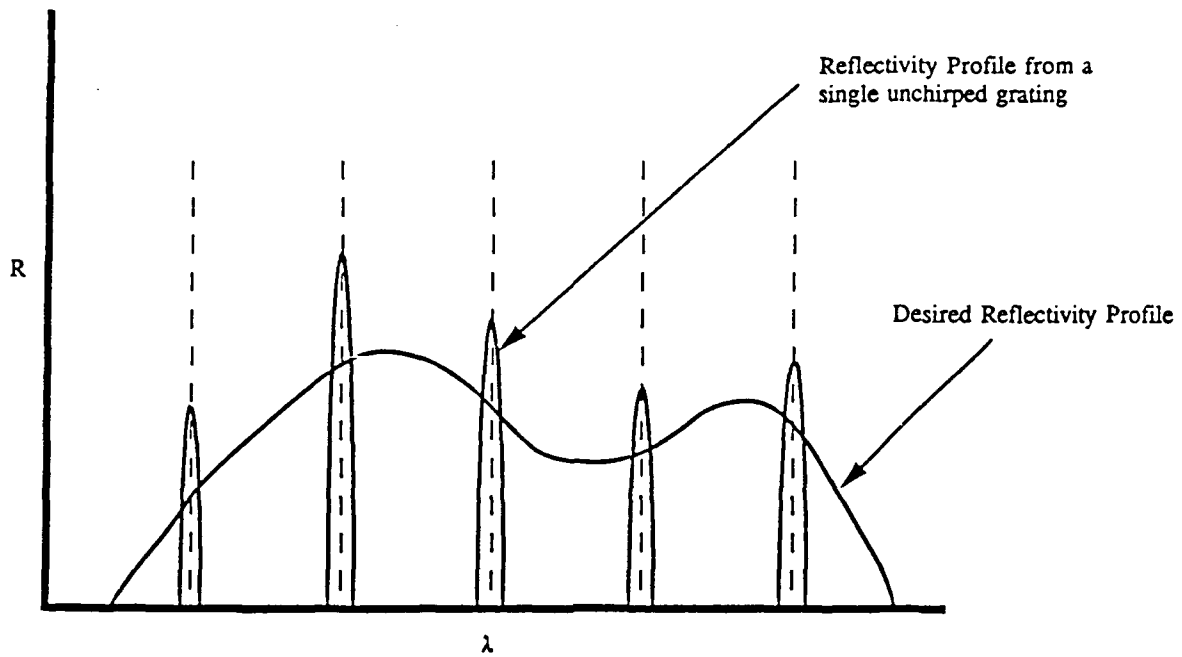


Figure 3.8a

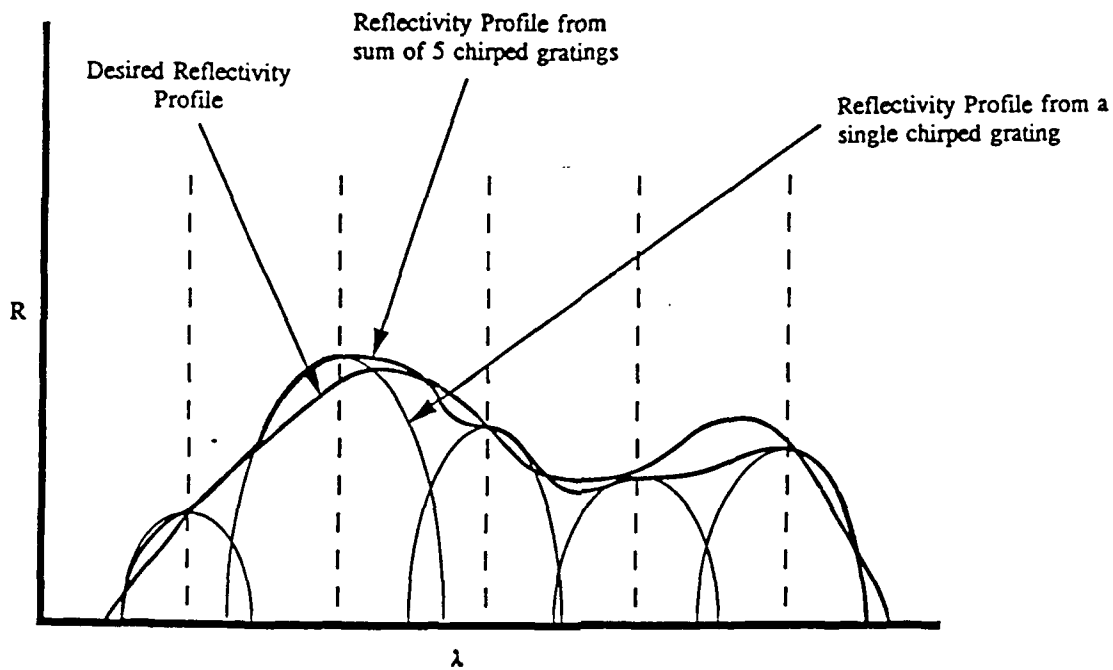


Figure 3.8b

Figure 3.8 Conventional recording and development of a series of holographic gratings cannot be used to accurately represent a desired spectral reflectivity profile (Figure 3.8a). Novel techniques for recording and development of gratings with a chirped profile allow the convenient fabrication of filters with any desired reflectivity profile (Figure 3.8b).

SECTION 3 REFERENCES

1. Amnon Yariv, Quantum Electronics (John Wiley and Sons, New York, 1975).
2. Amnon Yariv and Pochi Yeh, Optical Waver in Crystals (John Wiley and Sons, New York, 1984).
3. Jeffrey B. Shellan, "Aperiodic Structures in Optics and Integrated Optics," PhD thesis, California Institute of Technology, 1978.
4. Herwig Kogelnik, "Coupled Wave Theory for Thick Hologram Gratings," The Bell System Technical Journal, 48, 2909, 1969.

APPENDIX 3A. CONCEPT 1 PHASE FACTOR ANALYSIS

3A.1 ANALYSIS

In order to avoid "index stacking," we need to calculate the Fourier component phase term γ , or else the reflectance phase term β , which produces a uniform amplitude chirped grating. The angles γ and β are related through equation 3.32.

The square of the desired constant amplitude index of refraction modulation can be written as:

$$n^2(z) = n_0^2 + 2 n_0 n_1 \cos g(z) \quad 3A.1$$

The grating vector K_g is a function of z and is given by $\partial g(z)/\partial z$. The function $g(z)$ is real and will now be determined in terms of $R(k)$.

Combining equations 3A.1 and 3.24 yields:

$$n_0 n_1 \exp[i g(z)] = \frac{-4 i n_0^2}{\pi} \int \frac{1}{k} r^*(k) \exp(i 2 n_0 k z) dk \quad 3A.2$$

$$\Rightarrow n_1 \exp[i g(z)] = \frac{-4 i n_0}{\pi} \int \frac{1}{k} \sqrt{R(k)} \exp[i(2 n_0 k z + \beta(k))] dk \quad 3A.3$$

If we now multiply each side of equation 3A.3 by $\exp(-i K_g z)$ and integrate over all z from $-\infty$ to $+\infty$, the result is:

$$n_1 \int_0^L \exp [i(g(z) - K_g z)] dz \tag{3A.4}$$

$$= \frac{-8in_0}{K_g} \sqrt{R\left(\frac{K_g}{2n_0}\right)} \cdot \exp\left[i\beta\left(\frac{K_g}{2n_0}\right)\right]$$

We will not show the details, but the left hand side of equation 3A.4 can be approximated using the method of stationary phase. The result is:

$$n_1 \sqrt{\frac{2\pi i}{g''}} \exp [i(g - K_g z)] \tag{3A.5}$$

$$= \frac{-8in_0}{K_g} \sqrt{R\left(\frac{K_g}{2n_0}\right)} \cdot \exp\left[i\beta\left(\frac{K_g}{2n_0}\right)\right]$$

In equation 3A.5, the term g'' is shorthand for d^2g/dz^2 and the stationary phase requirement is:

$$g'(z) = K_g \tag{3A.6}$$

$$\left(g' = \frac{dg}{dz}\right)$$

If we take the square of the amplitude of each side of equation 3A.5 and use equation 3A.6, we find:

$$R \left(\frac{g'}{2n_0} \right) = \frac{\pi}{32} \frac{n_1^2}{n_0^2} \frac{g'^2}{g''} \quad 3A.7$$

Equation 3A.7 is our desired result. It is a non-linear second order differential equation for the function $g(z)$ in terms of known quantities n_1 , n_0 , and $R(k)$. If we define $h(z)$ as:

$$h(z) = \frac{2n_0}{g'(z)} \quad 3A.8$$

then equation 3A.7 can be converted to a simpler non-linear first order differential equation:

$$\frac{1}{R(1/h(z))} = \frac{-16}{\pi} \frac{n_0}{n_1^2} \frac{dh}{dz} \quad 3A.9$$

$$\Rightarrow \int R(1/h) dh = \frac{-\pi}{16} \frac{n_1^2}{n_0} z + c_1 \quad 3A.10$$

(c_1 = constant of integration)

If we define the function $G(h)$ in terms of the specified reflectivity function as:

$$G(h) = \int R(1/h) dh \quad 3A.11$$

and we define the function $G^{-1}(h)$ as the inverse function of G ($G^{-1}(G(h)) = h$), then:

$$\frac{1}{h} = \left[G^{-1} \left(\frac{\pi}{16} \frac{n_1^2}{n_0} z + c_1 \right) \right]^{-1} \quad 3A.12$$

$$\Rightarrow \frac{g'(z)}{2n_0} = \left[G^{-1} \left(\frac{\pi}{16} \frac{n_1^2}{n_0} z + c_1 \right) \right]^{-1} \quad 3A.13$$

Integrating equation 3A.13 gives us our desired result, the solution for $g(z)$:

$$g(z) = \int \frac{2n_0 dz}{G^{-1} \left(\frac{\pi}{16} \frac{n_1^2}{n_0} z + c_1 \right)} \quad 3A.14$$

If we return to equation 3A.5 and compare the phase terms on each side of the equation, we find:

$$\exp \left[i \left(\frac{\pi}{4} + g - K_g z \right) \right] = \exp \left[i \left(-\frac{\pi}{2} + \beta \right) \right] \quad 3A.15$$

$$\rightarrow \beta \left(\frac{g'}{2n_0} \right) = \frac{3\pi}{4} + g - z g' \\ (g' = K_g)$$

Combining equations 3A.15 and 3.32, we can derive our final result, an equation for the Fourier phase term γ needed to minimize index stacking:

$$3A.16$$

$$\gamma = g - z g' + \text{constant}$$

(The "constant" in 3A.16 can be any value--it does not impact the performance of the reflector)

In order to properly control the position of the back reflector plate during the recording of the HC, we must actually know γ as a function of θ , the recording beam's angle of incidence on the hologram during the angle sweep. This is easily found by the following process:

1. Use equation 3A.14 to solve for $g(z)$

2. Use the relationship

$$g'(z) = K_g(\theta) = \frac{4\pi}{\lambda_r} (n_o^2 - n_s^2 \sin^2 \theta)^{1/2}$$

to solve for $z = z(\theta)$

3. Use $z(\theta)$ in the right hand side of equation 3A.16 to find $\gamma(\theta)$.

3A.2 SAMPLE CALCULATION

We will now apply the results of the last section to the simple case of a HC with a constant reflectivity R_o between the wavelengths λ_{\min} and λ_{\max} . Since R_o is a constant, equation 3A.10 gives the result:

$$R_o h = \frac{-\pi}{16} \frac{n_1^2}{n_o^2} z + c_1 \quad 3A.17$$

$$\Rightarrow \frac{1}{g'(z)} = \frac{-\pi}{32} \cdot \frac{n_1^2}{n_o^2} \frac{z}{R_o} + \frac{c_1}{2n_o R_o} \quad 3A.18$$

The constant c_1 is easily found by evaluating equation 3A.18 at the point $z = 0$. We thus find:

$$g'(z) = \left[\frac{1}{g'(0)} - \frac{\pi}{32} \frac{n_1^2}{n_o^2} \frac{z}{R_o} \right]^{-1} \quad 3A.19$$

$$\Rightarrow g(z) = \frac{-32 n_o^2 R_o}{\pi n_1^2} \ln \left[\frac{1}{g'(o)} - \frac{\pi n_1^2}{32 n_o^2} \frac{z}{R_o} \right] \quad 3A.20$$

If we replace the left hand side of equation 3A.19 with $K_g(\theta)$ and solve for z , the result is

$$z = \frac{32 n_o^2 R_o}{\pi n_1^2} \left[\frac{1}{g'(o)} - \frac{1}{K_g(\theta)} \right] \quad 3A.21$$

Since $\gamma = g - zg'$ (equation 3A.16), we can use equations 3A.20, 3A.21, and $g' = K_g$ to find γ :

$$\gamma(\theta) = \frac{32 n_o^2 R_o}{\pi n_1^2} \left\{ 1 - \frac{K_g(\theta)}{g'(o)} + \ln \left[\frac{K_g(\theta)}{g'(o)} \right] \right\} \quad 3A.22$$

The function $K_g(\theta)$ is given in equation 3.28.

4. PROPERTIES OF HOLOGRAPHIC RECORDING MATERIALS

4.1 BACKGROUND

Dichromated gelatin (DCG) is probably the best material for fabricating high quality holograms. It offers one of the largest available refractive index modulations (~ 0.1), has excellent resolution ($> 10,000$ lines/mm), has low scattering, and requires moderate exposures ($50 - 300$ mJ/cm² in the wavelength range $350 - 520$ nm). It can be deposited in layers up to 50 microns thick, which is equivalent to over 300 periods for recording with radiation at 0.5 μm . The ability of DCG to provide an index modulation of 0.1 in layers up to 50 μm thick is an important feature for our intended application. Figure 4.1 is a table comparing the properties of four different materials which have been used for holographic recording. The high resolution of dichromated gelatin combined with its large index modulation make it the primary material for the Phase II work.

Another desirable property of DCG is its high optical damage threshold. JBS Technologies, Inc. received a $\$103,000$ subcontract from SAIC, as part of an SDIO coating development program, to investigate the potential of HCs for near IR lasers.^(*) Key findings of this work were that damage thresholds of over 1 MW/cm² cw were achievable for HCs deposited on Moly and that reflectivities of 99.5% were possible at a wavelength of 1.3 μm .⁽¹⁾

4.2 THE DCG RECORDING PROCESS

The unsensitized recording material is gelatin, which consists of the fibrous protein collagen; a material, normally obtained from animal skins and bones. Gelatin has the property that it can be cross-linked by certain polyvalent metallic ions when exposed to light. The chromium ion (Cr^{3+}) is the most commonly used metal ion for this purpose. It is obtained from

^(*)SAIC contract DAAH01-89-R-0065, D.O. #1 to the Army (supported by SDIO).

a reduced inorganic dichromate which reacts at the free carboxyl group sites in gelatin, provided by the constituent di-basic aspartic and glutamic amino acids. The photo-reduction of the dichromate ion and its effect on the crosslinking of gelatin through the carboxyl functional groups is illustrated in figure 4.2⁽²⁾

This crosslinking significantly increases the molecular weight and reduces the solubility of the material in warm water. Thus, portions of the DCG exposed to radiation in the range 3500 to 5200Å will become less water soluble (hardened) and this hardening will be proportional to the exposure level. When the material is then washed and subsequently dried in a dehydrating agent, such as isopropanol, the gelatin layer will have a varying refractive index structure recorded in it. This index of refraction pattern corresponds to the exposure levels which various parts of the DCG were subjected to during the holographic recording process. Figure 4.3 summarizes the DCG recording process.⁽²⁾

Of particular interest in the current work is how the index of refraction modulation pattern can be modified from the sinusoidal standing wave intensity pattern of the recording radiation. In other words, how a chirped or tapered grating can be created from the purely sinusoidal exposure pattern. There are four main stages in the DCG recording procedures: (1) preprocessing; (2) sensitization; (3) exposure and (4) development or processing (water washed followed by dehydration). It is primarily the procedure followed in the final processing stage which can be used to control grating chirp. We will discuss this step in detail in the following section. A description of the preprocessing, sensitization, and exposure steps will not be given here, but can be found in references by Cullen,⁽²⁾ Kubota,⁽³⁾ Sjölander,⁽⁴⁾ and Georgekutty.⁽⁵⁾

4.3 DCG PROCESSING PROCEDURE TO CONTROL GRATING CHIRP⁽²⁾

The development or processing step begins with a water wash to remove the unreacted ammonium dichromate after the exposure of the DCG. Increasing the water temperature and pH will increase the swelling of the gelatin layer which increases the index of refraction modulation. Gelatin molecules are transferred and rearranged in the water swollen layer to regions of higher

exposure, as illustrated in figure 4.3. Since the absorbed water produces swelling in the DCG, the period of the index modulation is greater than that of the sinusoidal intensity pattern created during the exposure step. The hologram, at this stage of the development process, would thus most strongly reflect radiation at a wavelength slightly longer than the recording wavelength. The procedure followed in the next step of the processing, dehydration, can be used to freeze in this swelling, reverse it, or to retain the swelling in certain parts of the DCG layer and reverse it in other parts. It is this third possibility that produces chirped gratings from a purely sinusoidal recording.

Isopropanol is considered to be the best dehydrating agent for DCG. When the sample is immersed in the isopropanol, the water in the swollen gelatin is rapidly removed, thus freezing the DCG molecular structure. If 100% isopropanol is used for the dehydration bath immediately after the water bath, the dehydration will occur so rapidly at the surface that some water will be trapped deeper in the DCG layer--closer to the substrate. This water is unable to escape through the dry hardened surface and the DCG layers closer to the substrate will remain permanently swollen. Thus the coating will naturally be chirped, with the longer period closer to the substrate.

An unchirped, faithful reproduction of the sinusoidal recording intensity pattern can be generated, on the other hand, if the rate of dehydration is carefully controlled. A slower rate of dehydration results if graduated water/alcohol mixtures are used. The sample is taken from the water bath and initially immersed in a 90/10 solution of water/alcohol. It can then be added to a 50/50 mixture of water and alcohol, followed by a 10/90 solution, and finally a bath of pure isopropanol. This allows sufficient time for a more uniform dehydration of the developing DCG and a sinusoidal, rather than chirped, index of refraction modulation will be achieved. The level of chirping can thus be carefully controlled by controlling the rate of dehydration. Table 4.1 summarizes typical processing procedures for making narrow bandwidth (no chirp) and wide bandwidth (chirped) coatings.

Table 4.1 Typical Processing Steps for Sinusoidal and Chirped Coatings

<u>Narrow Bandwidth Process</u>	<u>Wide Bandwidth Process</u>
<ul style="list-style-type: none">• Prepare water/IPA mixtures, 90/10, 50/50, 10/90, 0/100% and soak plate in each (starting with the 90/10%) for 4 min (20-25°C) with agitation.	Soak in 100% IPA (20-25°C) with agitation until maximum efficiency is obtained, typically 5-8 min.
<ul style="list-style-type: none">• Processed plates are transferred to a controlled RH environment of approx. 40% to stabilize. 10 - 20 hours.	
<ul style="list-style-type: none">• To protect the hologram against humidity changes a cover glass can be adhered using suitable transparent cyanoacrylate or epoxy resins.	

It has been demonstrated that the shape of the reflectivity profile, as well as its width, can be controlled through careful processing and variations in the gelatin formulation. Figure 4.4 illustrates how Cullen⁽²⁾ was able to fabricate a coating with a pointed reflectivity peak or a flat top, depending on the processing used.

The author of this report has also needed to fabricate chirped HCs for the previously referenced SDIO program.⁽¹⁾ The holographic coatings for that program were needed for a chemical laser (HF overtone) with a central wavelength of 1.35 μm and a bandwidth of a little over 0.1 μm . By following the development procedures discussed earlier, a broad-band high reflectivity coating with a flat top profile was produced. Figure 4.5 is a plot of the transmission and optical density of one of the fabricated coatings.

4.4 SEQUENTIAL RECORDINGS IN DCG

Sequential recording of different gratings in a single DCG hologram have been reported by numerous groups such as Magariños and Coleman,⁽⁶⁾ Rallison,⁽⁷⁾ and Physical Optics Corporation.⁽⁸⁾ In the work reported by Rallison, five overlapping gratings, each with near 100% diffraction efficiency, were recorded in DCG 20 μm thick. In another device fabricated by

Rallison, nine sequential exposures were made on a single hologram. The nine exposures were of lenses focusing a plane input beam to different locations. When the developed hologram was subsequently illuminated by a plane wave, the wave emerging from the back of the hologram focused down to nine diffraction limited spots. The nine separate gratings were recorded so that the energy in the nine output spots, making up the 3 x 3 array, was evenly distributed. Rallison has stated that the maximum number of separate high efficiency recordings that can be made in a single hologram is about equal to twice the index modulation times the thickness in microns. Thus a 50 micron thick layer of DCG should be sufficient for recording ten separate high efficiency chirped gratings, which when pieced together can form the desired reflectivity spectrum. Rallison's estimate is somewhat qualitative,^(*) and a much more precise prediction can be made with the computer codes written for this contract and discussed in the next section. These codes are based on the analysis presented in section 3 of this report.

Although many groups have fabricated chirped gratings in DCG and a number of groups have fabricated HCs with multiple gratings, none have combined these two features in order to make a coating with some prescribed reflectivity spectrum. The separately recorded coatings have nearly always been for wavelengths well separated, so that interaction effects could be ignored. In our case, we need to combine the spectral profiles of each recorded grating to form a variety of possible reflectivity profiles.

^(*)For example, what exactly is meant by "high efficiency" - 70%, 90%, 99% diffraction efficiency?

SECTION 4 REFERENCES

1. Jeffrey B. Shellan, "The Development of Holographic Rugate Coatings for High Energy Chemical Lasers," Final Technical Report submitted to Science Applications International Corp. (Contract No. DAAH01-89-R-0065, D.O. #1), December 1989.
2. R.A. Cullen, "Some characteristics of and measurements on dichromated gelatin reflection holograms," SPIE Vol. 369, 647.
3. Toshihiro Kubota, "Control of the reconstruction wavelength of Lippmann holograms recorded in dichromated gelatin," Appl. Opt. 28, 1845 (1989).
4. Sven Sjölander, "Bandwidth in dichromated gelatin holographic filters," Optica Acta 31, 1001 (1984).
5. Tharayil G. Georgekutty and Hua-Kuang Liu, "Simplified dichromated gelatin hologram recording process," Appl. Opt. 26, 372 (1987).
6. José R. Magariños and Daniel J. Coleman, "Holographic mirrors," Opt. Eng 24, 769 (1985).
7. Richard D. Rallison, "Holographic optical elements (HOES) in dichromated gelatin (DCG): progress," SPIE Vol. 523, Applications of Holography, 292 (1985).
8. "Laser Countermeasure Holographic Rugate Filters for Ultraviolet Radiation," Phase II SBIR proposal to SDIO by Physical Optics Corp., contract no. DNA001-87-C-0265, May 1988.

Material	Sensitivity (mJ/cm ²)	Refractive Index modulation	Resolution (lines/mm)	Advantages	Disadvantages
Silver Halide	0.001-0.01	0.08 or less	4000 depends on grain sz.	High speed	Complex processing
Dichromated Gelatin	40-600	0.01-0.1	> 10,000 lines/mm	High quality	Complex processing
Photo resist	2-6	-----	3,500	Easy replication	Low speed transmission only
DMP	4-15	0.08	4,000	Moderate quality	Complex processing, poor shelf life

Figure 4.1. Comparison of Four Materials Used in Holographic Recording.

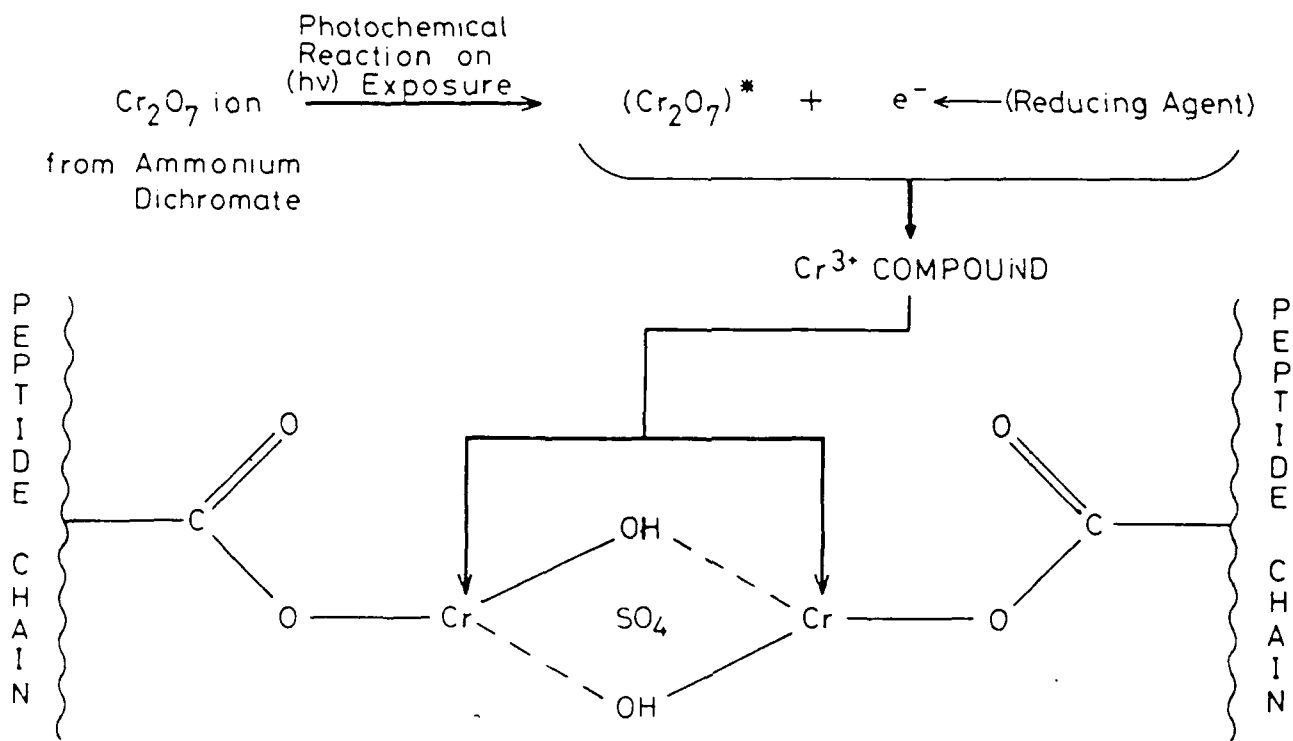


Figure 4.2 Photo-reduction of the dichromate ion and its effect on the crosslinking of gelatin via the carboxyl functional groups⁽²⁾

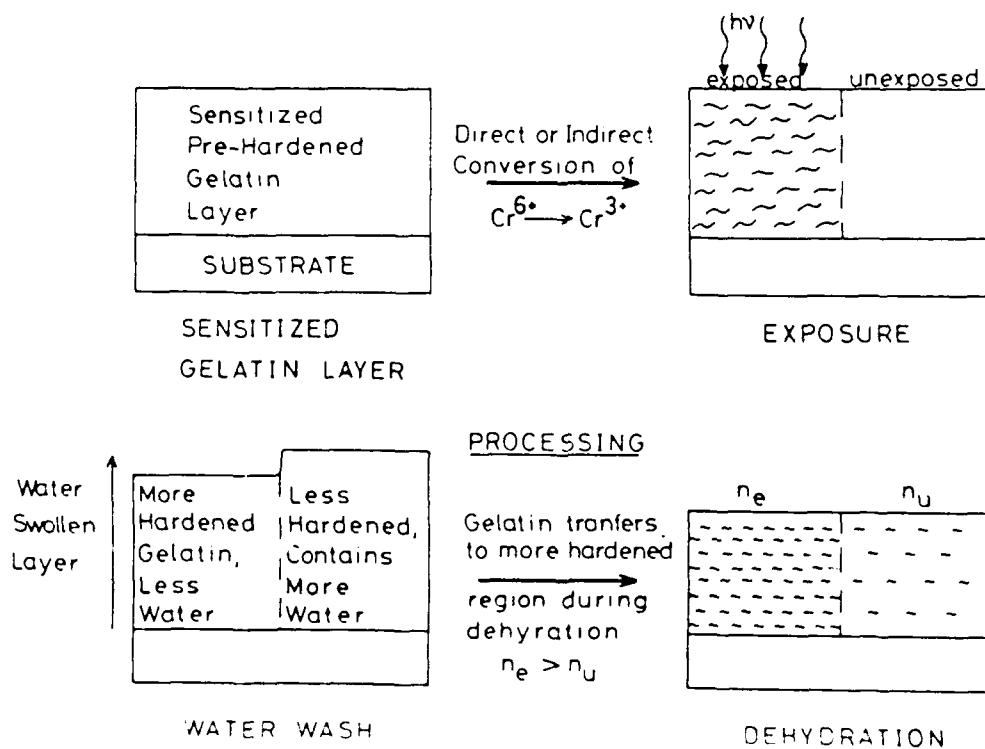


Figure 4.3 Generalized DCG recording process⁽²⁾

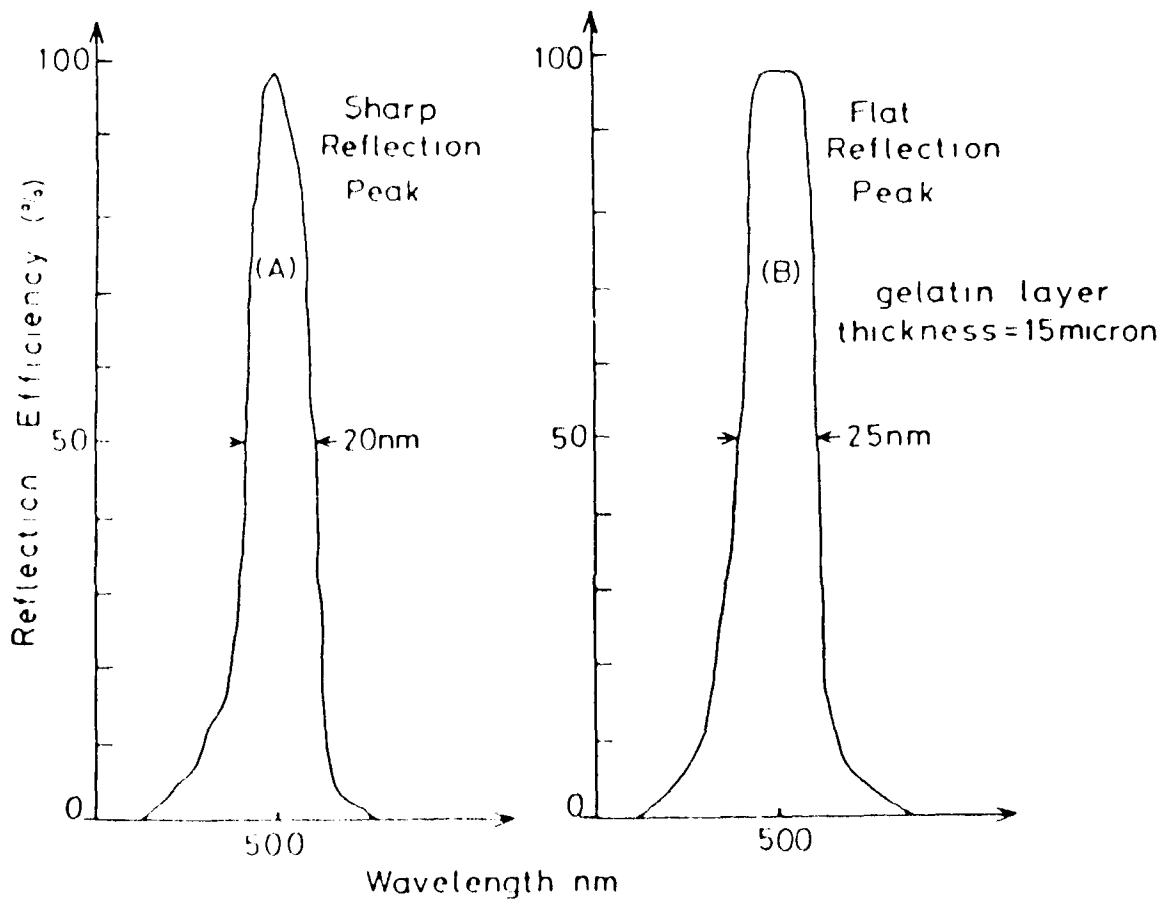


Figure 4.4 Reflection efficiency curves indicating the effect of narrow bandwidth processing (A) and the alternative "flat" peak processing (B). (reference 2)

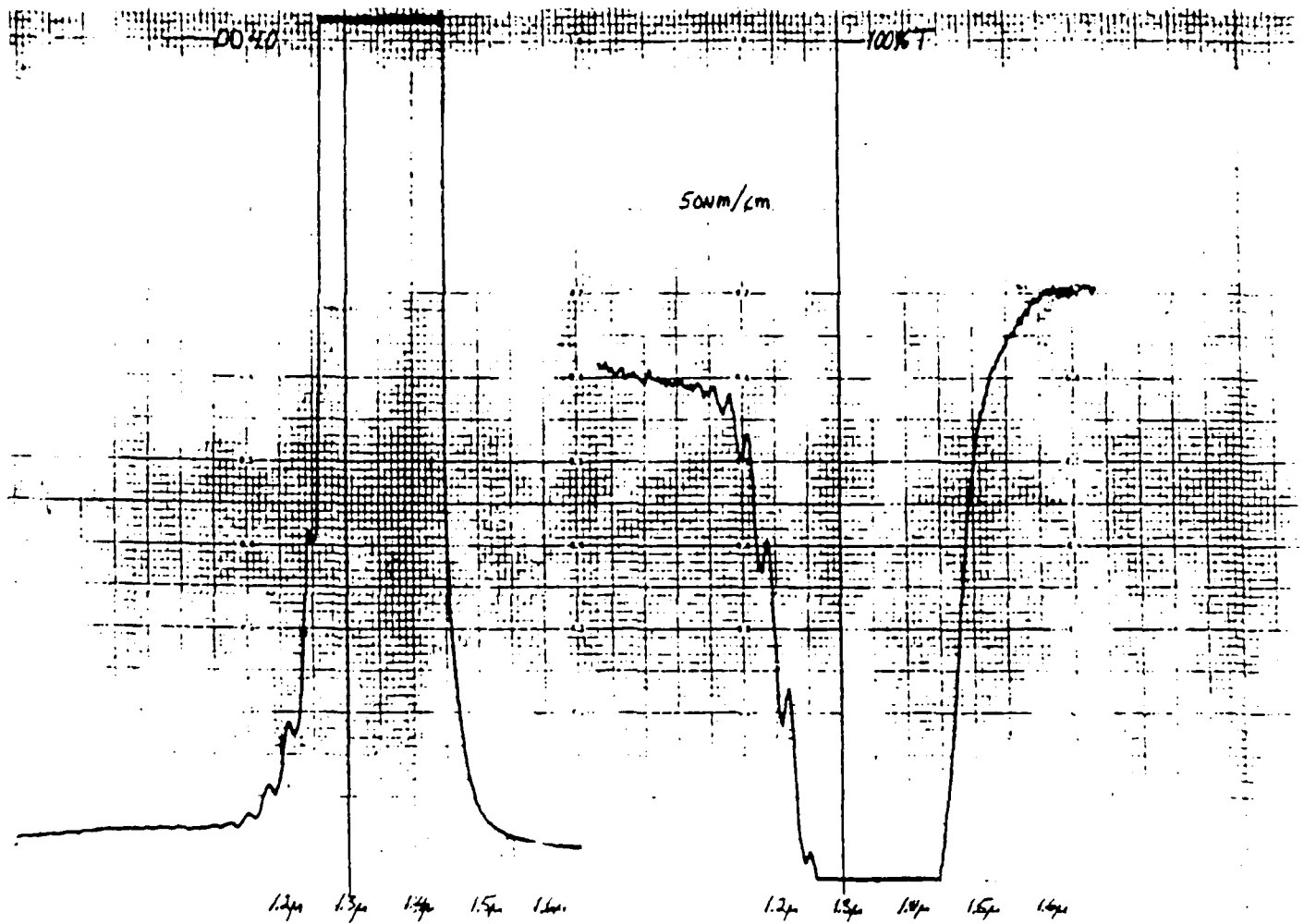


Figure 5. Measured Transmission and Optical Density of a Lippman Mirror on Glass Substrate.

5. COMPUTER MODELING OF OPTICAL COATING PERFORMANCES

A computer program has been written to find numerical solutions to the coupled mode equations. The program uses a subroutine based on the fifth order Runge-Kutta method with adaptive step size. Appendix 5A is a listing for this program.

The program was used to design three different filters:

1. A filter with a reflectivity profile matching the UV spectral signature (3000Å to 4000Å) of a typical solid propellant booster, as shown in figure 2.9.
2. A filter with a reflectivity profile given by the optimum matched filter characteristics used to detect a solid fueled booster against an Earth background (mid-latitude summer profile illustrated in figure 2.8).
3. High uniform reflectivity (ideally equal to 1.0) over the waveband 0.4 to 0.8 μm and zero elsewhere.

The first two filters listed above would be used in a reflectivity mode - they would be placed in the camera beam train so that light reflected from them would be focused on the detector used to detect the booster target. They would preferentially reflect radiation at the stronger spectral lines of the target and reflect a smaller fraction of Earth background radiation onto the detectors.

5.1 UV PLUME SPECTRAL PROFILE

Figure 5.1a illustrates the UV spectral signature of a solid booster, while figures 5.1b, c, d, and e show the calculated reflectivity profiles of four different HCs fabricated in DCG with slightly different parameters. All four reflectivity profiles are reasonably accurate representations of the plume signature, but the profiles in figure 5.1d and 5.1e are the best representations. The

design parameters for the four different reflectors are given in figure 5.2. All require very small chirp parameters (1.5%), so the slow, well controlled dehydration procedure described in section 4.3 would be used to fabricate the holographic reflectors in DCG. The exposure time for each of the four separate recordings will be proportional to the desired reflectivity. We have found that slightly better representations of the four peaks shown in figure 5.1a can be realized if the side lobes, that are normally present in fairly narrow band reflectors (1.5% chirp), can be suppressed. This can be accomplished by recording the four gratings in a manner that produces a tapered index modulation. The index modulation n_i ($i = 1$ to 4) used to arrive at the four profiles shown in figure 5.1 was quadratically tapered and of the form:

$$n_i = n_i^{(max)} + 4 \left(n_i^{(max)} - n_i^{(min)} \right) \frac{z}{L} \left(\frac{z}{L} - 1 \right) \quad 5.1$$

where:

- L = DCG thickness
- $n_i^{(max)}$ = maximum index modulation for the i^{th} recording (occurs at $z = 0$ and L , the hologram surface and DCG/substrate interface)
- $n_i^{(min)}$ = minimum index modulation for the i^{th} recording (occurs at $z = L/2$)

The index modulation taper can be adjusted through the selection of recording wavelength and preparation of the DCG (references 2 and 4 from section 4 of this report). As mentioned above, however, the curves plotted in figure 5.1 are not too sensitive to this parameter, so it will not have to be controlled too carefully during HC fabrication. The values of $n_i^{(min)}$ and $n_i^{(max)}$ are given in figure 5.2.

The HC thickness needed to achieve the four profiles shown in figure 5.1 is only 10 μm and the parameter $\lambda_i = 2n_0\Lambda_i^{(0)}$ for the four recordings is also given in figure 5.2

5.2 VISIBLE PLUME SPECTRAL PROFILE

Figure 5.3a illustrates the optimum matched filter profile for the detection of a solid booster against an Earth background, as calculated in section 2.1.5. Figures 5.3b, 5.4a, and 5.4b are plots of the reflectivity spectrum of several HCs designed to match the optimum filter. The coating illustrated in figure 5.3b is the best representation of the desired spectral profile. The parameters used to calculate these profiles are given in figure 5.5. All three HCs require a coating thickness of 22 μm , a small chirp (1%), and only two separate recordings (two chirped coatings recorded in the DCG) to produce the indicated spectral profiles.

5.3 HIGH REFLECTIVITY COATING FOR THE VISIBLE

Finally, a much more difficult spectral profile to produce holographically was the case of a reflectivity of 1.0 from 0.4 μm to 0.3 μm , and zero elsewhere. We attempted to design a HC with this profile using two and then four separate recordings. The total index modulation of the DCG, consisting of the sum of the modulation from each separate recording, was constrained to have a peak-to-valley value no greater than 0.2 (see section 4.1). The maximum allowable fractional chirp was constrained to be no greater than 15%, a conservative assumption for DCG.

Figure 5.6 shows the reflectivity profiles of HCs recorded with two different chirped periods. The input parameters are summarized in figure 5.7. Figure 5.6a used a 5% chirp, which is seen to be totally inadequate for spanning the wide spectral band of interest. Significantly better results are achieved by combining a 10% chirp with a smaller λ_2 value (0.75 μm - 0.60 μm), as illustrated in figures 5.6b and 5.6c. Surprisingly, increasing the chirp from 10% to 15%, while keeping other parameters fixed (figure 5.6c - 5.6d) did not improve the profile. The performance dropped somewhat in figures 5.6e and 5.6f, as compared to figure 5.6d, because the coating thickness was reduced from 50 μm to 40 μm . In figures 5.6g, h, and i the DCG thickness is increased to 50 μm and the average period of the shorter period grating is increased somewhat. This fills in the reflectivity drop centered at 0.57 μm in figures 5.6b

through 5.6f, producing a higher more uniform reflectivity profile. It does, however, result in a short wavelength spectral cutoff at around 0.45 to 0.5 μm , rather than the desired value of 0.4 μm .

Figure 5.8a through 5.8j illustrate the reflectivity profile when four separate recordings are made in the DCG to generate four separate chirped grating profiles. The coating input parameters for these ten cases are summarized in figure 5.9. These reflectivity profiles are not as close to our design goal as was the case for the two exposure profiles given in figure 5.6. This is primarily due to the fact that a smaller index modulation per recording (n_1 factor) had to be used for the four recording case, in order to avoid "index-stacking" (ensure that the peak-to-valley modulation was never more than 0.2).

The 15% maximum chirp profile and 50 μm DCG thickness assumed in generating the best reflectivity profiles for the $N = 2$ (two exposure) case may be a bit conservative. It may be possible to produce a slightly larger chirp (20%) on thicker DCG layers ($\sim 70 \mu\text{m}$), in which case a high reflectivity coating from 0.4 to 0.8 μm could be produced, based on the trends shown in figure 5.6.

5.4 PUBLICATION OF CONTRACT CONCLUSIONS

A summary of the results of this report, including the "plume filter" examples in section 5.1 and 5.2, have been submitted for publication and presentation at the 1991 SPIE International Symposium on Optical Applied Science and Engineering (21-26 July 1991, San Diego, CA; Conference No. 15). A draft copy of the paper is given in Appendix 5B.

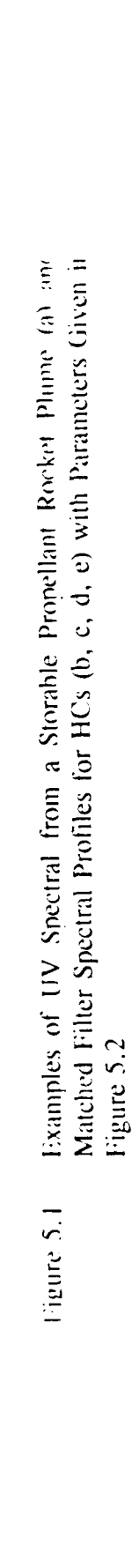
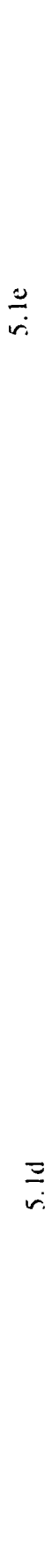
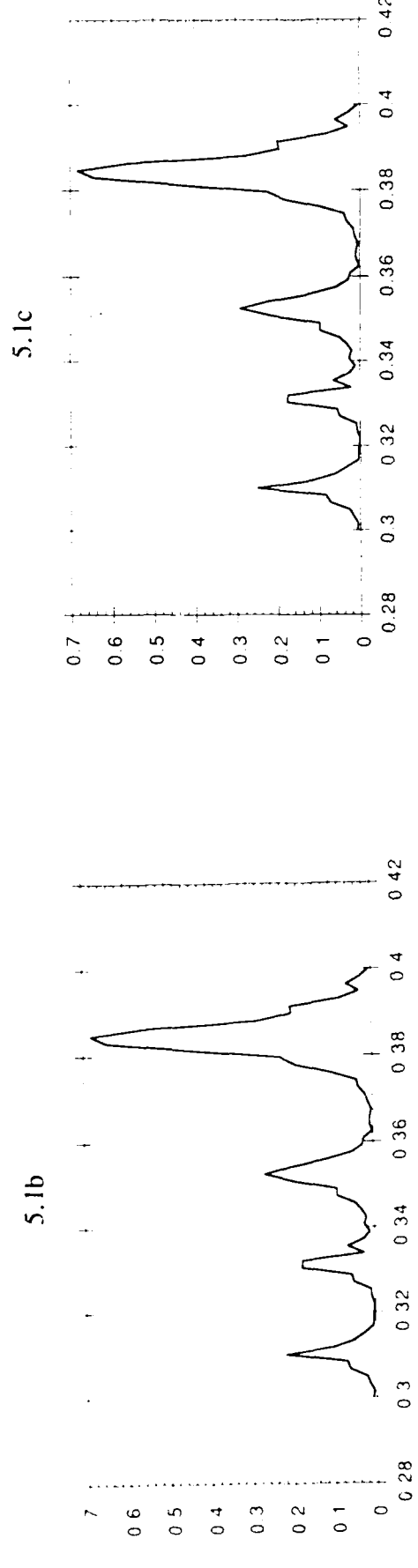
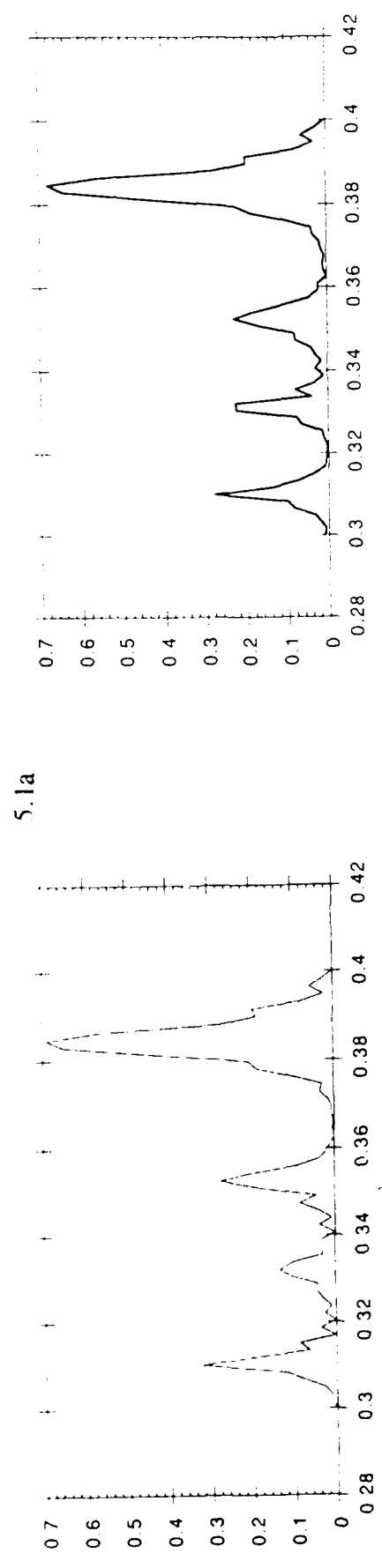
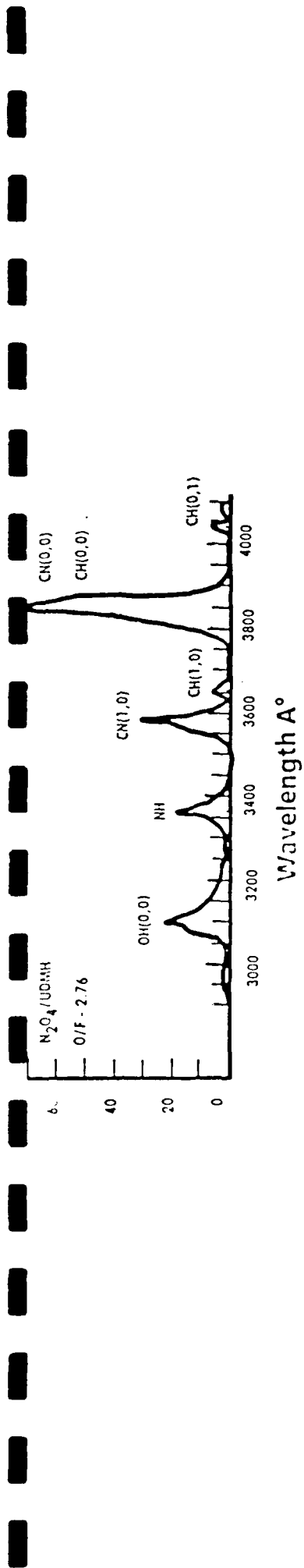
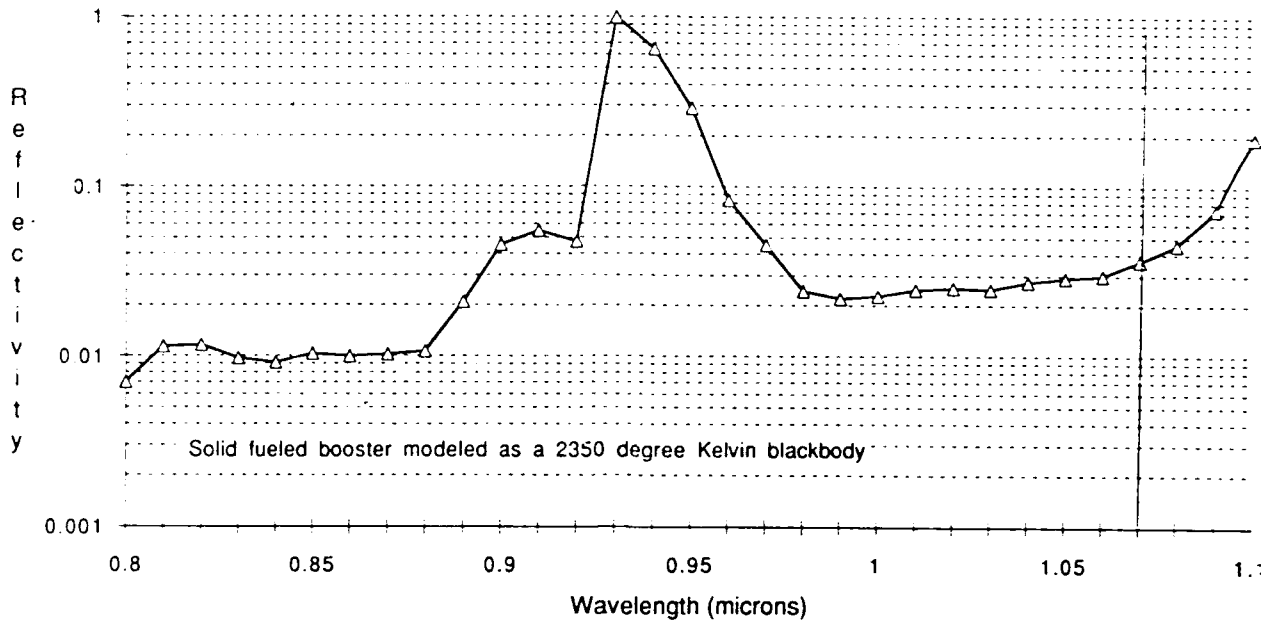


Figure 5.1 Examples of UV Spectral from a Storable Propellant Rocket Plume (a) and Matched Filter Spectral Profiles for HCs (b, c, d, e) with Parameters Given in Figure 5.2

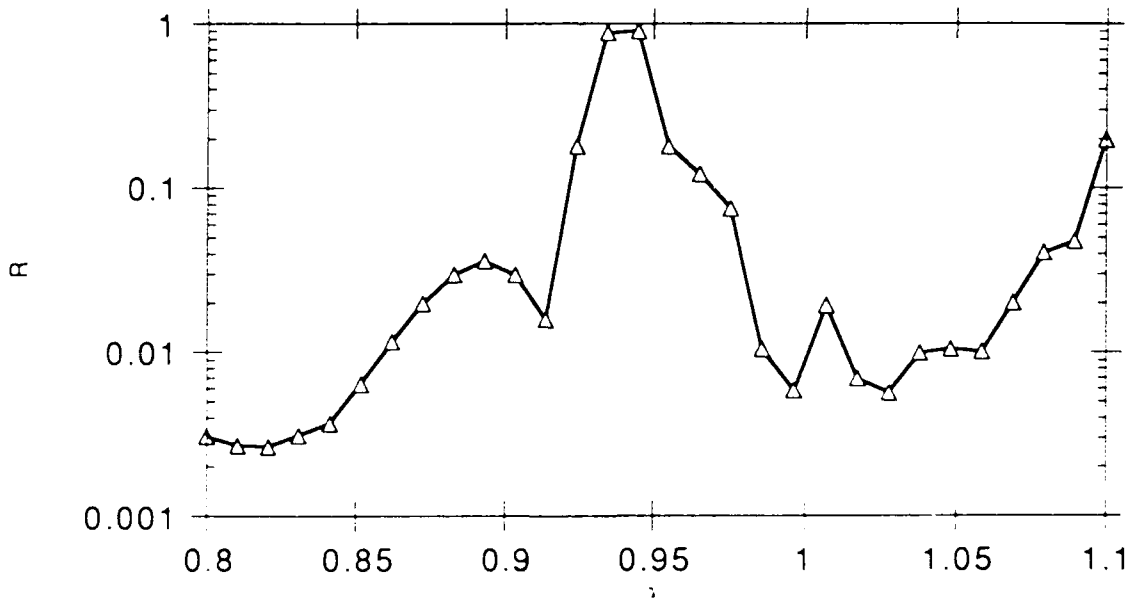
Figure	N	$\lambda_i (\mu\text{m})$				$n_i \begin{pmatrix} \min \\ \max \end{pmatrix}$				α_i				L (μm)	
		λ_1	λ_2	λ_3	λ_4	n_1	n_2	n_3	n_4	α_1	α_2	α_3	α_4		
5.2b	4	0.315	0.3365	0.358	0.390	0.007 0.009	0.0055 0.0065	0.0075 0.0085	0.0162 0.0180	0	π	0	0	0.015 z/L	10
5.2c	*	"	"	"	"	0.006 0.008	0.006 0.007	"	"	"	0	"	"	"	"
5.2d	*	"	"	"	"	0.005 0.007	0.005 0.006	0.008 0.009	"	"	"	"	"	"	"
5.2e	*	"	"	"	"	0.0055 0.0075	"	0.0085 0.0095	"	"	"	"	"	"	"

Figure 5.2 Holographic Coating Parameters Used to Generate the Coating Reflectivity Profiles Illustrated in Figures 5.1b, c, d, and e. (The min and max n_i Values Represent the Extremes for a Small Quadratic Taper in n_i).

OPTIMUM MATCHED FILTER REFLECTIVITY AS A FUNCTION OF WAVELENGTH FOR THE DETECTION OF A SOLID FUELED BOOSTER AGAINST AN EARTH BACKGROUND USING A SILICON DETECTOR

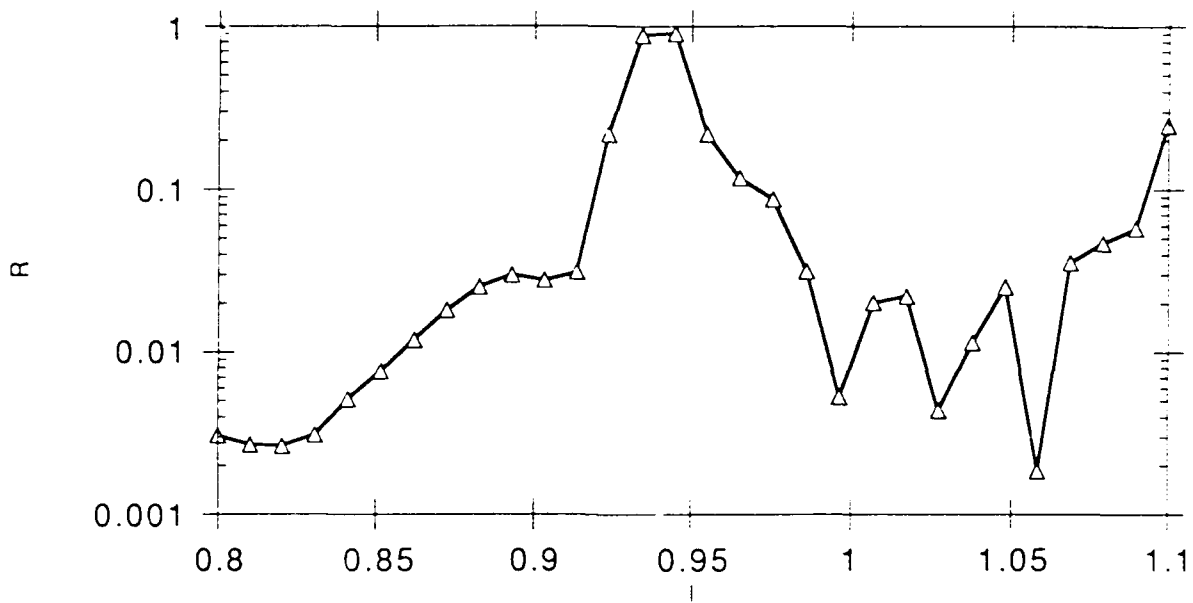


5.3a

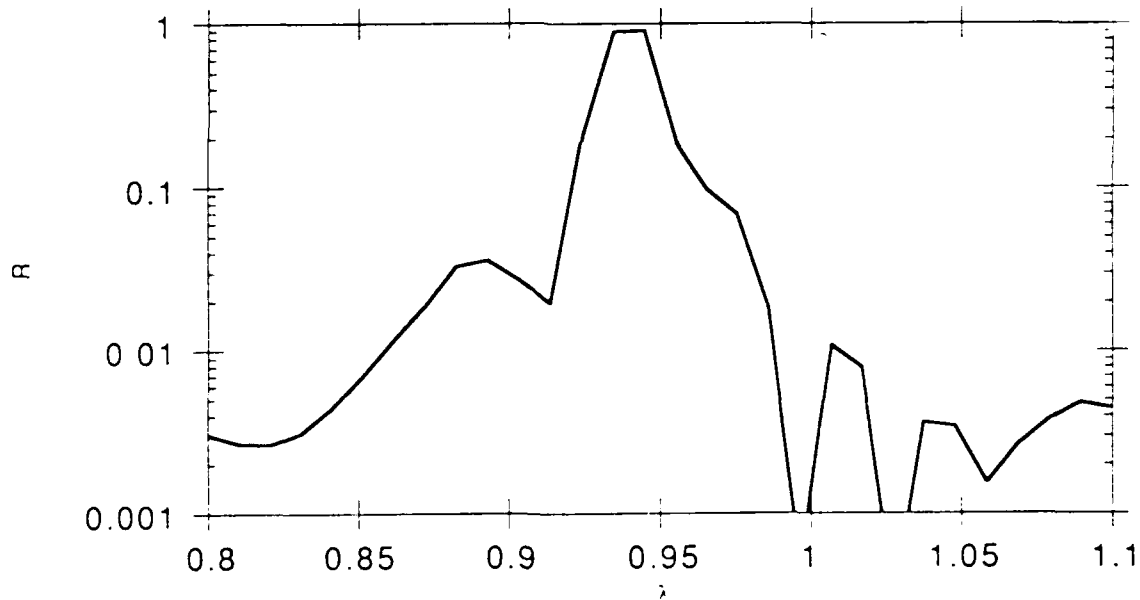


5.3b

Figure 5.3 Optimum Matched Filter Reflectivity, as Calculated for a Solid Fueled Booster Against an Earth Background (5.3a) and the Reflectivity Profile of an HC (5.3b) with Parameters Given in Figure 5.5.



5.4a

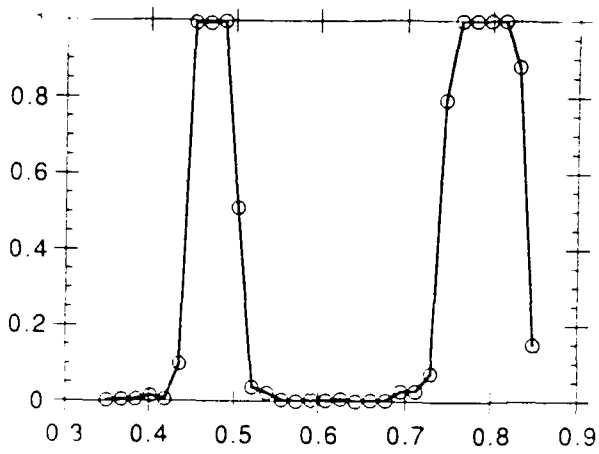


5.4b

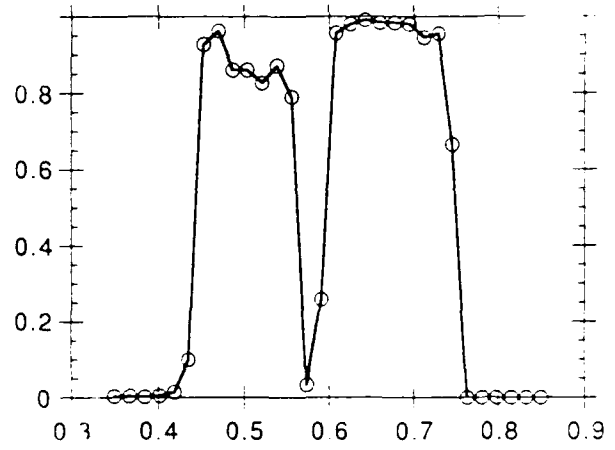
Figure 5.4 Holographic Matched Filters for the Detection of a Solid Fueled Booster Against an Earth Background, with Coating Parameters Given in Figure 5.5. These Filters do not Reproduce the Optimum Profile (Figure 5.3a) Quite as well as the HC Shown in Figure 5.3b.

Figure	N	$\lambda_i (\mu\text{m})$		$n_i \begin{pmatrix} \min \\ \max \end{pmatrix}$		α_i		$\epsilon(Z)$	L (μm)
		λ_1	λ_2	n_1	n_2	α_1	α_2		
5.3b	2	0.95	1.12	0.025 0.030	0.01 0.02	0	0	0.01 Z/L	22
5.4a	"	"	"	"	"	"	π	"	"
5.4b	"	"	1.17	"	"	"	0	"	"

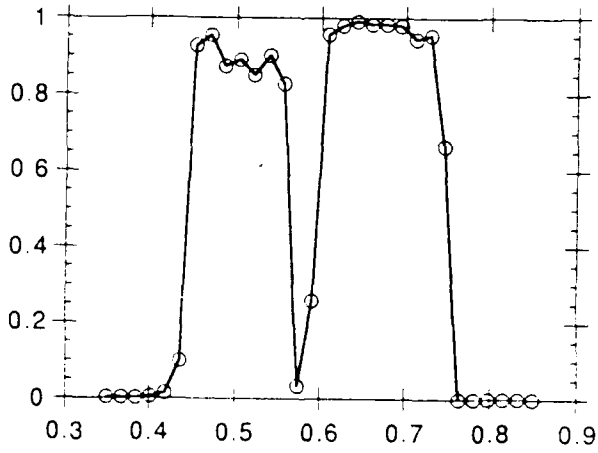
Figure 5.5 HC parameters for the filter reflectivity profiles illustrated in figures 5.3 and 5.4. (The min and max n_i values represent the extremes for a quadratic taper in n_i).



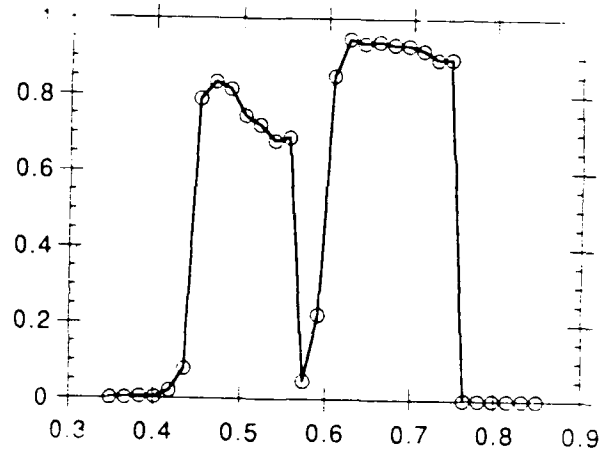
a



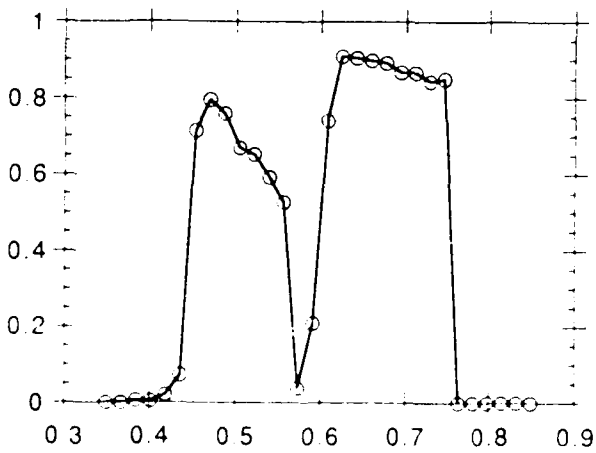
b



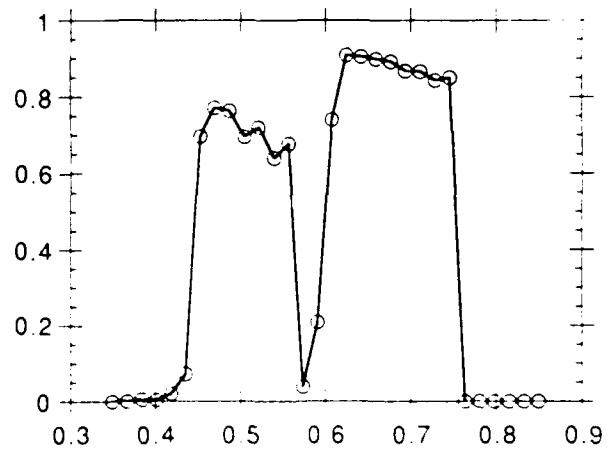
c



d

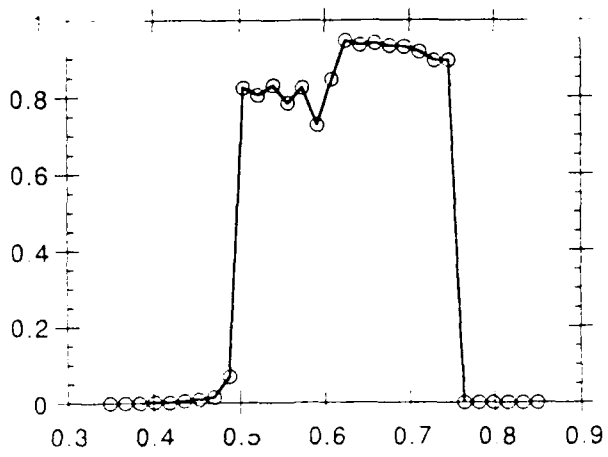


e

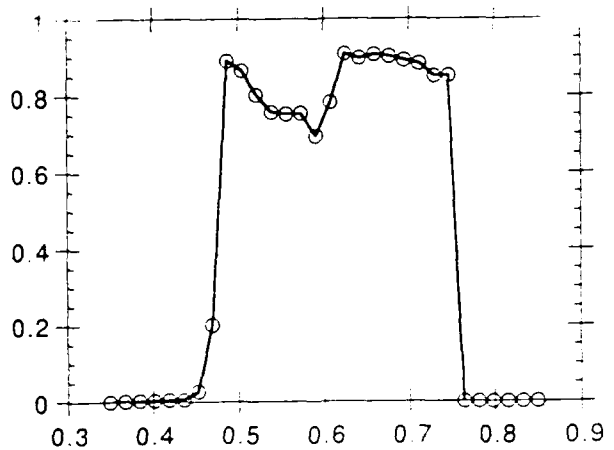


f

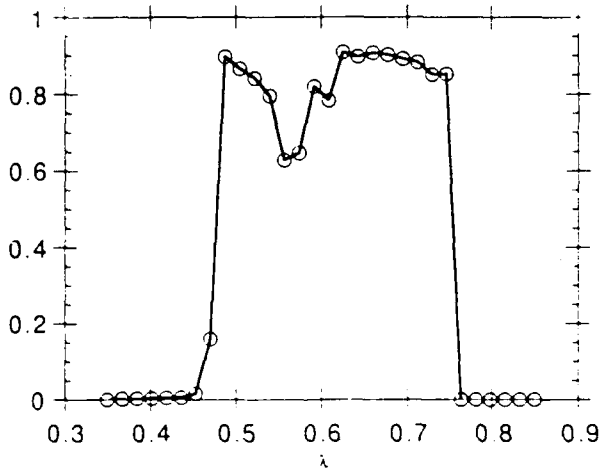
Figure 5.6 Attempts to Design a HC with a Reflectivity of 1 Over the Wavelength Regime 0.4 to 0.8 μm , by Using Two Chirped Periods. HC Parameters Given in Figure 5.7.



g



h

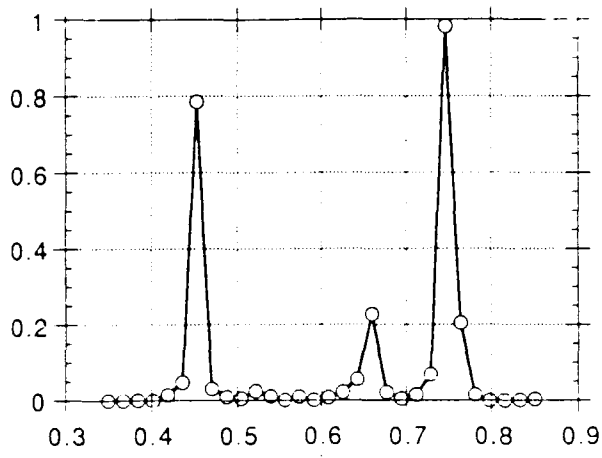


i

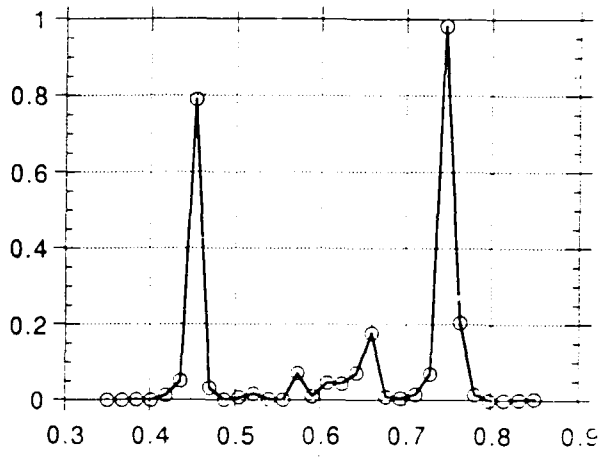
Figure 5.6 (continued)

Figure	N	λ_i (μm)		n_j		α_i		$\epsilon(Z)$	L (μm)
		λ_1	λ_2	n_1	n_2	α_1	α_2		
5.6a	2	0.45	0.75	$0.05 + 0.05(Z/L) (Z/L - 1)$	$-0.05 + 0.05 (Z/L) (Z/L - 1)$	0	0	$-0.05 Z/L$	50
5.6b	"	"	0.60	"	"	"	"	$-0.1 Z/L$	"
5.6c	"	"	"	"	"	"	π	"	"
5.6d	"	"	"	"	"	"	"	$-0.15 Z/L$	"
5.6e	"	"	"	"	"	"	"	"	40
5.6f	"	"	"	"	"	"	0	"	"
5.6g	"	0.50	"	"	"	"	"	"	50
5.6h	"	0.48	"	"	$-0.045 + 0.05 (Z/L) (Z/L - 1)$	"	π	"	"
5.6i	"	"	"	"	"	"	0	"	"

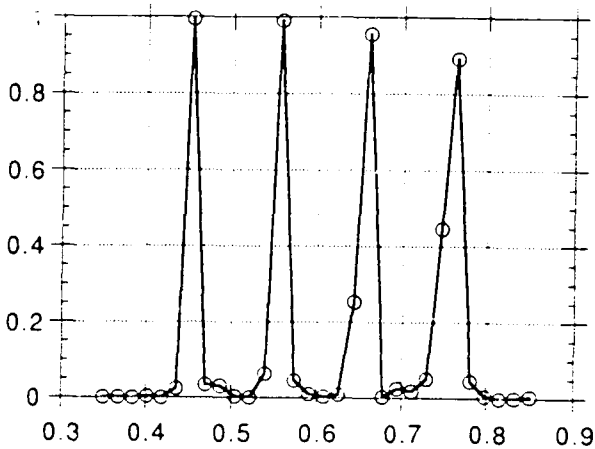
Figure 5.7 HC parameters used to generate the reflectivity plots in figure 5.6 (two chirped coatings; maximum allowable peak-to-valley index of refraction modulation = 0.2).



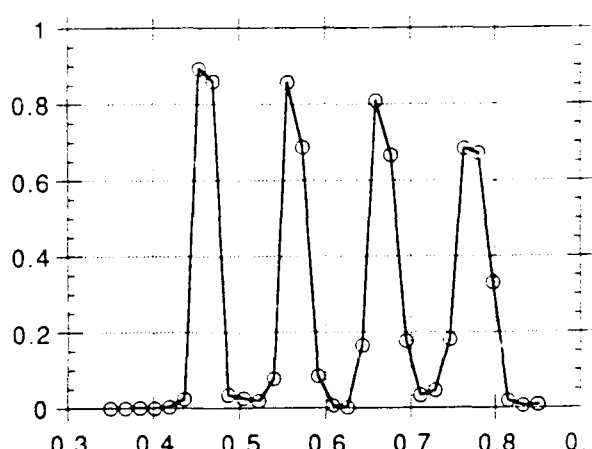
a



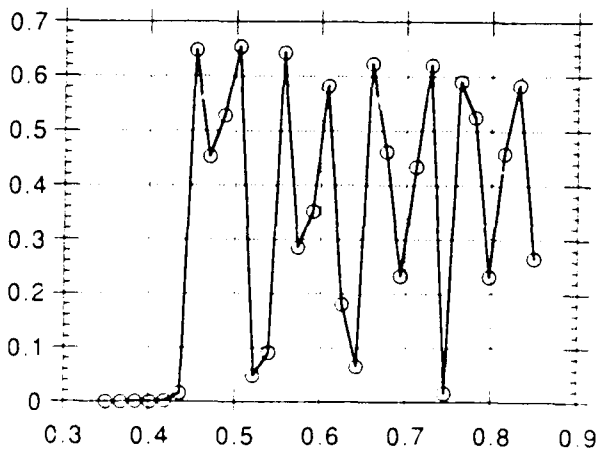
b



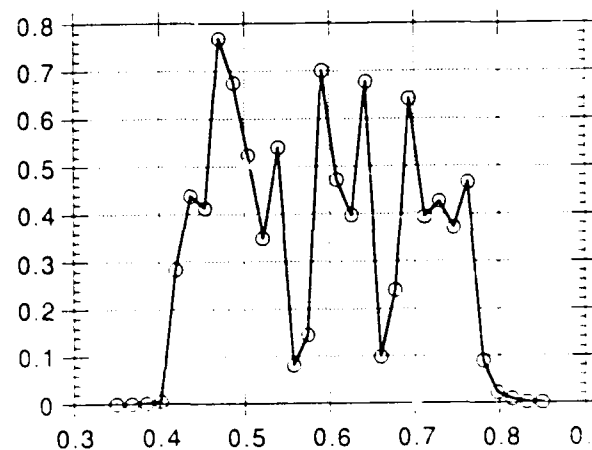
c



d

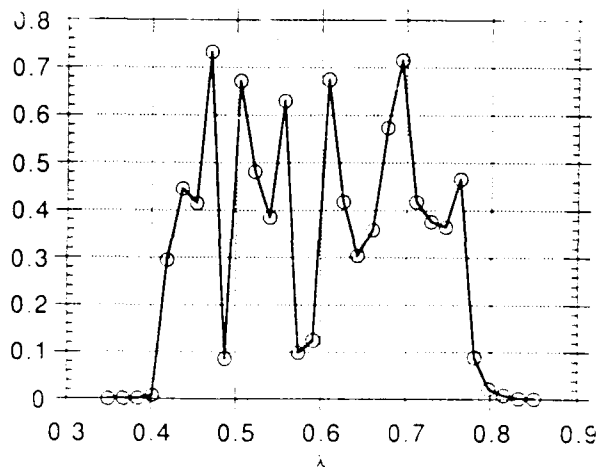


e

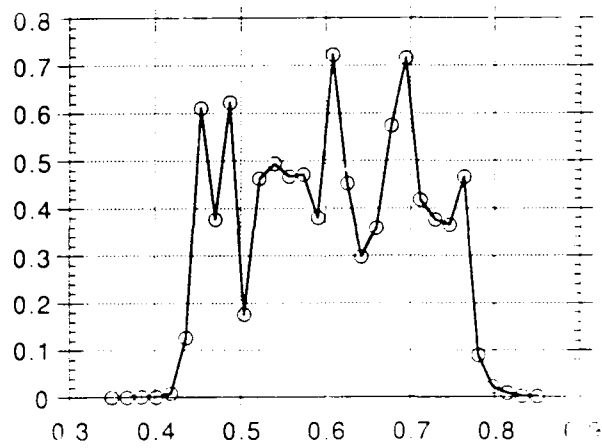


f

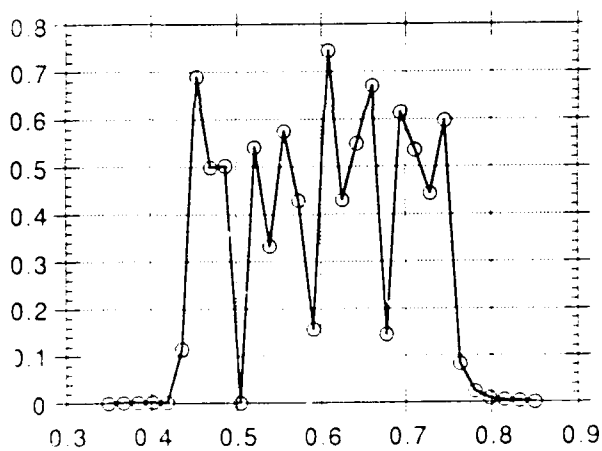
Figure 5.8 Attempts to design a HC with a Reflectivity of 1 Over the Wavelength Regime 0.4 to 0.8 μm , by Using Four Chirped Periods. HC Parameters Given in Figure 5.9.



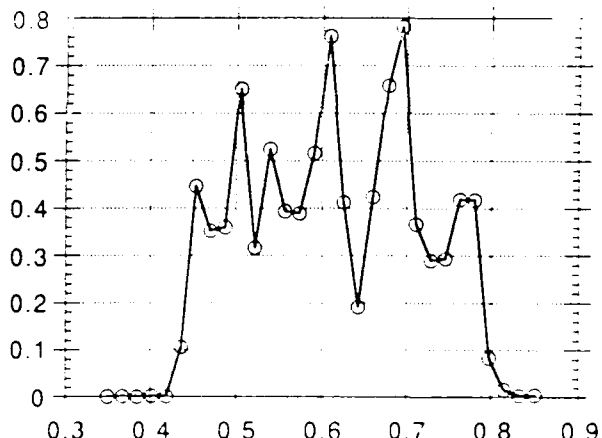
g



h



i



j

Figure 5.8 (continued)

Figure	N	$\lambda_i(\mu\text{m})$				$n_i \begin{pmatrix} \min \\ \max \end{pmatrix}$				α_i				L(μm)	
		λ_1	λ_2	λ_3	λ_4	n_1	n_2	n_3	n_4	α_1	α_2	α_3	α_4		
5.8a	4	0.45	0.55	0.65	0.75	0.015 0.025	0.015 0.025	0.015 0.25	0.015 0.025	0	0	0	0	0	50
5.8b	"	"	"	"	"	"	"	"	"	"	π	"	"	"	"
5.8c	"	"	"	"	"	"	"	"	"	"	π	"	π	-0.01 Z/L	"
5.8d	"	"	"	"	"	0.014 0.024	0.014 0.024	"	"	"	"	"	"	-0.03 Z/L	"
5.8e	"	"	"	"	"	"	"	"	0.016 0.026	"	"	"	"	-0.06 Z/L	"
5.8f	"	0.42	0.48	0.58	0.68	"	"	"	"	"	"	"	"	"	"
5.8g	"	"	0.50	0.60	"	"	"	"	"	"	"	"	"	"	"
5.8h	"	0.44	0.52	"	"	"	"	"	"	"	"	"	"	"	"
5.8i	"	"	"	"	"	"	"	"	"	"	"	"	"	-0.05 Z/L	"
5.8j	"	"	"	"	"	"	"	"	"	"	"	"	"	-0.07 Z/L	"

Figure 5.9 HC parameters used to generate the reflectivity plots in figure 5.8 (four chirped coatings; maximum allowable peak-to-valley index of refraction modulation = 0.2).

APPENDIX 5A

COMPIER LISTING OF THE PROGRAM USED TO SOLVE THE
COUPLED MODE EQUATIONS

```
program CaseTwo
c
c   This is a program for calculating the reflectivity
c   profile of multiple chirped gratings.
c   The program uses
c   Runge-Kutta driver with adaptive stepsize control.
c   Integrate the NVAR starting values YSTART from X1 to X2
c   with accuracy EPS, storing intermediate results in the
c   OUTPUT file. H1 should be set as a guessed first
c   stepsize. HMIN as the minimum allowed stepsize (can be 0).
c   YSTART is replaced by values at the end of the
c   integration interval. DERIVS is
c   the subroutine for calculating the right-hand
c   side derivative, while RKQC is the name of the stepper
c   routine to be used.
c
c   complex ystart(17),y(17),dydx(17)
c   real yscal(17)
c   real ynorm(2)
c   real x1,wvl,wvk,thk
c   real zeron
c   real pi
c   complex ci
c
c   common/mainp/x1,wvl,wvk,thk
c   common/allcom/zeron,pi,ci
c
c   ----- parameters -----
c   two=2.0
c   zero=0.0
c   tiny=1.e-30
c   call params(nwvl,wvlmin,wvlmax,delwvl)
c   ----- parameters -----
c
c   open(2,file='case2.d1')
c
c   hmin=1.e-7
c   eps=1.e-3
c   write(*,*)'input cutoff factor (0.5 ?)
c   read(*,*)ctff
c   ctff=0.5
c
c   ----- start of the big loop -----
```

```

do 90 iwvl=1,nwvl
wvl=wvlmin+delwvl*float(iwvl-1)
wvk=2.*pi*zeron/wvl
thk=wvk*ctff
c      maxstp=max. number of points from x1=L to x2=0
maxstp=10000
c      L=10 micron
x1=10.
x2=0.
nvar=2
dxsav=0.01
h1=0.01
x=x1
h=h1
ystart(1)=(1.,0.)
ystart(2)=(0.,0.)
do 11 i=1,nvar
      y(i)=ystart(i)
11     continue
      xsav=x-dxsav*two
do 16 nstp=1,maxstp
      call derivs(x,y,dydx)
c      write(*,*)nstp
do 12 i=1,nvar
      yscal(i)=cabs(y(i))+cabs(h*dydx(i))+tiny
12     continue
      if((x+h-x2)*(x+h-x1).gt.zero) h=x2-x
      call rkqc(y,dydx,nvar,x,h,eps,yscal,hdid,hnext,derivs)
      if(abs(x-xsav).ge.dxsav) then
      xsav=x
      endif
      if((x-x2)*(x2-x1).ge.zero) then
do 14 i=1,nvar
      ystart(i)=y(i)
14     continue
do 100 i=1,nvar
      ynorm(i)=cabs(y(i))
100    continue
      yt1=ynorm(1)*ynorm(1)
      yt2=ynorm(2)*ynorm(2)
      R=yt2/yt1
      write(2,5000)wvl,R
5000   format(1x,g20.10,'          ',g20.10)

```

```

                goto 90
            endif
            if(abs(hnext).lt.hmin)
*                pause 'Stepsize smaller than minimum.'
                h=hnext
16          continue
            pause 'Too many steps.'
90          continue
            stop
            end

c
c
c
        subroutine rkqc(y,dydx,n,x,htry,eps,yscal,hdid,hnext,derivs)
c          Fifth-order Runge-Kutta step with monitoring of local
c          truncation error to ensure accuracy and adjust stepsize.
c          Input are the dependent variable vector Y of length N
c          and its derivative DYDX at the starting value of the
c          independent variable X. Also input are the stepsize to be
c          attempted HTRY, the required accuracy HNEXT is the
c          estimated next stepsize. DERIVS is the user-supplied
c          subroutine that computes the right-hand side derivatives.
c          parameter (pgrow=-0.2,pshrnk=-0.25,fcor=1./15.,
*             one=1.,safety=0.9,errcon=6.e-4)
c          The value ERRCON equals (4/SAFETY)**(1/PGROW)
            external derivs
            complex y(17),dydx(17),ytemp(17),ysav(17),dysav(17)
            real yscal(17)
            xsav=x
            do 11 i=1,n
                ysav(i)=y(i)
                dysav(i)=dydx(i)
11          continue
            h=htry
1          hh=0.5*h
            call rk4(ysav,dysav,n,xsav,hh,ytemp,derivs)
            x=xsav+hh
            call derivs(x,ytemp,dydx)
            call rk4(ytemp,dydx,n,x,hh,y,derivs)
            x=xsav+h
            if(x.eq.xsav)pause 'stepsize not significant in RKQC'
            call rk4(ysav,dysav,n,xsav,h,ytemp,derivs)
            errmax=0.

```

```

do 12 i=1,n
    ytemp(i)=y(i)-ytemp(i)
    errmax=max(errmax,cabs(ytemp(i)/yscal(i)))
12 continue
errmax=errmax/eps
if(errmax.gt.one)then
    h=safety*h*(errmax**pshrnk)
    goto 1
else
    hdid=h
    if(errmax.gt.errcon)then
        hnext=safety*h*(errmax**pgrow)
    else
        hnext=4.*h
    endif
endif
do 13 i=1,n
    y(i)=y(i)+ytemp(i)*fcor
13 continue
19 return
end

```

c
c
c

```

subroutine rk4(y,dydx,n,x,h,yout,derivs)
c Given values for N variables Y and their derivatives
c DYDX known at X, use the fourth-order Runge-Kutta method
c to advance the solution over an interval H and return the
c incremented variables as YOUT, which need not be a distinct
c array from Y. The user supplies the subroutine
c DERIVS(X,Y,DYDX) which returns derivatives DYDX at X.
external derivs
complex y(17),dydx(17),yout(17),yt(17),dym(17)
hh=h*0.5
h6=h/6.
xh=x+hh
do 11 i=1,n
    yt(i)=y(i)+hh*dydx(i)
11 continue
call derivs(xh,yt,dym)
do 12 i=1,n
    yt(i)=y(i)+hh*dym(i)
12 continue

```

```

        call derivs(xh,yt,dym)
        do 13 i=1,n
            yt(i)=y(i)+h*dym(i)
            dym(i)=dym(i)+dym(i)
13      continue
        call derivs(x+h,yt,dyt)
        do 14 i=1,n
            yout(i)=y(i)+h6*(dydx(i)+dym(i)+2.*dym(i))
14      continue
        return
    end

c
c
    subroutine params(nwvl,wvlmin,wvlmax,delwvl)
c
    real alpha
    real phi(15),grtk(15)
    integer ngrt
    real zeron
    real pi
    complex ci

c
    common/prmtrs/alpha,phi,grtk,ngrt
    common/allcom/zeron,pi,ci

c
c
    ----- parameters -----
    ci=(0.,1.)
    pi=3.14159
c
    zeron=n_0 :
    zeron=1.5
c
    alpha=absorption constant ( 1/micron) :
    alpha=0.
c
    ngrt=number of gratings (N) :
    ngrt=4
c
    grating phase shift :
    phi(1)=0.
    phi(2)=pi
    phi(3)=0.
    phi(4)=0.
c
    grating wave length (micron) grtk=4 n_0 pi/wvl:
    grtk(1)=4.*zeron*pi/0.315
    grtk(2)=4.*zeron*pi/0.3365
    grtk(3)=4.*zeron*pi/0.3580

```



```

      delk=2.*wvk-epsilon(i)*grtk(i)
c      g=coefficient in the coupled mode equation
      g=g+(ci*pi*deln(i)/wvl)*cexp(ci*(delk*x-phi(i)))
10     continue
      gcc=conjg(g)
c      ----- parameters -----
      dydx(1)=g*y(2)-0.5*alpha*y(1)
      dydx(2)=gcc*y(1)-0.5*alpha*y(2)
      return
      end
```

APPENDIX 5B

Reflection Spectrum of Multiple Chirped Gratings

Jeffrey B. Shellan

JBS Technologies, Inc.

Thousand Oaks, CA 91360

ABSTRACT

We analyze the reflection spectrum of multiple chirped gratings using coupled-mode theory. We also design filters with desired reflection spectrum by adjusting the parameters of multiple chirped gratings.

1. INTRODUCTION

It is important to design filters with desired reflection spectrum. These filters require certain variation of index of refraction in a medium. Holography is one of the most practical methods to generate any desired index variation in a medium. In this paper, we report the design of filters with multiple chirped holographic gratings. We first analyze the reflection spectrum of multiple chirped gratings. Then, we adjust different parameters to design filters with desired reflection spectrum.

2. COUPLED-MODE ANALYSIS

Referring to Fig. 1, a beam of light is incident upon a medium with thickness L . The transmittance and reflectivity depend on both the index of refraction of the medium and the wavelength of light. The reflection spectrum can be obtained by calculating the reflectivity of plane waves with different wavelength.

Consider a medium where the index variation is generated by a set of N holographic gratings. The total index of refraction can be written as

$$n(z) = n_0 + \sum_{p=1}^N n_p(z) \cos\left[\frac{2\pi}{\Lambda_p}(1 + \epsilon(z))z + \phi_p + \alpha\right], \quad (1)$$

where

$$n_p(z) = n_p^{(0)} + n_p^{(1)} \frac{z}{L} + n_p^{(2)} \frac{z^2}{L^2} \quad (2)$$

is the amplitude of each grating which is tapered during manufacturing, ϵ is the chirp factor, L is the thickness of the medium, Λ_p is the grating spacing of the

p -th grating, ϕ_p and α are the phase and absorption constant respectively. A plane wave incident upon the medium will be reflected. The total electric field inside the medium is

$$E = A(z)e^{i(\omega t - kz)} + B(z)e^{i(\omega t + kz)}, \quad (3)$$

where $A(z)$ and $B(z)$ represent the amplitudes of the forward and backward propagating plane waves respectively. Under the approximation of slow varying envelopes, the coupled-mode equations [1] can be written as

$$\frac{d}{dz}A = i \sum_p \frac{\pi n_p(z)}{\lambda} e^{i[(2k - K_p)z - \phi_p]} B - \frac{1}{2}\alpha A, \quad (4)$$

$$\frac{d}{dz}B = -i \sum_p \frac{\pi n_p(z)}{\lambda} e^{i[(K_p - 2k)z + \phi_p]} A + \frac{1}{2}\alpha B, \quad (5)$$

where

$$K_p = \frac{2\pi}{\Lambda_p}(1 + \epsilon(z)) \quad (6)$$

is the grating wavevector of the p -th chirped grating.

The above coupled mode equations Eq. (4) and Eq. (5) can not be easily solved analytically. We have obtained numerical solutions by using the fifth-order Runge-Kutta method with adaptive step size. Since we have neglected fast varying phase terms in deriving the coupled mode equations, it will be consistent to neglect those terms with very large phase mismatch. In our numerical

calculations, we have neglected terms with phase mismatch

$$\Delta k = \left| 2k - \frac{2\pi}{\Lambda_p} \right| > 0.5k. \quad (7)$$

With this cutoff value of phase mismatch, the program runs much faster than directly integrating Eqs. (4) and (5).

By calculating reflectivities for plane waves with different wavelength, we can obtain the reflection spectrum. Fig. 2 shows the reflection spectrum of three chirped gratings. We have used the following parameters: $n_0 = 1.5$, $\alpha = 0$, $L = 10\mu m$, $\phi_1 = 0$, $\phi_2 = \frac{\pi}{3}$, $\phi_3 = \frac{\pi}{2}$, $\lambda_1 = 0.5\mu m$, $\lambda_2 = 1.0\mu m$, $\lambda_3 = 1.4\mu m$, $n_1 = 0.02 + 0.01(\frac{\lambda}{L})^2 - 0.01(\frac{\lambda}{L})$, $n_2 = 0.03 + 0.01(\frac{\lambda}{L})^2 - 0.01(\frac{\lambda}{L})$, $n_3 = 0.01 + 0.01(\frac{\lambda}{L})^2 - 0.01(\frac{\lambda}{L})$, $\epsilon_1 = -0.1(\frac{\lambda}{L})$, $\epsilon_2 = 0.1(\frac{\lambda}{L})$, $\epsilon_3 = 0.05(\frac{\lambda}{L})$, where λ_p is the center wavelength which is related to Λ_p by $\Lambda_p = \frac{\lambda_p}{2n_0}$. We notice that by chirping the grating, the side lobes are suppressed and the band width is increased. In addition, different gratings will interfere with one another only in the region where they overlap.

3. FILTER DESIGN

The shape of the reflection spectrum of a set of chirped gratings depends on their grating amplitudes, chirping rates, thickness of the medium, and their relative phases. We can adjust these parameters to design a filter with desired reflection spectrum. By increasing the grating amplitude, we can increase the peak reflectivity and the band width of the reflection spectrum. However, since

the dynamic range of the gratings is usually limited, sometimes we cannot reach the required reflectivity by increasing the amplitude of the gratings. Another way to increase the reflectivity is to increase the thickness of the medium. A thicker medium can give a higher reflectivity with a relatively smaller grating amplitude. In addition, a thicker medium will also result in a smaller band width. However, as we increase the thickness, we will have more side lobes. These side lobes can be suppressed by tapering and chirping the grating. On the other hand, tapering or chirping the grating will also increase the band width of the spectrum. Sometimes, a large chirping rate will produce two peaks in the reflection spectrum. When we use more than one grating, the relative phases of the gratings will also affect the spectrum in the region where they overlap. In order to fit a required reflection spectrum, we need to consider the effect due to all these parameters.

We have designed several filters with multiple chirped gratings. Fig. 3 shows one of the examples. Fig. 3a is the desired reflection spectrum. Fig. 3b shows the reflection spectrum of four chirped gratings. We notice that the two profiles match quite well. The parameters used to generate Fig. 3b are given by $n_0 = 1.5$, $\alpha = 0$, $L = 10\mu m$, $\phi_1 = 0$, $\phi_2 = \pi$, $\phi_3 = 0$, $\phi_4 = 0$, $\lambda_1 = 0.315\mu m$, $\lambda_2 = 0.3365\mu m$, $\lambda_3 = 0.3580\mu m$, $\lambda_4 = 0.39\mu m$, $n_1 = 0.009 + 0.008(\frac{z}{L})^2 - 0.008(\frac{z}{L})$, $n_2 = 0.0065 + 0.004(\frac{z}{L})^2 - 0.004(\frac{z}{L})$, $n_3 = 0.0085 + 0.004(\frac{z}{L})^2 - 0.004(\frac{z}{L})$, $n_4 = 0.018 + 0.007(\frac{z}{L})^2 - 0.007(\frac{z}{L})$, $\epsilon_1 = -0.015(\frac{z}{L})$, $\epsilon_2 = 0$, $\epsilon_3 = 0$, $\epsilon_4 = 0.015(\frac{z}{L})$. This example demonstrates the reflection spectrum of multiple chirped gratings with relatively large separation between their center wavelengths.

Another example is shown in Fig. 4. Fig. 4a shows the two desired reflection

curves. Fig. 4b and Fig. 4c show the two fitting curves. This example shows the reflection spectrum of multiple chirped gratings with their center wavelengths close to each other. By adjusting the thickness of the medium, the amplitudes of the gratings, the relative phases, center wavelengths, and the tapering and chirping factors, we can fit the two different curves in Fig. 4a by using two chirped gratings. Fig. 4b and Fig. 4c show the fitting curves corresponding to the upper and lower curve in Fig. 4a respectively. The parameters used to generate Fig. 4b are: $n_0 = 1.5$, $\alpha = 0$, $L = 10\mu m$, $\phi_1 = 0$, $\phi_2 = \pi$, $\lambda_1 = 0.985\mu m$, $\lambda_2 = 1.05\mu m$, $n_1 = 0.1 + 0.1(\frac{z}{L})^2 - 0.1(\frac{z}{L})$, $n_2 = 0.08 + 0.04(\frac{z}{L})^2 - 0.04(\frac{z}{L})$, $\epsilon_1 = 0.07(\frac{z}{L})$, $\epsilon_2 = -0.05(\frac{z}{L})$. The parameters used to generate Fig. 4c are: $n_0 = 1.5$, $\alpha = 0$, $L = 22\mu m$, $\phi_1 = 0$, $\phi_2 = 0$, $\lambda_1 = 0.95\mu m$, $\lambda_2 = 1.17\mu m$, $n_1 = 0.03 + 0.01(\frac{z}{L})^2 - 0.01(\frac{z}{L})$, $n_2 = 0.02 + 0.04(\frac{z}{L})^2 - 0.04(\frac{z}{L})$, $\epsilon_1 = 0.01(\frac{z}{L})$, $\epsilon_2 = 0.04(\frac{z}{L})$. We notice that thicker medium and smaller grating amplitude result in narrower spectral band width.

4. CONCLUSION AND DISCUSSION

We have analyzed the reflection spectrum of multiple chirped gratings using coupled-mode theory. Based on the analysis, we have designed filters with desired reflection spectrum by adjusting the parameters of multiple chirped gratings.

In the above discussions, we have used slowly varying envelope approximation and neglected the terms with large phase mismatch. This approximation is very practical, if we need only to know the general shape of the reflection spectrum. When we design filters to fit desired reflection spectrum, we simply adjusted the

parameters according to the past experience. A more general approach would be to vary the parameters systematically so that the optimum fitting curve can be found.

REFERENCES

1. See, for example, P. Yeh, "Two-Wave Mixing in Nonlinear Media," IEEE J. Quantum Electron., 25, 484-519, (1989).

FIGURE CAPTIONS

Fig.1 Schematic drawings of the incident, transmitted and reflected beams.

Fig.2 Reflection spectrum of three chirped gratings where $n_0 = 1.5$, $\alpha = 0$.

$$L = 10\mu m, \phi_1 = 0, \phi_2 = \frac{\pi}{3}, \phi_3 = \frac{\pi}{2}, \lambda_1 = 0.5\mu m, \lambda_2 = 1.0\mu m, \lambda_3 = 1.4\mu m,$$

$$n_1 = 0.02 + 0.01\left(\frac{\lambda}{L}\right)^2 - 0.01\left(\frac{\lambda}{L}\right), n_2 = 0.03 + 0.01\left(\frac{\lambda}{L}\right)^2 - 0.01\left(\frac{\lambda}{L}\right), n_3 =$$

$$0.01 + 0.01\left(\frac{\lambda}{L}\right)^2 - 0.01\left(\frac{\lambda}{L}\right), \epsilon_1 = -0.1\left(\frac{\lambda}{L}\right), \epsilon_2 = 0.1\left(\frac{\lambda}{L}\right), \text{ and } \epsilon_3 = 0.05\left(\frac{\lambda}{L}\right).$$

Fig.3 Reflection spectrum of (a) the desired profile, and (b) the fitting curve with

four chirped gratings: $n_0 = 1.5$, $\alpha = 0$, $L = 10\mu m$, $\phi_1 = 0$, $\phi_2 = \pi$, $\phi_3 = 0$,
 $\phi_4 = 0$, $\lambda_1 = 0.315\mu m$, $\lambda_2 = 0.3365\mu m$, $\lambda_3 = 0.3580\mu m$, $\lambda_4 = 0.39\mu m$,
 $n_1 = 0.009 + 0.008\left(\frac{\lambda}{L}\right)^2 - 0.008\left(\frac{\lambda}{L}\right)$, $n_2 = 0.0065 + 0.004\left(\frac{\lambda}{L}\right)^2 - 0.004\left(\frac{\lambda}{L}\right)$,
 $n_3 = 0.0085 + 0.004\left(\frac{\lambda}{L}\right)^2 - 0.004\left(\frac{\lambda}{L}\right)$, $n_4 = 0.018 + 0.007\left(\frac{\lambda}{L}\right)^2 - 0.007\left(\frac{\lambda}{L}\right)$,
 $\epsilon_1 = -0.015\left(\frac{\lambda}{L}\right)$, $\epsilon_2 = 0$, $\epsilon_3 = 0$, $\epsilon_4 = 0.015\left(\frac{\lambda}{L}\right)$.

Fig.4 (a) Reflection spectrum of the two desired profiles. (b) The fitting curve

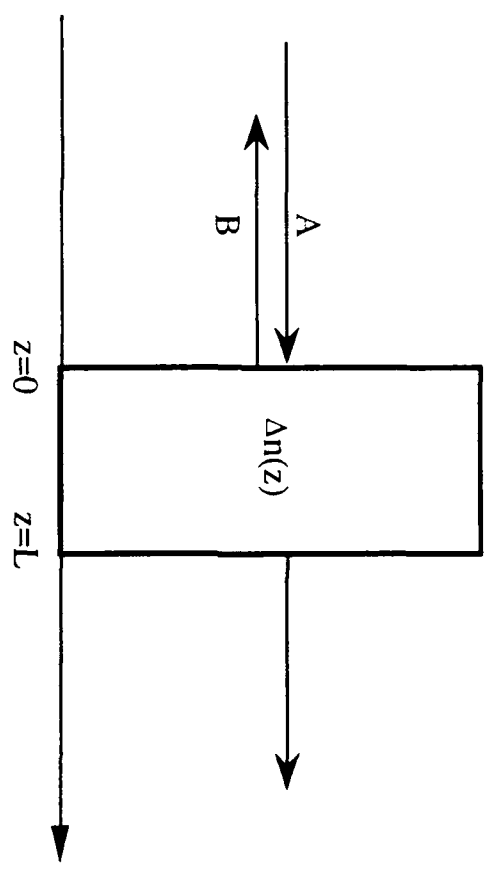
for the upper curve in (a) with two chirped gratings: $n_0 = 1.5$, $\alpha = 0$, $L =$
 $10\mu m$, $\phi_1 = 0$, $\phi_2 = \pi$, $\lambda_1 = 0.985\mu m$, $\lambda_2 = 1.05\mu m$, $n_1 = 0.1 + 0.1\left(\frac{\lambda}{L}\right)^2 -$
 $0.1\left(\frac{\lambda}{L}\right)$, $n_2 = 0.08 + 0.04\left(\frac{\lambda}{L}\right)^2 - 0.04\left(\frac{\lambda}{L}\right)$, $\epsilon_1 = 0.07\left(\frac{\lambda}{L}\right)$, $\epsilon_2 = -0.05\left(\frac{\lambda}{L}\right)$.

(c) The fitting curve for the lower curve in (a) with two chirped gratings:

$$n_0 = 1.5, \alpha = 0, L = 22\mu m, \phi_1 = 0, \phi_2 = 0, \lambda_1 = 0.95\mu m, \lambda_2 = 1.17\mu m,$$

$$n_1 = 0.03 + 0.01\left(\frac{\lambda}{L}\right)^2 - 0.01\left(\frac{\lambda}{L}\right), n_2 = 0.02 + 0.04\left(\frac{\lambda}{L}\right)^2 - 0.04\left(\frac{\lambda}{L}\right), \epsilon_1 = 0.01\left(\frac{\lambda}{L}\right),$$

$$\epsilon_2 = 0.04\left(\frac{\lambda}{L}\right).$$



1 2

Data from "chirp.d2"

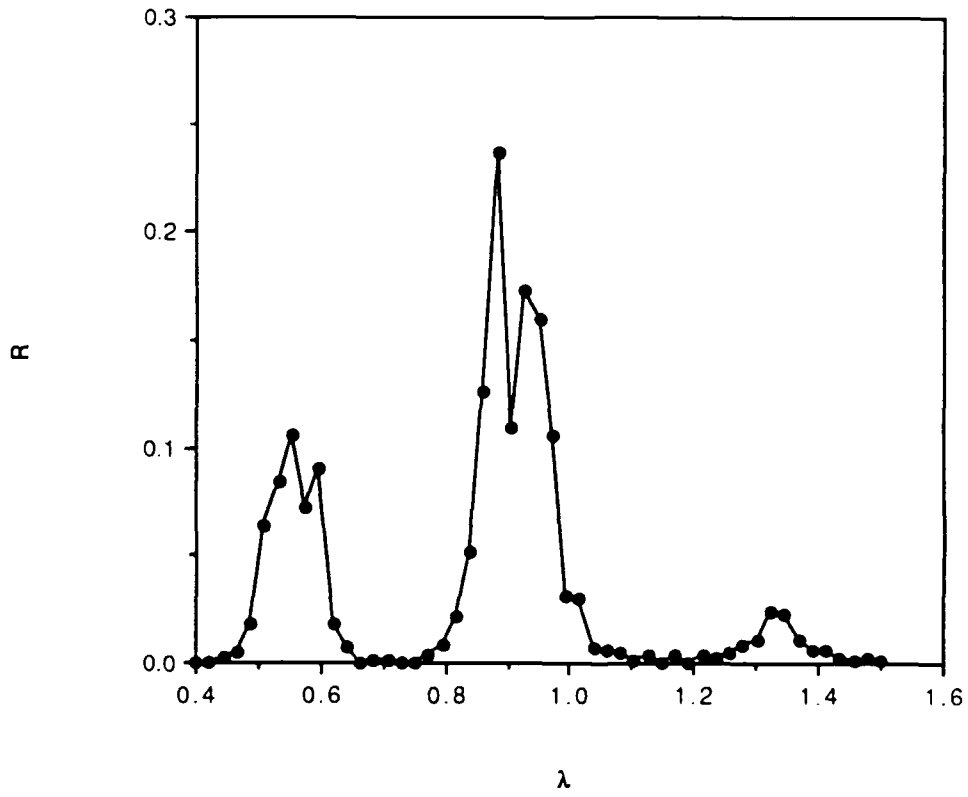


Fig. 3a

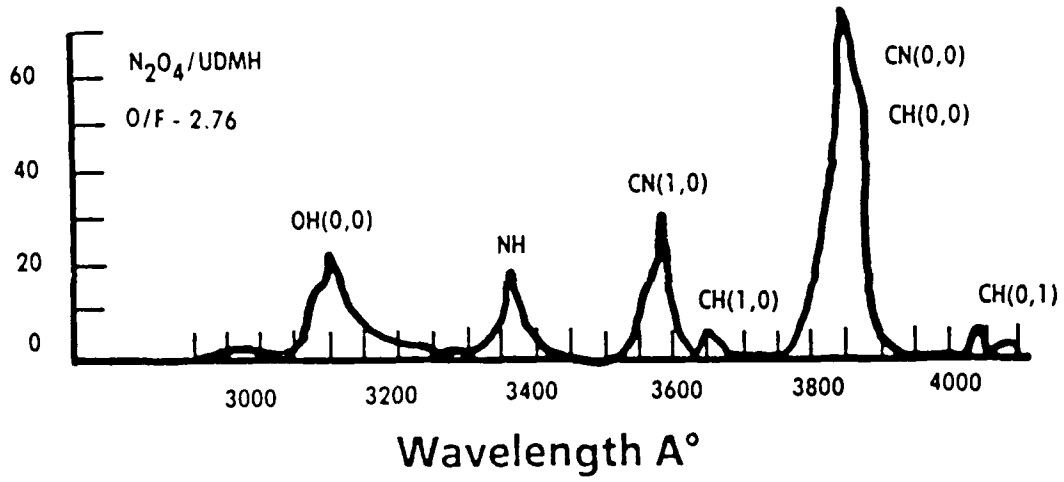


Fig. 30

Data from "case2.p1"

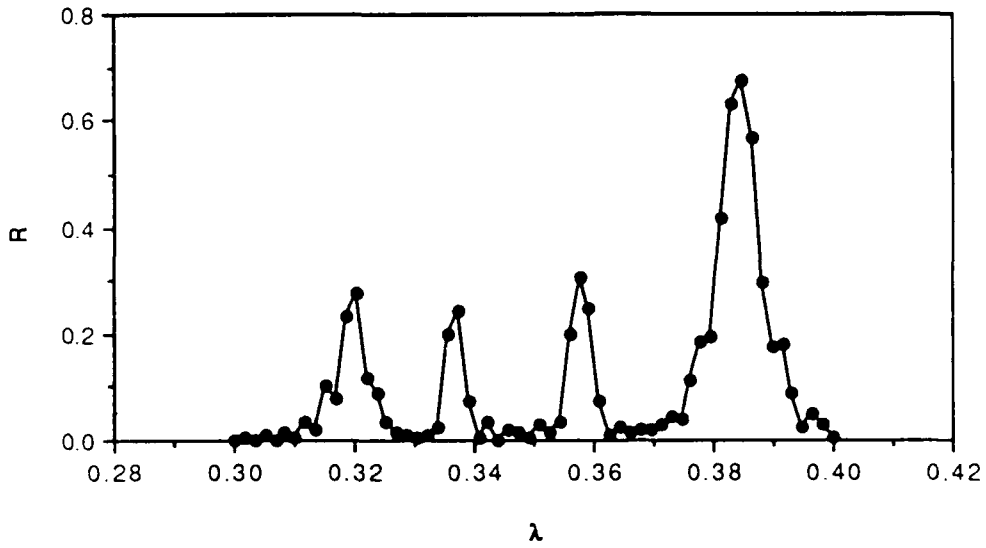


Fig. 4a

OPTIMUM MATCHED FILTER REFLECTIVITY AS A FUNCTION OF WAVELENGTH FOR THE DETECTION OF A SOLID FUELED BOOSTER AGAINST AN EARTH BACKGROUND USING A SILICON DETECTOR

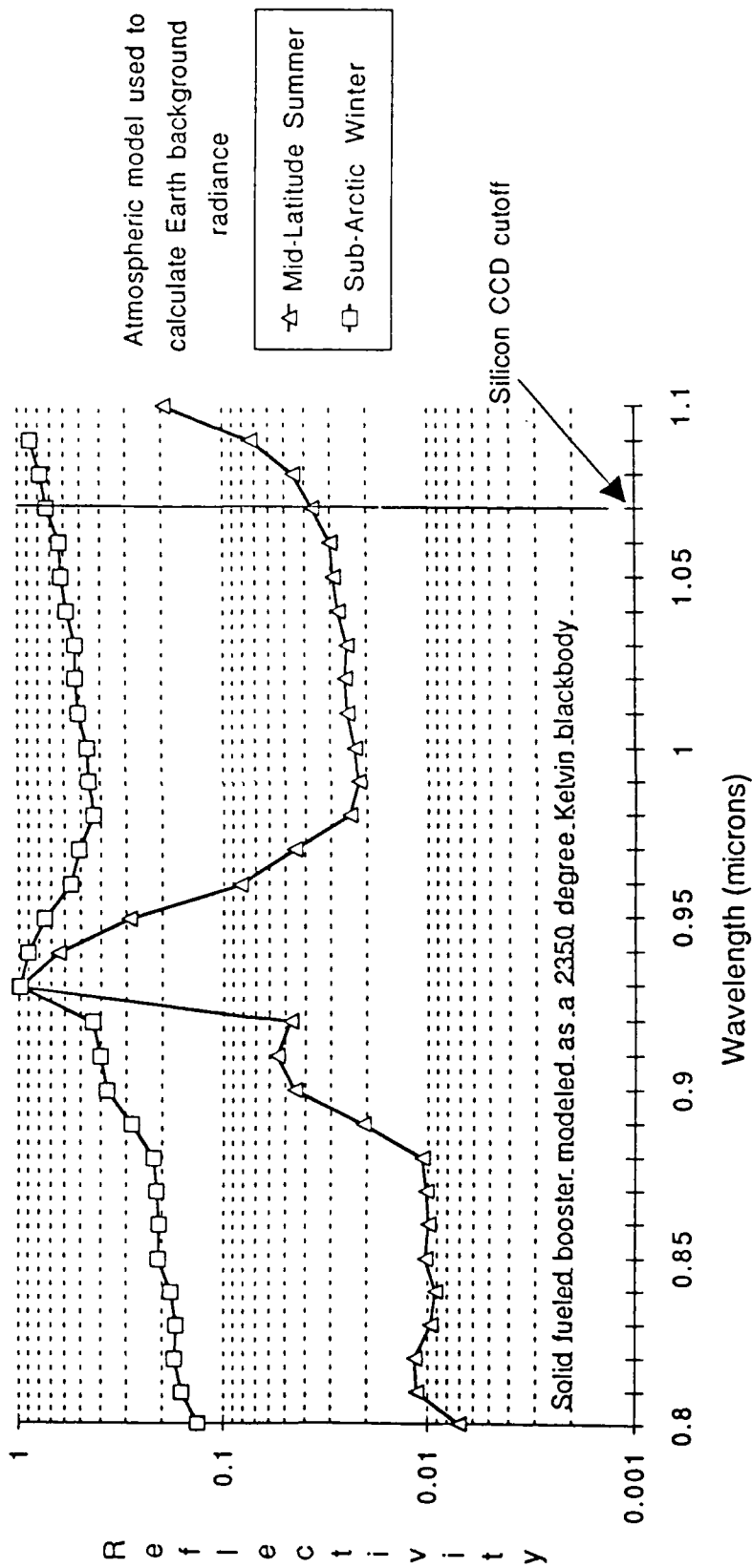


Fig 4b

Data from "case3.p1"

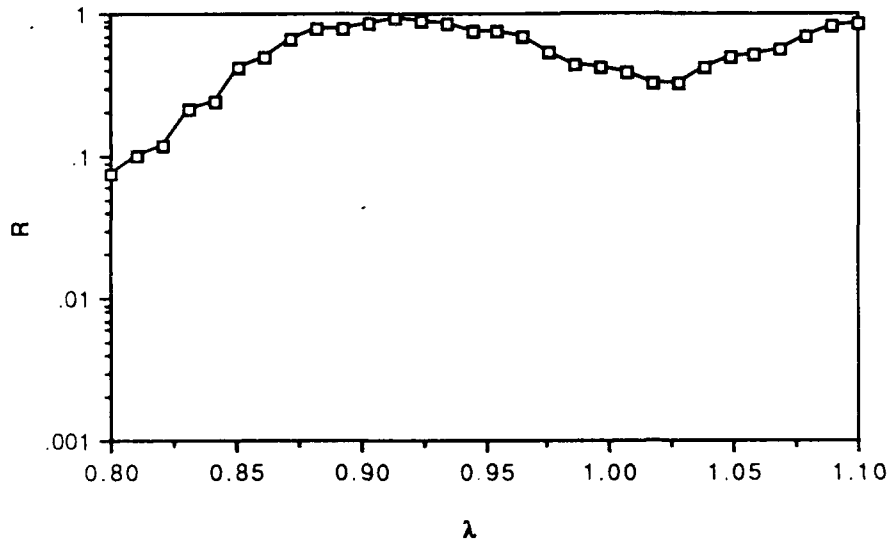


Fig. 2c

Data from "case3.p2"

